Computational Modelling of Fructose Metabolism and Lipid Deposition in Non-Alcoholic Fatty Liver Disease

Yunjie Liao

Department of Chemical Engineering & Institute for Liver and Digestive Health

University College London

Supervisors: Prof. David Bogle, Prof. Nathan Davies

This dissertation is submitted for the degree of

Doctor of Philosophy

Declaration

I, Yunjie Liao, confirm that the work presented in this thesis is my own. Where information has been derived from other sources, I confirm that this has been indicated in the thesis.

In loving memory of my grandmother, Shiping Li (1933-2019).

Acknowledgements

First of all, I would like to express my deepest and sincerest gratitude to my supervisors Professor David Bogle and Professor Nathan Davies for their enlightening advice, invaluable guidance and continuous encouragement throughout my PhD. Their profound knowledge, their dedication and determination in work deeply inspire me, motivate me and push me further than I dare. It was a great privilege and honour to complete this research project under their supervision.

Secondly, I would like to bring this acknowledgement to Dr Helen Jones, who has offered me not only experimental skills training, but also kindness and empathy. In addition, I am very grateful to Dr Fausto Andreola, Dr William Ashworth, Ms Abe Habtesion and the Liver Failure Group as well as the Department of Chemical Engineering for their friendly help and assist. I also would like to thank UCL and the China Scholarship Council for their financial support.

Last but not least, I would be remiss if I did not thank my parents and my family for all the faith and trust they placed in me. I am extremely grateful for their unconditional love, caring and understanding. I also must recognize Yue Wang, Dr Shengnan Li and other friends for their constant company and support during these years.

Abstract

Introduction: Non-alcoholic fatty liver disease (NAFLD) is the commonest chronic liver condition that is globally affecting 20-30 % of the general population. It covers a spectrum of conditions resulting from excess lipid accumulation in the liver without alcohol abuse. Among all the risk factors, fructose has been identified as a problematic component by recent clinical and experimental studies.

Methodology: A systems biology approach has been applied to explore the metabolic mechanisms whereby fructose consumption can induce dyslipidaemia associated with NAFLD and to explore whether the pathological conditions can be reversed during the early stages of disease. Both *ex vivo* experiments and computational modelling are employed in an iterative process.

Results: A computational model of the hepatic fructose metabolism has been established, containing approximately 120 parameters, 25 variables and 25 first order differential equations. Model predictions and experimental results presented a clear deposition of lipid profiles within the liver cells as a direct consequence of high-fructose feeding.

Furthermore, the model was also used to identify the potential regulatory targets for novel therapeutic interventions. Synergistic application of PK, KHK and PPARα *in silico* has been predicted as the most effective treatment to reduce the production of both fatty acids and triglycerides under both moderate and severe insulin resistance conditions.

Conclusion: Fructose over-consumption has a significant influence on the development of NAFLD. The results suggest that the constructed model is robust and it has sufficient detail to present the kinetic relationship between fructose and fatty liver under both

healthy and insulin-resistant conditions. Regulatory point identification provides a guidance for further experimental conduction.

Keywords: Fructose metabolism, Lipid, NAFLD, Computational modelling, Systems biology.

Impact Statement

Non-alcoholic fatty liver disease (NAFLD) is recognised as the commonest chronic liver condition that is not only associated with liver-oriented metabolic dysfunction like obesity and metabolic syndrome (Craig, 2014, Williams et al., 2014), but also contributing to other diseases such as chronic kidney disease (Byrne and Targher, 2020), cardiovascular disease (Anstee et al., 2013), hypertension (Ryoo et al., 2014), T2DM (Fracanzani et al., 2008) and so on.

Currently NAFLD and non-alcoholic steatohepatitis (NASH) are globally affecting 20-30 % and 3-5% of the general population, respectively (Byrne and Targher, 2020, Younossi et al., 2016, Nomura and Yamanouchi, 2012). In the last decade, the requirement of liver transplantation procedure resulted from NAFLD has increased ten times, and in the next decade, it is estimated that NAFLD will become the primary cause, even surpasses alcohol-related liver disease (British Liver Trust, 2019). This growing prevalence has greatly increased the clinical burden and costs.

Among all the risk factors of NAFLD, over-consumption of fructose has been repeatedly reported in both clinical and experimental studies to be highly associated with the development of NAFLD as well as other abnormal metabolic conditions. Therefore, in this thesis, a systems biology approach has been adopted to investigate the relationship between high-fructose intake and the progression of NAFLD by applying both *in vitro* experiments and computational modelling in an iterative progress.

A detailed kinetic model of fructose metabolism was constructed as a result and this computational model can directly serve as a tool to make predictions under both healthy

and pathological conditions, providing a better understanding within the liver system. Furthermore, it can be used to identify and test potential interventional targets for NAFLD and other related diseases. From a systematic perspective, this research can also be integrated into a more comprehensive and sophisticated biological network platform to explore the intrinsic complexity of human body.

In addition, this project can be beneficial to the subjects in a wider range of scope other than academia.

Firstly, this research enables to elevate the public awareness and facilitate public health policy developing. Since asymptomatic liver damage can last for as long as 20 years (British Liver Trust, 2019), the majority people tend to overlook this issue and often fail to realise the occurrence of liver diseases, especially NAFLD. Additionally, the outcomes provide the evidence to support and encourage the current public health campaigns like sugar reduction programme to lessen daily fructose intake.

Secondly, the use of the constructed model would be of interest to pharmaceutical industry, as to date, neither effective diagnostic approach nor pharmaceutical medicine is available for NALFD. Therefore, biomarker identification by modelling can be transferable into diagnostic testing kit intervention and drug production. As reported by the British Liver Trust (2019), around 25%-64% patients with non-alcoholic fatty liver would progress to non-alcoholic steatohepatitis, but only approximately 7% of which could be reversed. Therefore, if the combination therapy proposed by the current project was to be successful, this population would be the main beneficiaries.

Last but not least, the ultimate and ideal goal of this project is to improve personalised medicine. This would result in enhancing survival rates and improving life quality for patients. With the aid of systems biology approach, we can tailor each individual's therapeutic plans through adjust constant rate, making the medical treatment more accurate, accessible and affordable.

Table of Contents

List of Figures

List of Tables

List of Equations

List of Abbreviations and Symbols

β-NADH - β-Nicotinamide Adenine Dinucleotide
ACC - Acetyl-CoA Carboxylase
ACLF - Acute-on-Chronic Liver Failure
ADP - Adenosine Diphosphate
ALD - Alcohol-Related Liver Disease
AldB - Aldolase B
ALF - Acute Liver Failure
ALT - Alanine Aminotransferase
AMP - Adenosine Monophosphate
AMPK - Adenosine Monophosphate Kinase
apoB - Apolipoprotein B
apoE - Apolipoprotein E
AST - Aspartate Transaminase
ATP - Adenosine Triphosphate
BCA - Bicinchoninic Acid
BMI - Body Mass Index
boxi - Beta-Oxidation
BSA - Bovine Serum Albumin
CLD - Chronic Liver Disease
CoA - Coenzyme A
CPT-1 - Carnitine Palmitoyltransferase I
CT - Computed Tomography
DHAP - Dihydroxyacetone-Phosphate
DMEM - Dulbecco'S Modified Eagle Medium
DNL - De Novo Lipogenesis
DPBS - Dulbecco’s Phosphate Buffered Saline
DTT - Dl-Dithiothreitol
EDTA - Trypsin-Ethylenediaminetetraacetic Acid
EMEM - Eagle’s Minimum Essential Medium

F1P - Fructose-1-Phosphate

F6P - Fructose-6-Phosphate

FA - Fatty Acid

FAS - Fatty Acid Synthase

FBS - Foetal Bovine Serum

FFA - Free Fatty Acids

Fru - Fructose

G1P - Glucose-1-Phosphate

G6P - Glucose-6-Phosphate

GA - Glyceraldehyde

GA3P - Glyceraldehyde-3-Phosphate

GEMNs - Genome-Scale Metabolic Networks

Glu - Glucose

GLUT2 - Glucose Transporter 2

GLUT5 - Glucose Transporter 5

GLUT8 - Glucose Transporter 8

GTP - Guanosine Triphosphate

^{1}H-MRS - Proton Magnetic Resonance Spectroscopy

HBSS - Hanks' Balanced Salt Solution

HBV - Hepatitis B Virus

HCV - Hepatitis C Virus

HDL - High-Density Lipoprotein

HE - Hepatic Encephalopathy

HFCS - High Fructose Corn Syrup

HHL-5 - Human Hepatocyte Line 5

HHL-7 - Human Hepatocyte Line 7

HHLs - Human Hepatocyte Lines

IDL - Intermediate-Density Lipoprotein

IL-1 - Interleukin 1

IL-6 - Interleukin 6

IR - Insulin Resistance

IRS-1/2 - Insulin Receptor Substrate 1/2

JNK-1 - Jun Amino Terminal Kinase 1

KCl - Potassium Chloride

KHK - Fructokinase (also known as Ketohexokinase)

Km - Michaelis Constant

KOH - Potassium Hydroxide

LDL - Low-Density Lipoprotein

Lply - Lipolysis

LSECs - Liver Sinusoidal Endothelial Cells

LSM - Liver Stiffness Measurement

MEM - Minimum Essential Medium

MRI - Magnetic Resonance Imaging

MTP - Microsomal Triglyceride Transfer Protein

NADH - Nicotinamide Adenine Dinucleotide

NAFL - Non-Alcoholic Fatty Liver

NAFLD - Non-Alcoholic Fatty Liver Disease

NASH - Non-Alcoholic Steatohepatitis

NEAA - Non-Essential Amino Acids

NEFAs - Non-Esterified Fatty Acids

NF-kB - Nuclear Factor Kappa B

NKT - Natural Killer T

OAT - One at A Time

ORO - Oil Red O

P/S - Penicillin-Streptomycin

PDC - Pyruvate Dehydrogenase Complex

PEPCK - Phosphoenolpyruvate Carboxykinase

PI-3 kinase - Phosphatidylinositol-3 Kinase

PK - Pyruvate Kinase

PPARs - Peroxisome Proliferator-Activated Receptors

PPARα - Peroxisome Proliferator-Activated Receptor Alpha

PTP-1B - Protein-q Phosphatase-1B

SBC - Section Bloodstream Circulation

SD - Standard Deviations

SH - Section Hepatocytes

SHB - Section Hepatic Bloodstream

SREBPs - Sterol Regulatory Element-Binding Proteins

T2DM - Type 2 Diabetes Mellitus

TG - Triglycerides

TGS - Triglyceride Synthesis

Th-1 - T Helper 1

TNF- α - Tumour Necrosis Factor Alpha

TPI - Triose Phosphate Isomerase

Tri - Triokinase

UK - United Kingdom

US - Ultrasound

VLDL - Very-Low-Density Lipoprotein

1 Chapter 1: Framework and Context

1.1 Problem Statement and Hypothesis

Liver is the chemical reaction factory of the human body and it is responsible for a multitude of physiological regulations. A series of metabolic disturbances can induce lipid deposition and subsequently cause non-alcoholic fatty liver disease (NAFLD), potentially leading to hepatic cirrhosis and other advanced liver diseases.

In spite of tremendous strides in life science, the mortality rate of liver disease in UK is still increasing. Among which, NAFLD is affecting as high as 30% of the general population around the world and it is likely to become the biggest cause of liver disease in UK in the next decade.

NAFLD is a multifactorial and multisystem disease. Among all the risk factors, from genetic to environmental aspects, growing consumption of fructose has been repeatedly reported in both clinical and experimental studies to be highly associated with the development of NAFLD.

Therefore, the hypothesis of the current project is that fructose over-consumption has a significant influence on the development of NAFLD.

1.2 Objectives and Purposes

As the underlying mechanisms of how high-fructose consumption would lead to deranged liver (fatty liver in particular) remain partially understood, a systems biology approach that combined computational modelling with biomedical experiments is an attractive

option to acquire a more comprehensive insight into the relationship between high fructose intake and the development of NAFLD.

Therefore, the primary goal in the current project is to develop a kinetic and dynamic computational model of fructose metabolism to explore the potential pathophysiological mechanisms. Secondly, we aim to generate prediction of the regulatory and metabolic consequences to fructose under both healthy and disease status. Finally, the ultimate objective is to assess potential interventional targets for reversing and treating fatty liver caused by fructose during the early stages of disease progression.

1.3 Thesis Layout and Structure

As stated above, we applied both *in vitro* experiments and computational model to test the hypothesis. Therefore, the thesis layout would be presented in an "experiment-model-experiment" process, which reflects the iterative nature of systems biology approach.

The next chapter (Chapter 2: Literature Review) presents a literature review introducing the background research of this project. Chapter 3: Experimental Attempt and Exploration then briefly explores the impact of fructose on the hepatic lipid profiles by conducting two biomedical experiments on both cell culture model and animal model.

Chapter 4: Model Construction of Fructose Metabolism and Chapter 5: Model Validation and Enhancement describe the whole process of model construction, simulation and validation of fructose metabolism in details. Model simulation consisting of four stages, predicting model basic behaviours, dietary impacts on hepatic lipid accumulation,

fructose impacts under the insulin resistance conditions and testing potential therapeutic targets.

In Chapter 6: Experimental Assessment and Validation, *in vitro* experiments are introduced again specifically targeting at the potential regulatory points to evaluate and validate the model predictions.

Finally, the conclusions are drawn in the Chapter 7: Conclusions and Future work.

2 Chapter 2: Literature Review

A literature review is presented in this chapter. In Section 2.1, a brief review of normal liver structure and functions is provided. Section 2.2 demonstrates different catalogues of liver diseases. The alarming crisis, non-alcoholic fatty liver disease (NAFLD), is reviewed in Section 2.3. Then in Section 2.4, fructose metabolism as well as its interactions with other abnormal metabolic conditions are presented. Last but not least, systems biology approaches are introduced briefly in Section 2.5 focusing on the existing hepatic computational models.

Text descriptions in Section 2.3.1, 2.4.1 and 2.5.1were published in Liao et al. (2020).

2.1 Liver – the Chemical Reaction Factory

2.1.1 Anatomy and Structure

As the largest solid organ, a healthy human liver is brown and it accounts for approximately 2-3% of the total body weight in an adult. It normally locates in the right upper quadrant of the abdomen, below the diaphragm. As presented in Figure 2-1, the liver is divided into a large right lobe and a small left lobe from the perspective of anatomical structure. In regard of functional anatomy, the liver can be divided into eight functional segments in a clockwise order according to Couinaud classification. Individual segment comprises its own bile duct, portal branch and hepatic arterial branch, then drains the blood flow into different hepatic veins (Sibulesky, 2013).

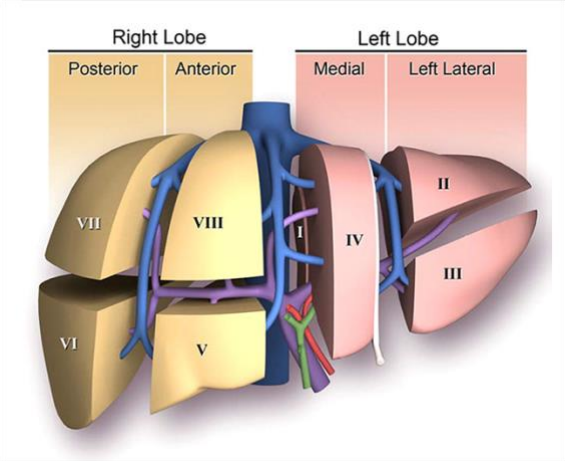

Figure 2-1. Anatomical structure and functional anatomy of the liver.

(adapted from Sibulesky (2013))

Around four fifths of blood flow in the liver come from the portal vein and the other one fifth is supplied by the hepatic artery (Sibulesky, 2013). The portal vein is considered to be the main blood supply to the liver as it gathers the most amount of absorbed nutrients. Also, it is the place where pancreatic hormone and gastrointestinal peptide are released. The blood flow then leaves the liver through hepatic veins (Bizeau and Pagliassotti, 2005).

As shown in Figure 2-2, portal vein, hepatic artery, hepatic vein and liver sinusoid are the four kinds of vasculatures in the liver (Enomoto et al., 2004). These hepatic vascular networks are responsible for exchanging a substantial amount of nutrients, hormones and oxygens within the liver as well as between the liver and the rest of the body (Hijmans et al., 2014).

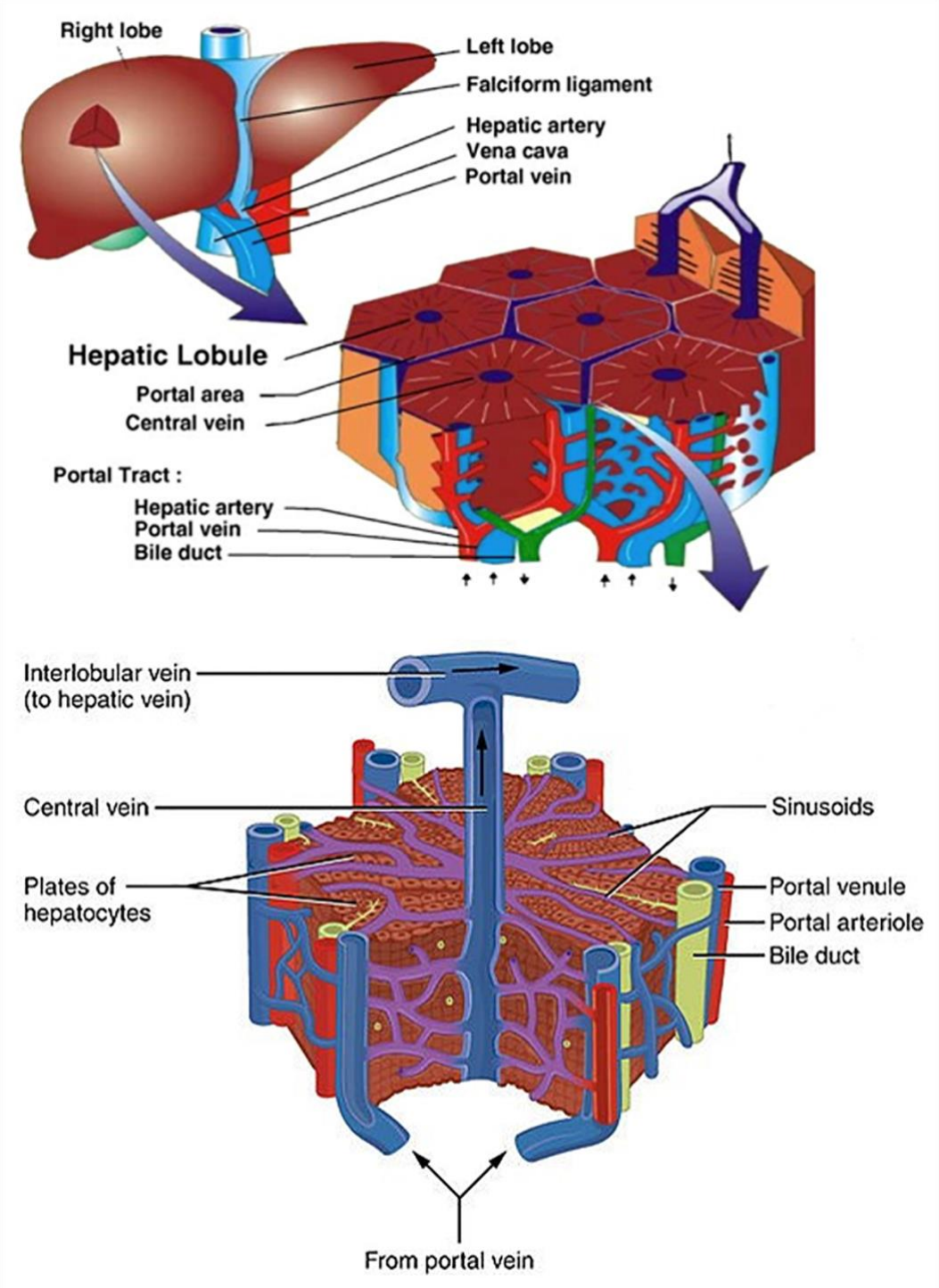

Figure 2-2. The structure of liver lobules.

(adapted from Rani et al. (2006) and Betts et al. (2013))

Regarding the histological structure, the liver is made by approximately one million hepatic lobules (also seen in Figure 2-2). Each lobule is a multilateral structure (diamond-shape) of parenchyma around the central vein, which contains about one thousand paths through the sinusoids (Chalhoub et al., 2007, Jungermann and Katz, 1989).

Table 2-1. Cell types and essential functions in the liver.

(simplified from (Damania et al., 2014))

Cell type	% of the hepatic volume	Essential function
Parenchymal cell		
Hepatocytes	80	Metabolism of protein, carbohydrate, lipid, micronutrients and xenobiotics, also bile secretion
Non-parenchymal cells		
Liver sinusoidal endothelial cells (LSECs)	2.8	Filtration and transport of nutrients from the blood; blood clearance and endocytosis; secretion of inflammasome molecules
Kupffer cells	2.1	Phagocytosis, cytokines responsible for inflammatory response and liver regeneration; iron metabolism
Stellate cells	1.2	Fat-storing cells; vitamin A storage; secretion of growth factors
Pit cells	Minor	Liver-specific natural killer cells; antitumor function
Biliary epithelial cells	3.5% of cell mass	Cytokine secretion, regulation role in inflammation, regulation of hepatic glutathione

There are two typical types of cells can be found in the liver: one is parenchymal cell (i.e., hepatocyte), contributing to about 80% to 90% of the hepatic volume and around 60% of hepatic cell numbers; the other cell type is non-parenchymal cells, including liver sinusoidal endothelial cells (LSECs), Kupffer cells, stellate cells, pit cells and biliary epithelial cells, which can be commonly found in the hepatic sinusoid *in vivo* (Enomoto et al., 2004). Hepatic cell types and their functions are summarised in Table 2-1.

Hepatocyte is the main focus of this project as it plays the major role in accomplishing the liver functions, especially the metabolic-related ones.

2.1.2 The Concept of Liver Sinusoid and Hepatic Zonation

The structure of the liver is complex and the hepatic lobule is regarded as the fundamental unit in the liver. Individual lobule receives a mixed blood supply from liver bile ducts, portal veins and hepatic arteries, then drains it into central veins, and eventually, to hepatic veins (Hijmans et al., 2014).

The blood flow across the liver sinusoid is displayed in Figure 2-3. Along this direction of hepatic bloodstream, hepatocytes are exposed to different concentrations of nutrients, hormones and oxygens according to their position. In other words, liver cell behaviours reacted to changes in the constituents and rates of substrate deliveries can be determined depending on their anatomic positions (Bizeau and Pagliassotti, 2005).

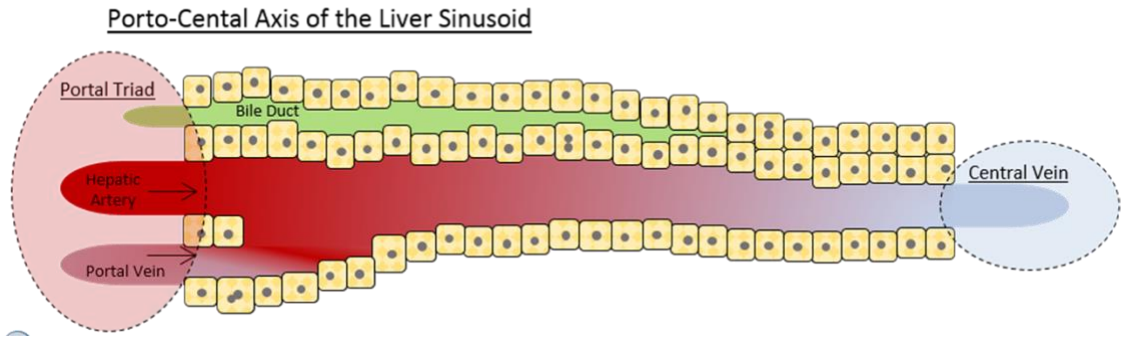

Figure 2-3. The structure of the liver sinusoid.

(adopted from Ashworth (2017))

As for hepatic zonation, the “acinus” model has been broadly accepted, in which three zones are divided across the liver sinusoid, namely periportal zone, intermediate zone and perivenous zone (Hijmans et al., 2014, Jungermann and Keitzmann, 1996, Jungermann and Katz, 1989). Hepatocytes in these three zones of the liver perform different metabolic capacities (Katz, 1992).

2.1.3 Normal Functions and Regulations

The liver is the chemical reaction factory of the body. It performs a broad range of biochemical functions for the maintenance of metabolic and energetic homeostasis, including the synthesis and catabolism of protein, the regulation of carbohydrate, the moderation of lipid, the storage of micronutrients and the secretion of toxic xenobiotics (Baynes and Dominiczak, 2005). Among all these complicated metabolic processes, the focus of the present project is fructose metabolism, which will be discussed extensively in Section 2.4.2 and 2.4.3.

Abnormal metabolic changes would lead to hepatic lipid deposition, which can subsequently result in NAFLD and potentially lead to hepatic cirrhosis as well as other advanced liver diseases. However, the liver can maintain all its normal functions with as little as one fifth of the original mass. In fact, the liver is the only internal organ that has the ability to regenerate back to a full size in about three months even when 80% of the liver tissues have been removed (Fausto et al., 2006). As a result, there are only a few warning signals and symptoms prior to severe hepatic impairment. Asymptomatic liver damage can last for as long as 20 years (British Liver Trust, 2019).

2.2 Liver Disease – the Leading Cause of Death in UK

According to British Liver Trust (2019), liver disease has become the third leading cause of mortality in those aged under 75 years old in United Kingdom (UK), only after cardiovascular disease and cancer. Surprisingly, liver disease is now the most common cause of death in the 35-49 age group, accounting for approximately 10% of the deaths.

As displayed in Figure 2-4, with huge endeavour made in health during the last five decades, mortality rates have declined for almost all diseases in UK, except for liver disease, which has increased four times as it was in 1970. In 2016/2017, it is estimated that over 14,600 people in UK died from liver diseases. Furthermore, it is predicted that numbers of premature deaths caused by liver diseases will overtake those result from cardiovascular diseases in the next few years (Williams et al., 2018).

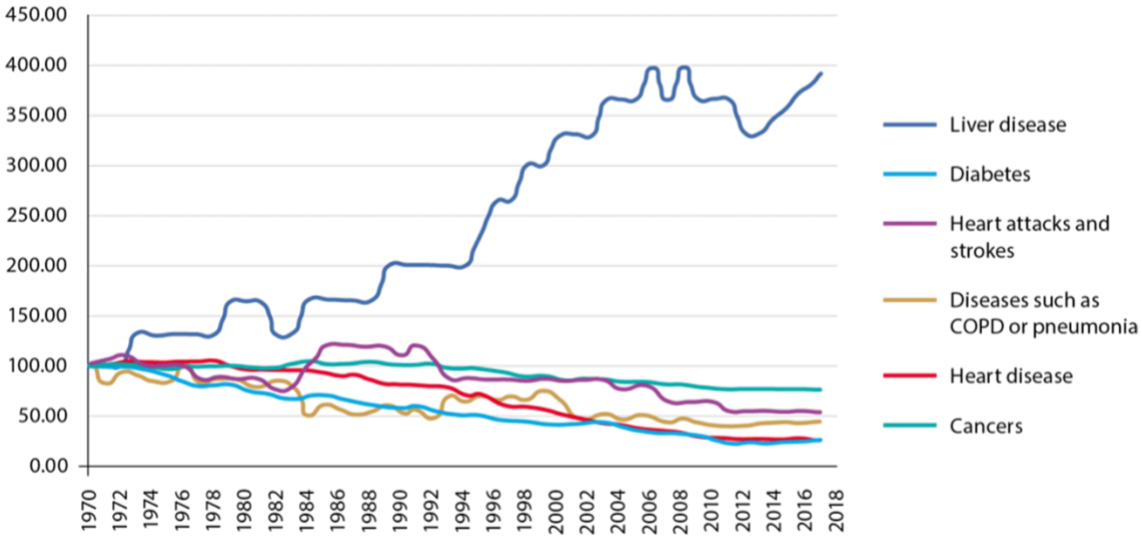

Figure 2-4. Standardised UK mortality rate data.

(adopted from Williams et al. (2018))

Liver disease can be roughly divided into two classifications, those which lasts over six months, known as chronic liver disease, and those which lasts less than three month after the first sign of liver injury, known as acute liver failure (Pratt and Kaplan, 2000, O'Grady et al., 1993).

Before getting into those two liver disease categorisations, a dynamic process called liver cirrhosis should also be noted. Caused by various mechanisms of liver damage, cirrhosis is often regarded as the end-stage liver disease, which can result in necroinflammation and fibrogenesis, leading to hepatic functional abnormalities. Histologically, cirrhosis is characterised by scar tissues and collapse of liver structures, resulting in alteration of hepatic vascular architecture (Tsochatzis et al., 2014).

2.2.1 Acute Liver Failure

Acute liver failure (ALF) refers to a rapid and sudden severe hepatic dysfunction condition that can progress within an acute period, normally hours or weeks without any previous liver damage (Amin et al., 2019). This rare clinical manifestation can often result rapidly in jaundice, coagulopathy, hepatic encephalopathy (HE) and multisystem failure (Dong et al., 2020).

Recognising the prognostic importance of HE, ALF has been redefined by O'Grady et al. (1993) in 1993. The classifications of hyperacute, acute and subacute have been proposed, which are corresponding to 0-1 week, 1-4 weeks and 4-12 weeks, respectively, of the time interval between the onset of jaundice and the appearance of HE. These criteria have become the most commonly used clinical tool as the ALF aetiology, the possible complications and the medical prognosis can be identified by it.

Viral infection (hepatitis A, B, and E viruses) and drug poisoning are identified as the predominant triggers of ALF in the developing and developed countries, respectively (Bernal et al., 2010). Apart from spontaneous recovery and cause-oriented intervention, emergency liver transplant is considered as the most effective treatment for ALF (Dong et al., 2020, Bernal et al., 2010).

It is worth mentioning that chronic liver disease, such as non-alcoholic fatty liver disease (NAFLD), is unable to cause ALF. However, NAFLD can be an aetiology underlying cirrhosis in acute-on-chronic liver failure (ACLF), which refers to the condition that ALF occurs in an individual with pre-exist chronic liver disease (Bernal et al., 2015).

2.2.2 Chronic Liver Disease

On the contrary to ALF, chronic liver disease (CLD) is the term defining hepatic impairment with progressive changes over a time period of six months. While the incidence of ALF is around one to six individuals per million population around the world per year (Amin et al., 2019), the incidence of CLD is approximately 20 per million population (Moon et al., 2019).

In 2017, a total of 1,500,000,000 people globally is estimated to be suffering from CLD and about 2,000,000 are died annually caused by CLD. The aetiology and pathogenesis of CLD includes but not limit to hepatitis B virus (HBV), hepatitis C virus (HCV), alcohol-related liver disease (ALD) and NAFLD (Moon et al., 2019). As high as 90% of CLD in the UK is believed to be preventable (British Liver Trust, 2019).

Even though over 86% of mortality from liver diseases result from alcohol over-consumption, a fact should not be neglected that other lifestyle-induced liver-related

deaths are also rising rapidly (British Liver Trust, 2019). Among which, NAFLD is considered to be the most common chronic liver condition with around 30% of global population affected and is usually linked with obesity, type 2 diabetes mellitus (T2DM) and metabolic syndrome (Craig, 2014, Williams et al., 2014, Cohen et al., 2011, Lim et al., 2010).

Furthermore, it has been predicted that it is highly possible for NAFLD to surpass ALD becoming the biggest cause of liver disease in the near future (British Liver Trust, 2019). Therefore, a concern has been raised and NAFLD is the main focus of the current study, which will be discussed in the next section (2.3).

2.2.3 Liver Failure and Transplantation

Liver transplant procedure has been performed since 1963 by Starzl et al. (Meirelles Júnior et al., 2015, Starzl et al., 1982). It is a surgical operation that replaces a diseased or damaged liver with part or all of a healthy one. The criteria of liver transplantation are: liver fails to perform its normal functions and lose its regeneration capability, especially when it meeting one of the following conditions: ALF, a life-threatening systemic complication of liver disease, or a liver-based metabolic defect or, more frequently, cirrhosis with complications such as hepatic encephalopathy, ascites, hepatocellular carcinoma, hepatorenal syndrome, or bleeding caused by portal hypertension. In short, irreversible hepatic failure and/or liver cancer are the primary indications for liver transplantation (O'Leary et al., 2008).

The necessity of liver transplantation can be divided into two catalogues, elective and emergency, depending on the how fast liver failure would progress. Among elective liver

transplant waiting-list, ALD is the main reason to apply for the procedure. Second to it is NAFLD.

2.3 NAFLD – the Alarming Crisis

Non-alcoholic fatty liver disease (NAFLD) is the commonest chronic liver dysfunction globally (Younossi et al., 2016, Miele et al., 2009). It covers a spectrum of conditions resulting from excess lipid accumulation in the liver without excessive alcohol consumption. The pathologic manifestations of NAFLD are shown in Figure 2-5. Data was taken from British Liver Trust (2019) and Perumpail et al. (2017). The histological section figures were taken from Cohen et al. (2011).

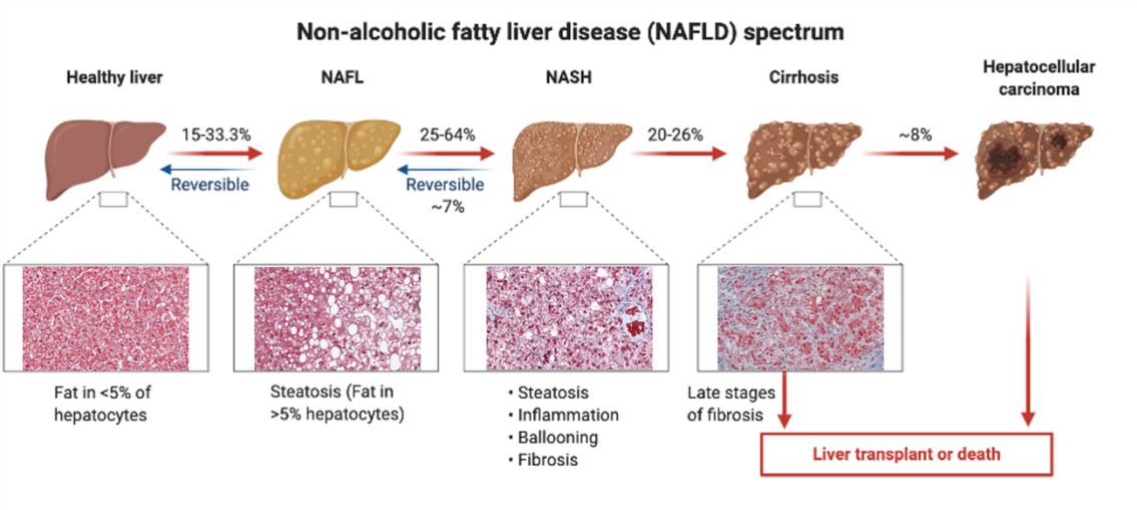

Figure 2-5. The spectrum of NAFLD progress.

NAFLD can develop from simple steatosis (intrahepatic lipid deposition, also known as non-alcoholic fatty liver, NAFL) to non-alcoholic steatohepatitis (NASH), an advanced stage that combines steatosis with inflammation. NASH can then further progress to

fibrosis (excess fibrous connective tissues) and cirrhosis (a late stage of scarring), and potentially to hepatocellular carcinoma (Cohen et al., 2011, Ouyang et al., 2008). Among these conditions, steatosis and NASH are reversible, while fibrosis and cirrhosis are often considered irreversible (Maldonado et al., 2018).

Increasing evidence have suggested that NAFLD is a multisystem condition (Byrne and Targher, 2015), which is not only associated with liver-oriented diseases, but also contributing to chronic kidney disease (Byrne and Targher, 2020), cardiovascular disease (Anstee et al., 2013), hypertension (Ryoo et al., 2014), T2DM (Fracanzani et al., 2008) and so on.

In 2020, it has been proposed that NAFLD should change its name to Metabolic Associated Fatty Liver Disease (MAFLD) due to its metabolic risk factors (Younossi et al., 2020). However, we remain using the term "NAFLD" in this thesis.

2.3.1 Prevalence

In the recent three decades, the prevalence of NAFLD has risen by 20-fold, mainly linked with obesity, T2DM, insulin resistance (IR) and many other metabolic disorders. Currently NAFLD and NASH are globally affecting 20-30 % and 3-5% of the general population, respectively (Byrne and Targher, 2020, Younossi et al., 2016, Nomura and Yamanouchi, 2012). It has been estimated that, between 2016 and 2030, NAFLD prevalence would continue to grow at a steady rate of up to approximately 30% (Estes et al., 2018).

In UK, one in three people is speculated to be having pro-steatosis conditions (the early phrase in NAFLD development) and around 3,300,000 individuals are having NASH. In

the last decade, the requirement of liver transplantation procedure resulted from NAFLD has increased in ten times (British Liver Trust, 2019).

Among obese subjects, an estimation of 30-37% are having NAFLD (Perumpail et al., 2017), while among non-obese population (including normal weight and overweight), the prevalence of NAFLD is still as high as 12% (Ye et al., 2020). The classification of obese and non-obese can be found in Table 2-2. In addition, NAFLD has been reported to be highly associated with T2DM. Among T2DM patients, there is around 56% and 37% individuals that are also suffering from NAFLD and NASH, respectively (Younossi et al., 2016).

Table 2-2. Calculation and classification of BMI.

$\boldsymbol{Body\ Mass\ Index\ (BMI) = \frac{Weight(kg)}{Height^2(m)}}$	**Classification**
$\boldsymbol{BMI < 18.5}$	Underweight
$\boldsymbol{18.5 \leq BMI \leq 24.9}$	Normal weight
$\boldsymbol{25 \leq BMI \leq 29.9}$	Overweight
$\boldsymbol{30 \leq BMI \leq 39.9}$	Obese

2.3.2 Diagnosis

From histological perspective, NAFLD can be diagnosed when there is more than 5% fat are observed in the hepatocytes (Petäjä and Yki-Järvinen, 2016). When it comes to diagnostic methodology of NAFLD, liver biopsy is widely accepted as the gold standard (Petta et al., 2016). However, since the biopsy procedure is expensive and invasive, it is impractical and unrealistic to be performed to monitor population.

In terms of non-invasive detection, there are proton magnetic resonance spectroscopy (^{1}H-MRS), magnetic resonance imaging (MRI), ultrasound (US) and computed tomography (CT). Among them, the ^{1}H-MRS technique has been regarded as the most accurate non-invasive method and US is the most widely used measurement for NAFLD diagnosis. However, the limitations of these two diagnostic methodologies are high-cost and low sensitivity, respectively (Piazzolla and Mangia, 2020, Petäjä and Yki-Järvinen, 2016, Petta et al., 2016).

Another widely used non-invasive measure technique for NAFLD in the recent years is transient elastography (FibroScan). This tool is to assess the severity degree of fibrosis in individuals with chronic liver disease by measuring liver stiffness (Nguyen et al., 2020). Even though the diagnostic efficiency of liver stiffness measurement (LSM) by FibroScan is satisfied for hepatitis B and C, advanced liver fibrosis and cirrhosis, the accuracy of diagnosing NAFLD still remains unclear as LSM tends to lack of stability in NAFLD. Taking these into consideration, routine measurement by FibroScan in every 6 months is recommended to monitor the progress of NAFLD (Nguyen et al., 2020).

Additionally, even though liver enzymes such as alanine aminotransferase (ALT) and aspartate transaminase (AST) serve as hepatic biomarkers in regular liver function tests, they cannot be used as the indicators for NAFLD diagnosis. Approximately up to 80% NAFLD patients are tested having normal level of ALT. Also, there is no difference in histological observation between normal and abnormal liver enzyme level within NAFLD population (Petäjä and Yki-Järvinen, 2016, Fracanzani et al., 2008).

Therefore, the actual number of people with NAFLD might be highly underestimated and a novel, accurate, non-invasive diagnostic methodology is urgently needed.

2.3.3 Potential Pathophysiological Mechanisms

Despite the fact that the prevalence of NAFLD is increasing globally, the underlying pathophysiological mechanisms of it still remain poorly understood. Over the last decade, the proposed pathogenesis of NAFLD has evolved from the "two-hit" theory to the "multiple-hit" hypothesis (Buzzetti et al., 2016, Petta et al., 2016).

The "first hit" is simply intracellular lipid accumulation in the liver, often induced by sedentary lifestyle, obesity and insulin resistance. Then with inflammatory factors activation, the "second hit" occurs, leading to chronic hepatic inflammation. However, apart from lipid deposition and inflammation, the "multiple-hit" theory proposes that gastrointestinal microbiome balance, hormonal regulation as well as other risk factors are also "hitting" the development of NAFLD in parallel and the first two hits do not necessarily appear in sequence (Buzzetti et al., 2016, Benedict and Zhang, 2017).

Therefore, it has been widely accepted that the pathogenesis of NAFLD is multifactorial, including genetic factors, environmental factors, dietary factors and other metabolic factors.

In terms of the "first hit" simple lipid deposition, a brief of lipid definition and classification is presented as follow. Although no agreement has been reached in the definition of lipid, it can be considered as a catalogue of macro biomolecules that are hydrophobic and soluble in nonpolar solvents (Baynes and Dominiczak, 2005).

Together with proteins and carbohydrates, lipids are the primary sources of energy in the body and they are mainly distributed in plasma, adipose tissue and biological membranes. As listed in Table 2-3, four forms of lipids are commonly known as they play significant roles in regulatory functions, which are fatty acids, triglycerides, phospholipids and cholesterol (Baynes and Dominiczak, 2005).

Furthermore, lipoproteins, including chylomicrons, very low-density lipoprotein (VLDL), low-density lipoprotein (LDL), intermediate-density lipoprotein (IDL) and high-density lipoprotein (HDL), are essential components in lipid transportation (Baynes and Dominiczak, 2005).

Table 2-3. The catalogue of common lipids.

Category	Subtype/Example	Main function	Relevant lipids *
Fatty acids	Short-chain/medium-chain/long-chain Saturated/monounsaturated/polyunsaturated	Fundamental biological lipids	√
Glycerolipids	Monoglyceride Diglyceride Triglyceride	Energy storage	√
Glycerophospholipids	Phospholipid	Biological membranes	
Sterols	Cholesterol Bile acids	Component of membrane lipids	

* Relevant to hepatic lipid metabolism and NAFLD in this thesis

More details regarding lipid classification can be found in Liebisch et al. (2020).

2.3.4 Therapeutic Treatment

Unsurprisingly, the ambiguity in the underlying mechanism of NAFLD directly results in the absence of effective therapeutic interventions. So far, lifestyle intervention is

commonly recommended for NAFLD and NASH patients. Weight losing through improving dietary choices and increasing physical activity is considered as an effective method for the reversal of NAFLD and NASH conditions (Younossi et al., 2018).

In addition, a few other medical treatments can be introduced to alleviate NAFLD-associated symptoms and dysfunctions, such as Orlistat for obesity (Zelber–Sagi et al., 2006), angiotensin-converting enzyme inhibitors for hypertension (Stokkeland et al., 2018), metformin for T2DM (Mazza et al., 2011). Despite the fact that there are almost 30 potential medicines that have been experimentally exploring and testing (Dibba et al., 2018). To date, no pharmaceutical drug has been approved specifically targeting at NALFD.

2.4 Fructose – a "Sweet" Burden

As mentioned above, NAFLD is a multifactorial and multisystem disease. Apart from genetic factors, overnutrition and a sedentary lifestyle have often been blamed as the cause of NAFLD. However, recent clinical and experimental studies repeatedly suggest that the climbing consumption of fructose may also be a crucial risk component (Jensen et al., 2018, Sellmann et al., 2015, Schultz et al., 2015, Nomura and Yamanouchi, 2012, Ouyang et al., 2008). Therefore, research topic around fructose and NAFLD is put under the spotlight.

Paralleling the increasing concern about the impact of fructose on NAFLD, the number of researches has mounted remarkably in the past two decades. Figure 2-6 presented the searching results from 2005 to 2020 by applying the keywords "Fructose and NAFLD" in

PubMed (Accessed in January 2021). There were only 2 publications studying the relationship between fructose and NAFLD in 2005 but 131 papers in 2020.

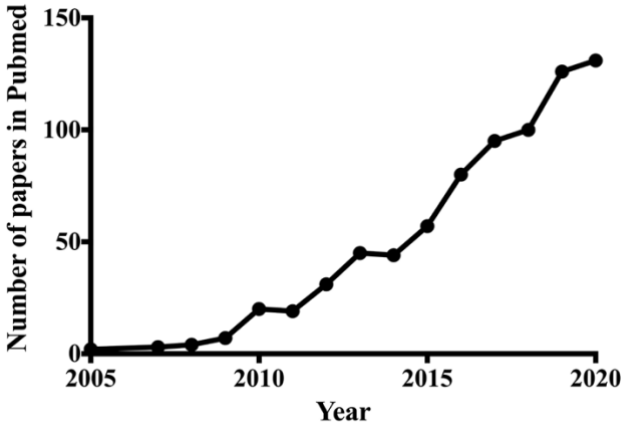

Figure 2-6. Searching results by year (2005-2020) in PubMed.

(Keywords: Fructose & NAFLD)

Fructose, along with glucose and galactose, is one of three primary dietary monosaccharides. Unlike glucose and galactose, which are aldohexose, fructose is the only ketohexose that exists in the body with a notable quantity (Baynes and Dominiczak, 2005). Historically, fructose was proposed as a beneficial sweetener and recommended for the obese and for patients with diabetes, because of its inability of inducing insulin secretion and its capability of decreasing postprandial hyperglycaemia. However, a new accusation has been made in the recent two decades that high-fructose intake is prevalent in parallel with a series of health issues such as metabolic syndrome, obesity, T2DM and NAFLD (Basaranoglu et al., 2013). Therefore, this section is to review the current knowledge regarding the relationship between dietary fructose and those metabolic abnormal conditions.

2.4.1 Changes in Dietary Fructose Consumption

Between 1900 and 1950, approximately 20g fructose (5% of total energy) was consumed in the daily meals, mainly from fruits and honey (Douard and Ferraris, 2008). Nowadays, fructose has become a ubiquitous ingredient that accounts for a large proportion of energy intake (approaching 15%-25% of total energy) (Softic et al., 2016, Jensen et al., 2018). A 30% increase in total fructose consumption has been observed in recent decades (Ventura et al., 2011).

Refined and processed fructose is responsible for this dramatic rise. Since fructose is considered to be sweeter than glucose, it is relatively low-cost for manufacture to produce sweetener that contains it (Silliman and Coulston, 1991). Therefore, sucrose and high fructose corn syrup (HFCS) have become the main sources of fructose consumption, with a fructose/glucose ratio of 50/50 and 55/45, respectively (Jensen et al., 2018, Ventura et al., 2011). HFCS, a key component of sugar sweetened beverages, has been considered as an inexpensive substitute for other simple sugars in the food industry, accounting for 40% of all added sugars (Bray et al., 2004).

The average fructose intake for the whole population in America has been reported as 49g/day in 2004. For the age groups 15-18 and 19-22, a total of 75g fructose is consumed per day (Douard and Ferraris, 2013). In 2008, the consumption amount of fructose then raised to 54.7g/day (Vos and Lavine, 2013).

In UK, it has been reported that the average intake of sugar sweetened beverages is 106g per day for adults during the period of 2016-2019 (Public Health England and the Food Standards Agency, 2019). Recently, this sugar has been targeted by public health

campaigns (e.g. sugar reduction programme in UK) and with a sugar tax levy in several countries (Jones, 2016, Briggs et al., 2017, Hashem et al., 2019).

2.4.2 Hepatic Fructose Metabolism

Even though fructose and glucose share the same chemical formula $C_6H_{12}O_6$, their structures are different (Silliman and Coulston, 1991). It is proposed that fructose is strongly associated with those chronic health issues due to its unique and distinct metabolic pathways which exclusively take place within the liver. Therefore, in the current section, hepatic fructose metabolism would be reviewed.

2.4.2.1 Dietary absorption

Fructose is essentially absorbed and transported across the brush border membrane into the hepatic portal vein via an energy-dependent process involving glucose transporter 5 (GLUT5) and glucose transporter 2 (GLUT2). In the liver, it has been reported that dietary fructose is mainly consumed by periportal hepatocytes (Tappy and Lê, 2010).

It should be noted that massive pure fructose intake would lead to stomach ache, often along with diarrhoea, because of the hyperosmolar environment caused by inefficient intestinal absorption. However, it has been suggested that co-intake of glucose with fructose or consuming sucrose directly are able to improve dietary fructose ingestion and attenuate the malabsorption. A possible reason for this phenomenon is that glucose stimulates transporter to co-transport fructose, enhancing fructose absorption (Laughlin, 2014, Sun and Empie, 2012, Havel, 2005, Mayes, 1993). Therefore, the liver is rarely exposed to fructose alone in human.

As mentioned in the last section (2.4.1), sucrose is a disaccharide consisting of two monosaccharides (glucose and fructose) at 1:1 ratio. However, whether the absorption rate of equal amount of free glucose and fructose combination is different from that of sucrose still remains unknown (Sanchez-Lozada et al., 2010).

2.4.2.2 Fructose metabolic pathways

The metabolic activities of fructose primarily take place in the liver. Fructokinase (also known as ketohexokinase, KHK), aldolase B and triokinase are three specialized enzymes for fructose metabolism. The most significant distinction between fructose metabolism and glucose metabolism is their phosphorylation process.

As presented in Figure 2-7, after entering the liver, dietary fructose is swiftly phosphorylated by KHK to produce fructose-1-phosphate, which bypasses the key rate-controlling regulatory enzyme (phosphofructokinase) of glycolysis in glucose metabolism. Two isoforms of KHK have been reported, which are KHK-C, mainly existing in hepatocytes, and KHK-A, distributed broadly in numerous organs.

Fructose-1-phosphate is then converted to dihydroxyacetone phosphate (DHAP) and glyceraldehyde (GA) by enzyme aldolase B, providing intermediates for further glycolysis process. Triokinase, as the third essential enzyme, functions by phosphorylating glyceraldehyde to form glyceraldehyde-3-phosphate (GA3P), which also produces intermediates for later reactions.

Then the pathways of glucose and fructose metabolism gather at the triose phosphate stage (as GA3P) and become the same from this point on (Laughlin, 2014, Ouyang et al., 2008, Rutledge and Adeli, 2007, Havel, 2005).

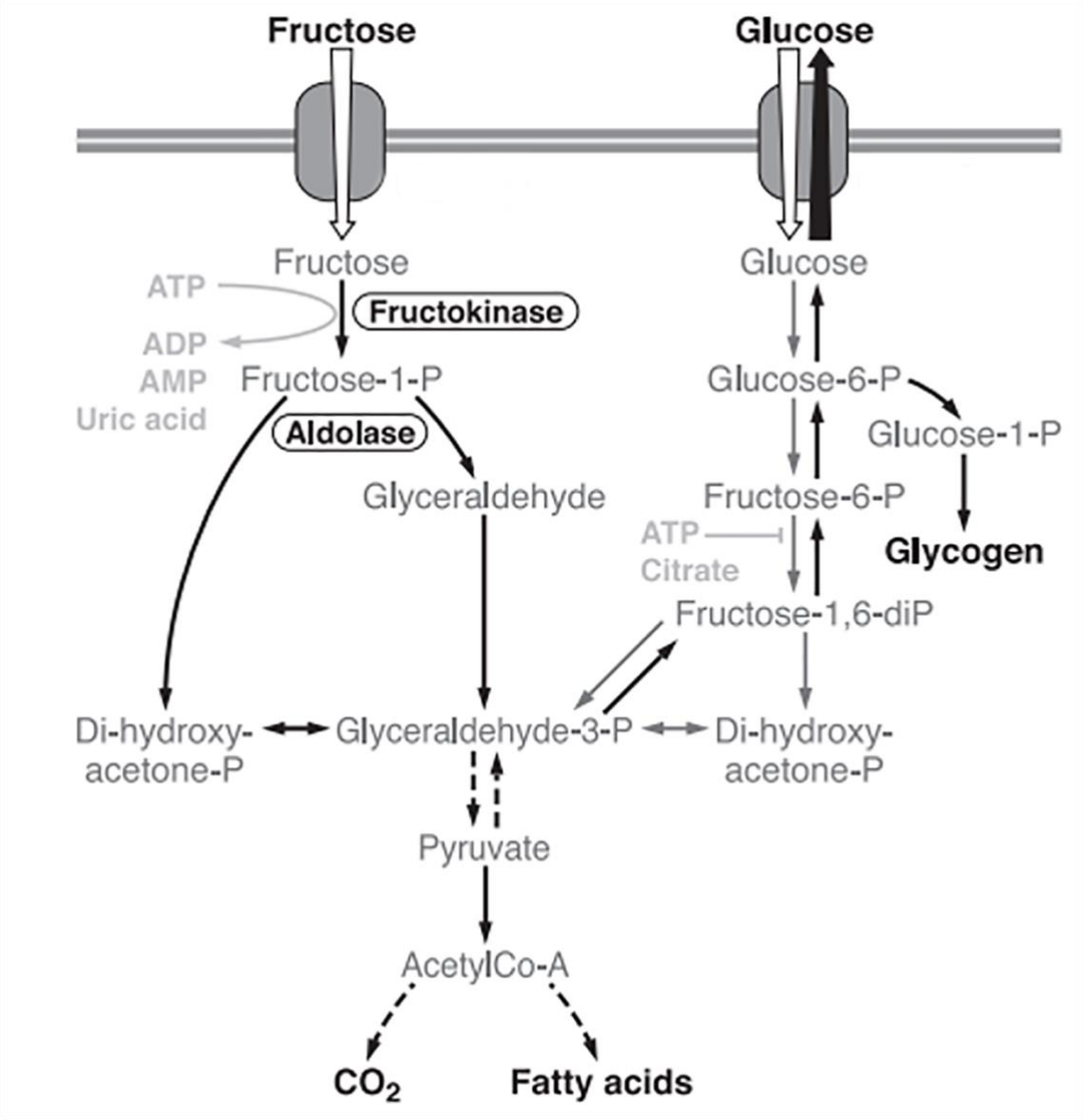

Figure 2-7. Hepatic Fructose VS Glucose metabolism.

(adopted from (Tappy and Lê, 2010))

From triose phosphate level, there are four possible pathways in hepatic fructose metabolism, which are glucose conversion, glycogen conversion, fructose oxidation and lactate conversion. To be specific, approximately two thirds of fructose carbon originated

from triose phosphates flows into gluconeogenesis and then be secreted as glucose in fasted condition. Thus, there is an increasing amount of glucose flux that can be measured after fructose intake. In fed condition, fructose tends to be converted to lactate than glucose or glycogen.

Apart from these, other carbons from dietary fructose can be found in all the further metabolic pathways including glycolysis, glycogenesis, *de novo* lipogenesis (DNL) as well as fatty acid esterification. The common intermediates and ultimate metabolites include pyruvate, acetyl-CoA, citrate, alpha-ketoglutarate, fatty acids, triglyceride and so on (Laughlin, 2014, Sun and Empie, 2012, Mayes, 1993).

In terms of energy utilisation, ATP is catalysed to produce adenosine monophosphate (AMP) and adenosine diphosphate (ADP) through hydrolysis during fructose metabolism. AMP then either regenerate ATP by AMP kinase (AMPK) or break down to adenosine and eventually produce uric acid. When fructose is quickly processing phosphorylation, the concentration of intracellular phosphate decrease, driving AMP to generate uric acid instead of regeneration of ATP. Consequently, fructose would stress the liver by depleting hepatic energy streams (Basaranoglu et al., 2013, Abdelmalek et al., 2012, Abdelmalek et al., 2010, Ouyang et al., 2008).

2.4.3 Interactions between Fructose Metabolism and other Metabolic Conditions

After reviewing the normal metabolism of dietary fructose, the following section (2.4.3) would discuss the putative mechanisms connecting fructose over-consumption and certain metabolic conditions, including interaction between fructose metabolism and lipid

metabolism, interaction between fructose metabolism and insulin resistance, as well as interaction between fructose metabolism and inflammation.

2.4.3.1 Interaction between fructose metabolism and lipid metabolism

Since fructose is unlikely to be limited through the inhibition of phosphofructokinase, which often induced by citrate and ATP, a large amount of fructose carbon will enter into the glycolytic pathway after a great portion of fructose consumption, further enhancing the process of triglyceride and very-low-density lipoprotein (VLDL) production in the liver. Once the intermediates of the glycolytic pathway excess their capacity, they would be converted into glycerol-3-phophate, which supplies the glycerol for triglyceride synthesis. This triglyceride would further be packed into VLDL and then released into the bloodstream.

A growing amount of studies demonstrate that, along with the increasing triglyceride synthesis, fructose consumption also reduces triglyceride clearance at the same time, thus the balance of triglyceride homoeostasis would be disturbed after consuming high-fructose diet (Song et al., 2013, Le et al., 2009, Basciano et al., 2005). Several feeding studies in adults (Vos and Lavine, 2013) display consistent results that high doses of fructose and fructose-containing sugars increase plasma triglyceride concentration in comparison with glucose feeding for 1 day, 6 days, 2 weeks, 4 weeks and 12 weeks.

Another significant lipid-related metabolic pathway affected by fructose-rich consumption is pyruvate dehydrogenation. Through this process, fructose is considered as an uncontrolled energy resource of acetyl-CoA, providing abundant essential components for subsequent DNL and long chain fatty acid synthesis (Havel, 2005).

Combined with ATP depletion caused by rapid fructose phosphorylation, a large quantity of fatty acids fails to be converted into other forms of lipid. Those fatty acids, therefore, accumulate in the liver, leading to lipotoxicity, insulin resistant, inflammatory and other undesired consequences (Abdelmalek et al., 2010, Basciano et al., 2005).

In addition, as the members of the ligand-activated nuclear receptor superfamily, peroxisome proliferator-activated receptors (PPARs) transcriptionally regulate a range of protein expressions that are related to lipid catabolism. In mammals, there are three isotypes, PPARα, PPARβ/δ and PPARγ, but only PPARα is highly expressed in hepatocytes (Hashimoto et al., 2000).

PPARα mainly exerts impacts on fatty acid transportation and β-oxidation in order to increase lipid removal from the liver (Staels et al., 2013). Also, it plays an essential role in inflammatory response modulation by inhibiting a certain kind of the inflammatory genes. To activate PPARα, it is known that fatty acid and prostaglandins are two natural ligands and the fibrates are the common synthetic ligands (Tailleux et al., 2012).

Recent evidence reports that PPARα has lower expression in both mRNA level and protein level after high fructose feeding compared to the control group in both rodent (Ohashi et al., 2015, Nagai et al., 2002, Roglans et al., 2002) and hamster model (Basciano et al., 2005), which suggests that fructose or/and its metabolic products (e.g. fructose-1-phosphate) have negative influences on lipid β-oxidation; thus lead to hepatic lipid accumulations (in the forms of both free fatty acid and triglyceride).

2.4.3.2 Interaction between fructose metabolism and insulin resistance

Hepatic insulin resistance can be defined as that cells like hepatocytes lose their sensitivity to insulin and then glucose level keeps rising (Santoleri and Titchenell, 2019). It is recognized as a remarkable pathophysiological manifestation of type 2 diabetes, metabolic syndrome and NAFLD. However, the causal relationship between hepatic insulin resistance and liver fat cannot be concluded.

It is interesting that even though fructose is considered to be unable to induce insulin secretion, the researchers often use fructose diet to construct animal insulin resistance models for other studies. There is always a debate about whether insulin level can still increase stimulated by fructose consumption and whether high-fructose diet will lead to compensatory hyperinsulinemia. However, the answer is still unclear.

A potential molecular mechanism of these insulin resistance models is displayed in Figure 2-8. It is speculated that high fructose intake would decrease tyrosine phosphorylation of the insulin receptor and damage insulin receptor substrate 1/2 (IRS-1/2) phosphorylation (Havel, 2005, Nomura and Yamanouchi, 2012). Also, the activity of phosphatidylinositol-3 kinase (PI-3 kinase), insulin-induced Akt-Ser473 and Akt-Thr308 phosphorylation have been reported that have a significant decrease in the liver after high-fructose infusion. These suggest that fructose is able to cause insulin resistance by impairing the insulin signalling pathway.

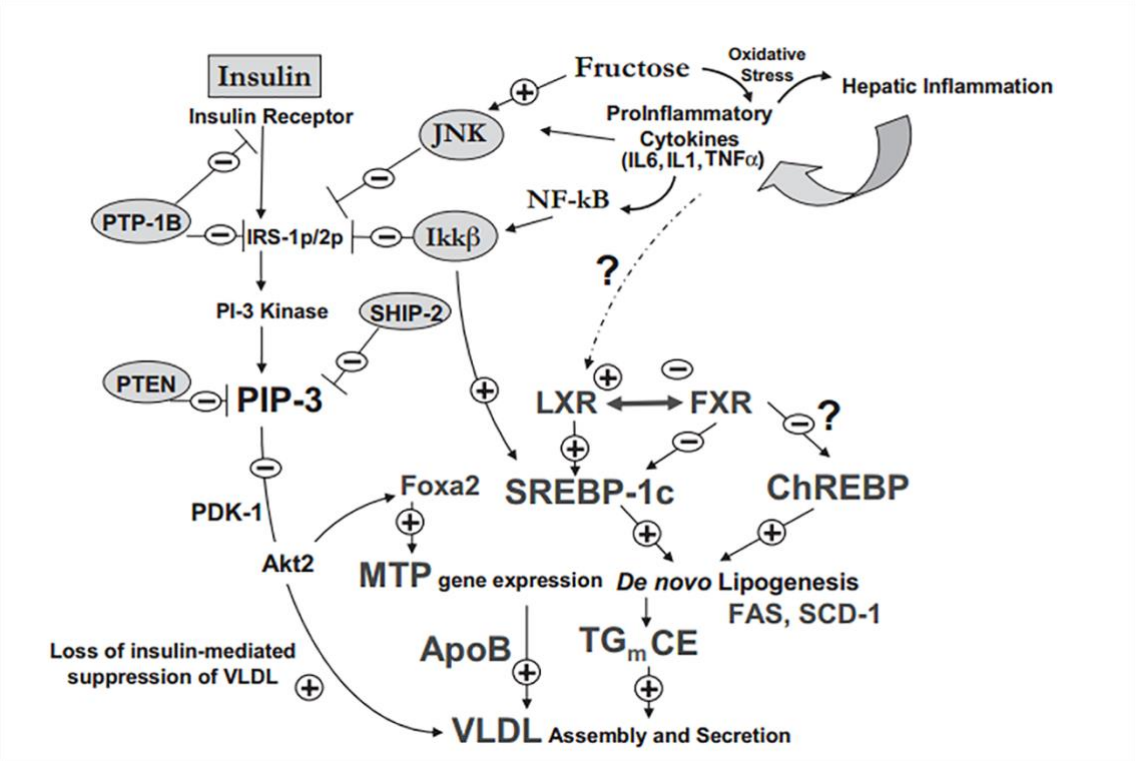

Figure 2-8. Mechanisms of fructose-induced hepatic insulin resistance, VLDL overproduction and hepatic inflammation.

(adopted from (Rutledge and Adeli, 2007))

Furthermore, protein-q phosphatase-1B (PTP-1B), a negative insulin signalling regulator, is observed that expresses a significant higher level in isolated hepatocytes with fructose exposure (Taghibiglou et al., 2002). As growing evidence claiming that PTP-1B is highly associated with Sterol Regulatory Element-Binding Proteins (SREBPs) expression via upregulating several certain transcriptional activities, PTP -1B is considered as a novel activator of lipogenesis (Shimizu et al., 2003).

Regarding to SREBPs, it is well known that they have remarkable effects on regulating cholesterol biosynthesis in a majority of cells (Brown and Goldstein, 2008). It has also

been demonstrated that high-fructose diet leads to higher expressions of SREBPs genes, even in the absence of insulin, which further enhances fatty acid synthase (FAS) and acetyl-CoA carboxylase (ACC) expression, eventually accelerates hepatic lipogenesis (Dekker et al., 2010, Miyazaki et al., 2004).

To sum up, inhibiting insulin receptor and improving PTP-1B activity by fructose would induce hepatic insulin resistance and augments SREBP-1c expression, leading to stimulation of DNL as well as escalation of microsomal triglycerides and cholesteryl ester.

In addition, the relationship between insulin resistance and VLDL overproduction has also been brought to the attention of scientists. Apolipoprotein B (apoB) and apolipoprotein E (apoE) are two important apolipoproteins of triglyceride assembly in VLDL production and these apolipoproteins are often employed to evaluate the lipoprotein particle secretion activities (Lavoie and Gauthier, 2006).

Previous researches reveal that, in the short term, insulin mainly targets on apoB pathways to conduct VLDL secretion regulation. Four possible mechanisms are proposed as follows: 1) suppression of apoB synthesis and degradation, 2) negative alteration of microsomal triglyceride transfer protein (MTP) expression, 3) inhibition of apoB phosphorylation, and 4) amendment of apoB translation (mRNA level). Constant stimulation of insulin exerts a positive effect on VLDL secretion (Taghibiglou et al., 2002).

Therefore, in animal insulin-resistant models, impaired insulin signalling pathways induced by fructose could result in hepatic MTP overexpression and apoB-containing VLDL overproduction.

2.4.3.3 Interaction between fructose metabolism and inflammation

As the high-fructose diet enhances fatty acids and triglyceride overproduction, a considerable amount of lipid gradually accumulates in the liver. These fat depositions in the liver can act as pathological stimuli that subsequently stimulates hepatocytes to produce pro-inflammatory cytokines, such as tumour necrosis factor alpha (TNF- α), interleukin 1 (IL-1) and interleukin 6 (IL-6), seen in Figure 2-8. Hepatic inflammation and intrahepatic production of cytokines would lead to the activations of nuclear factor kappa B (NF-kB) and c-Jun amino terminal kinase 1 (JNK-1) systems (Braunersreuther et al., 2012).

JNKs is a group of serine/threonine kinases that cannot only be triggered by TNF-α upon inflammation, but also by excessive amount of non-esterified fatty acids (NEFAs) and oxidative stress. It has been reported that fructose-feeding can activate JNKs systems directly and consequently diminish hepatic insulin signalling, provoking a cascade of pathologic changes, including insulin resistance and hepatic steatosis. The activation of JNKs plays an important role in the inhibitory serine phosphorylation of IRS-1 (Ser-307) in the liver (Rutledge and Adeli, 2007). Thus, JNKs is considered as a crucial inflammatory indicator of high-fructose feeding models.

Additionally, fat accumulation also leads to abnormal innate immune system, in which it enhances natural killer T (NKT) cell apoptosis, induces over-secretion of T helper 1 (Th-1) cytokines and subsequently develops hepatic inflammation (Li et al., 2005).

To sum up briefly, high-fructose consumption can result in hepatic lipid accumulation, insulin resistance and hepatic inflammation. These abnormal metabolic conditions can

occur independently but also simultaneously and interactively, leading to a cascade of metabolic dysfunctions and then promoting the development of obesity, T2DM, NAFLD and other diseases.

Despite the potential underlying metabolism and mechanism described above, the sole effect of fructose and whether there is a casual link between dietary fructose consumption and NAFLD in human has been constantly challenged.

Firstly, the increasing intake of fructose is questionable, simply because fructose is not recorded separately as an independent variable in dietary questionnaire. As a result, the estimated dietary fructose intake might be exaggerated. Secondly, since fructose is rarely consumed on its own, it is difficult to completely eliminate the adverse effects contributed by other diet components (i.e., fat). Most importantly, it has been pointed out that hypercaloric diet and/or unrealistic excessive fructose feeding, rather than fructose itself, are the casual factors of those metabolic dysfunctions in most of the animal experiments. Also, species diversity between animal and human should be taken into consideration.

Therefore, there is still no conclusive proof that NAFLD can directly results from fructose consumption and this project attempted to gain better understanding around it.

2.5 Systems Biology Approach - the Rising Star

The concept of systems biology was first introduced twenty years ago. The core of this modern cross-disciplinary field is to apply mathematics, statistics, bioinformatics and computer science to support complex biological researches at a systematic scale, from

genomics, proteomics, pathways, to cells, tissues, organs, organisms, populations and ecologies (Ideker et al., 2001).

Generally, systems biology approaches can be divided into two branches: one is data-based knowledge integration and interpretation, the other is simulation-based hypothesis prediction and exploration. Correspondingly, the former approach provides comprehensive insights for biological systems while the latter one allows the hypothesis to be tested and steer experiments into an appropriate direction (Holzhutter et al., 2012, Kitano, 2002, Ideker et al., 2001).

Therefore, the conventional framework of systems biology approach is an iterative cycle, as presented in Figure 2-9. This "make-test-validate-refine" process normally combines mathematical and computational modelling with quantitative experiments.

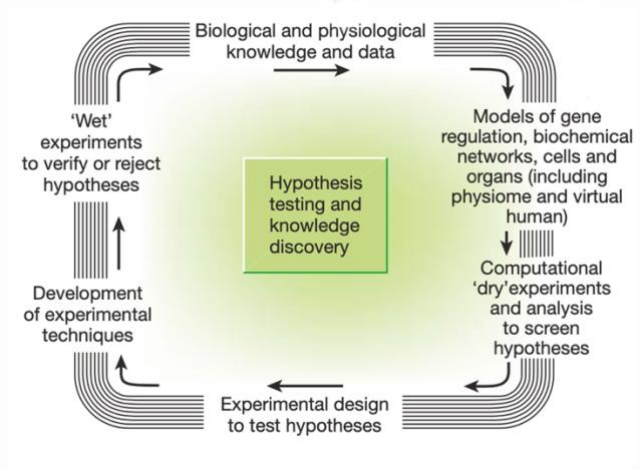

Figure 2-9. The iterative cycle of systems biology approach.

(Adopted from (Kitano, 2002))

2.5.1 Existing computational models of liver systems

With the benefit of extensive studies in modelling human metabolism over the last two decades, three well-known reconstructed human metabolic networks have been established to incorporate complex metabolic pathways and biochemical reactions in humans (Gille et al., 2010, Duarte et al., 2007, Ma et al., 2007). Among these, the model 'HepatoNet1' developed by Gille et al. (2010) mainly examines liver function at a system scale. It contains 777 components and over 2500 reactions in order to explore ammonia detoxification rates and the synthesis of bile acids under starvation conditions.

In addition, an ambitious program called "Virtual Liver Network" has been proposed by Holzhutter et al. (2012), aiming at representing all the central functions of human liver in detail and modelling the whole organ under both normal and pathological conditions on multiple scales.

However, the major limitation of these stoichiometry-based reconstructed models is that their static predictions failed to represent the dynamic flows of metabolic reactions.

Applying a kinetic model to study hepatic energy metabolism has been investigated since the 1970s. The first model of metabolic regulation was introduced by Garfinkel (1971), which listed 34 dynamic chemical expressions to conduct the TCA cycle simulation.

Most of the recent dynamic liver models are focusing on the regulation of glucose homeostasis. For instance, Naftalin (2016) constructed a computer model to simulate glucose absorption and illustrated the relationship between it and metabolic diseases. In addition, Hetherington et al. (2012) and Sumner et al. (2012) applied an innovative

engineering method to create a composite and flexible model to simulate hepatic glucose homeostasis regulated by glucagon and insulin based on liver-pancreas interaction.

Similarly, König et al. (2012) stimulated a hepatic kinetic model to represent glycolysis, gluconeogenesis pathways as well as glycogen metabolism. This model also examines the effect of hormonal regulation (insulin, glucagon and epinephrine) on glucose metabolism. On the basis of glucose metabolism, Chalhoub et al. (2007) even integrated part of lipid metabolism, fatty acid in particular, into a dynamic computational model.

Even though existing *in silico* modelling often consider liver as an ensemble piece, there still are some studies that have developed compartmental models to mimic zonation influence across the liver sinusoid.

The research conducted by Ohno (2008) proposes to divide the sinusoid into eight grading compartments in order to represent the hepatic heterogeneity along the direction from the periportal hepatocytes to the perivenous hepatocytes. This model mainly focuses on investigating ammonia metabolism, which examines the different distributions of three enzymes expressions, including carbonyl phosphate synthase, glutamine synthase and ornithine aminotransferase, within the compartments.

Similarly, the eight-compartment-model of simulating hepatic flexibility and elimination was introduced by Anissimov and Roberts (2002), using palmitate as the central parameter to make corresponding model predictions. Furthermore, Ashworth et al. (2016) have created a computational model with eight compartments that not only describes the zonated enzyme expression in hepatic glucose and lipid metabolism, but also simulates

insulin resistance and proposes the possible mechanism of NAFLD development across the hepatic sinusoid.

Despite the fact that abundant studies have highlighted the important role fructose plays in liver-related metabolic diseases, a model that only focuses on fructose metabolism is not available at the beginning of the current study. Later on, only a few models (Allen and Musante, 2017, Allen and Musante, 2018, Maldonado et al., 2018) have placed emphasis on the hepatic fructose metabolism and none of these have reflected the underlying dynamic mechanism of fructose metabolism and NAFLD development. A brief comparison of these models is listed in Table 2-4.

Table 2-4. What has and has not been done in the existing fructose models.

The existing fructose models	What has been done	What has not been done
Allen and Musante (2017)	1) Two fructose-specialized enzymes were included in the model (fructokinase and Aldolase B); 2) The relationship between fructokinase deficiency and essential fructosuria was explored; 3) Urine fructose concentration was included in the model.	1) Downstream fructose pathways after aldolase B were excluded; 2) The relationships between fructose and other metabolic conditions have not been done.
Allen and Musante (2018)	1) The relationship between fructose and de novo lipogenesis was discussed; 2) Simplification method has been applied in metabolic pathway of the fructose-pyruvate-fatty acids-triglyceride axis.	1) The relationship between fructose and NAFLD has not been explored; 2) The model does not have other inputs, i.e., glucose.
Maldonado et al. (2018)	1) The relationship between fructose and NAFLD has been investigated; 2) A fructose model was constructed that integrated the transport and signalling network with a hepatocyte-specific human genome-scale metabolic network (HepatoNet1). 3) Glucose input was included in the model.	1) The human genome-scale metabolic network produces static predictions which failed to represent the dynamic flows of metabolic reactions; 2) The fructose metabolism under the disease state has not been considered.

Therefore, this project aimed to develop a suitable model to fill the gaps in current understanding of the relationship between fructose and NAFLD.

2.6 Chapter Conclusions

To conclude, NAFLD is a multifactorial and multisystem disease but currently there is no pharmaceutical treatment available for NALFD. Even though abundant literatures have emphasized the essential role dietary fructose plays in NAFLD and other metabolic diseases, the possible underlying regulatory and molecular mechanisms are still not fully understood.

Biomedical studies and clinical trials tend to discover one specific molecule/component at a time and often lacks of a holistic perspective to integrate the complex interaction within the biology systems. Therefore, to adopt the systems biology approach to explore the relationship between fructose consumption and the development of NAFLD is able to provide a better understanding and identify potential interventional targets.

3 Chapter 3: Experimental Attempt and Exploration

3.1 Chapter Introduction

Before constructing a computational model of fructose metabolism, two biochemical experiments have been performed *in vitro* as an exploratory attempt. The purpose of these experiments is to briefly investigate whether the fructose-enrich diet can induce fatty liver and whether the experimental results are reconciled with the literature.

3.2 Experimental Design

Two kinds of biochemical experiments were performed at this stage. They are MTS proliferation assay and Oil red O staining test. Three hepatocyte cell lines as well as animal liver tissues were used to carry out the experiments.

Four treatments were employed in the cell lines, representing a 100% fructose meal, a 100% glucose meal, a sucrose meal, as well as a mixed meal (50:50 fructose and glucose). The concentration range of the carbohydrate treatments covers from 5mM to 20mM, simulating the consumption levels from normal to excessive.

In addition, two different diets were provided for the Sprague Dawley rats, including the control diet and the fructose diet. The fructose diet contains a total of 66.3g fructose per 100g chow, which accounts for 69.6% of the caloric consumption, simulating the fructose over-consumption model.

More details on sample collections and assay planning are demonstrated in the following sections (see 3.2.1 and 3.2.2).

3.2.1 Sample Harvest and Collection

3.2.1.1 Hepatocyte Cell Lines

Primary human hepatocytes and derived liver cell lines are commonly used *in vitro* models for hepatic phenotypic functions research (Wilkening et al., 2003). Although primary human hepatocytes are considered to be the most suitable material in resembling the hepatic process *ex vivo*, the shortage of available human liver source, the reluctance of growth in culture and the heterogeneous quality of the supply limit the feasibility of the experimental designs. Therefore, liver cell lines with stable, reproducible characteristics were chosen as the hepatic cell culture model in this study. Specifically, the three employed immortal hepatocyte cell lines are HepG2, HHL-5 and HHL-7.

HepG2, a human liver tumour cell line, has been widely used in liver-specific research since 1979 (Aden et al., 1979). HepG2 cells were originally derived from the liver tissue of a fifteen year old male Caucasian American with differentiated hepatoblastoma (Javitt, 1990, Wang et al., 1988). Over the recent decades, it has been well established that HepG2 have maintained a wide variety of specific-functions of normal hepatocytes (Wilkening et al., 2003).

However, a few concerns have been raised that the *in vivo*-like metabolic regulation of healthy hepatocytes might not be represented accurately by a tumorigenic origin liver cell line such as HepG2 (Sefried et al., 2018). Furthermore, it has been reported that there is a considerable amount of lipid has been observed in HepG2 cellular content due to its incapability in fatty acid secretion (Gibbons et al., 1994), which might jeopardize lipid-related researches.

Therefore, the immortalised human hepatocyte lines (HHLs) cell lines were also introduced to the current project. These cell lines were originally isolated from a healthy liver of a sudden deceased juvenile male. As a novel hepatic cell culture model, HHLs has been claimed having the capacity to successfully recapture the phenotype and function of the primary hepatocytes (Clayton et al., 2005). In this study, both HHL-5 and HHL-7 were applied in assays exploring the relationship between fructose stimulation and lipid accumulation.

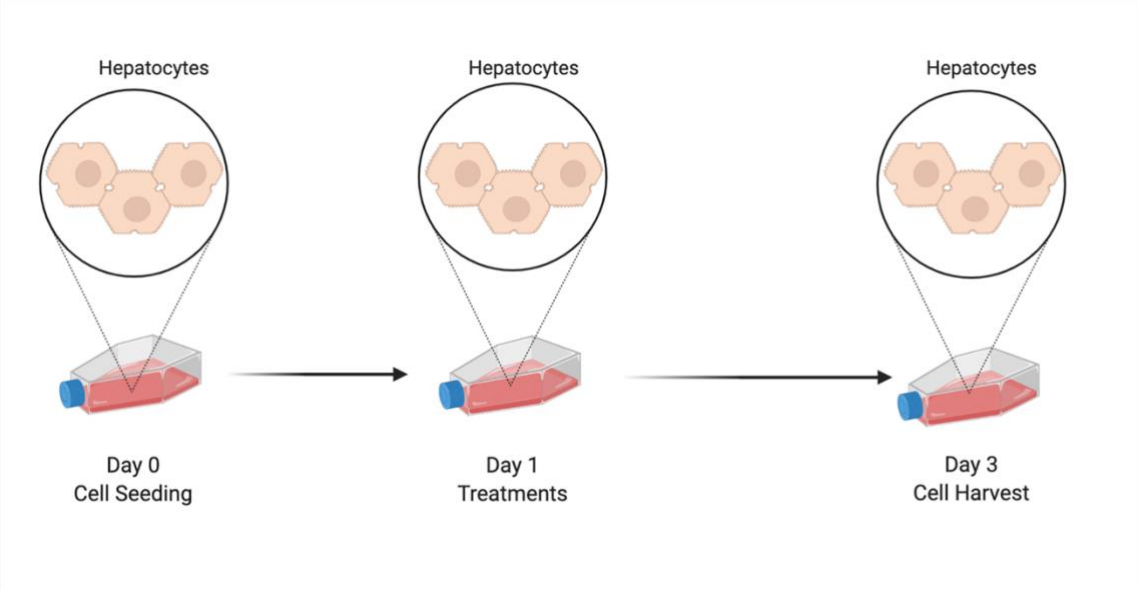

Figure 3-1. Experimental period of cell culture.

The typical experimental period of cell culture protocol is presented in

Figure 3-1. the cells were seeded at the density of 26,000 cells/cm^2 for 24 hours before exposing to any experimental treatments. Due to the fact that the doubling time of HepG2 cells is around 48 hours (Shafiee-Morrel et al., 2012) and the characteristics of HHLs

remain unclear, a 72-hour incubation period allows the hepatocytes to experience one proliferation cycle under the customised stimulations.

3.2.1.2 Animal Experiment Design

In spite of the species differences, animal model is considered as a valuable tool in biomedical research. In collaboration with Aarhus University, Denmark, 60 male Sprague Dawley rats were randomized into 6 groups. In 16 weeks, rats received either a fructose enriched diet to model NAFLD or a normal rat chow before injecting with yohimbine treatment or saline placebo.

As the current project is solely interested in investigating the effect of fructose on hepatic metabolism, only the control group and the fructose group samples were selected to conduct assays and analysis. One rat (No.35) in the fructose group was found dead in week 15; hence, frozen liver tissues and fixed histological slides from 10 rats in the control group and 9 rats in the fructose group were applied to the biochemical experiments in this chapter.

The caloric intake distribution provided by the control diet and fructose diet per 100g chow are shown in Figure 3-2. It can be seen that these two diets have similar proportion of protein. In addition, in the control diet 12.35% of calories were supplied by fat, in which the percentage is approximately 3% higher than that in the fructose diet. However, this 3% energy discrepancy is compensated by the source of carbohydrate in the fructose group.

The carbohydrate compositions of each diet are displayed in Figure 3-2 (A2) and (B2). Rats in the control group obtained carbohydrates from fibre, disaccharides and

polysaccharides, whereas the fructose-feeding rats were exposed to 66.3 fructose and 0.9g sucrose per 100g chow, accounting for 98.66% and 1.34% of the carbohydrate energy intake, respectively.

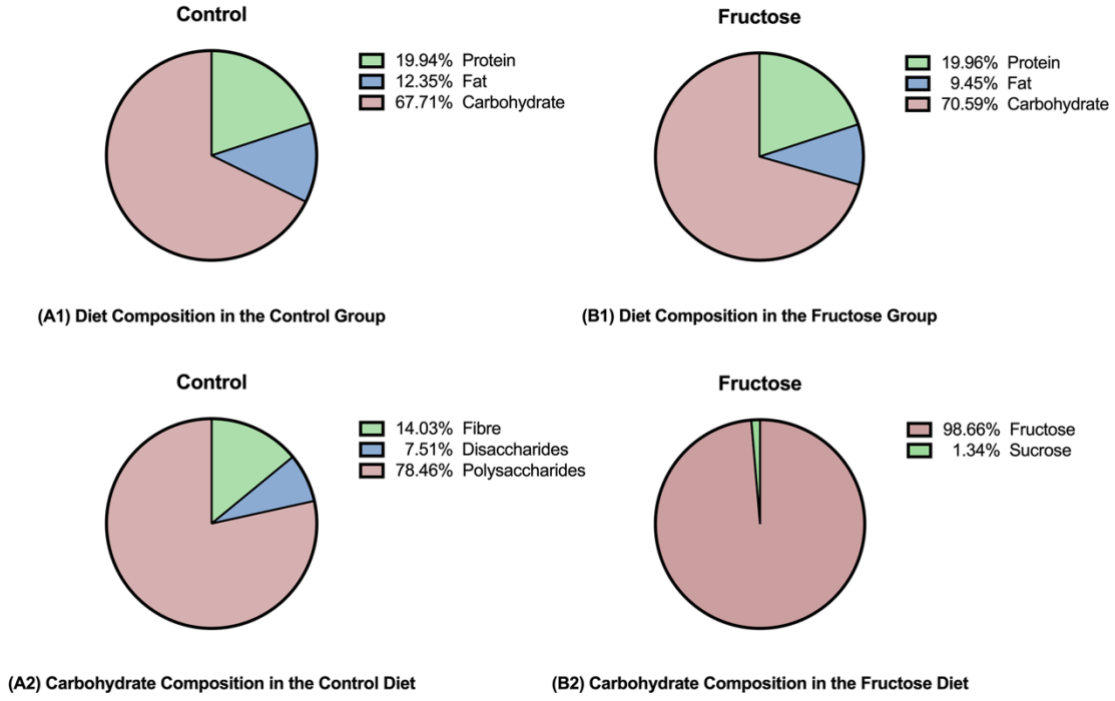

Figure 3-2. Diet compositions regarding energy contribution in the animal experiments.

(A1 and B1: the compositions of diet in the control group and the fructose group;

A2 and B2: the composition of carbohydrates in the control diet and the fructose diet.)

In Week 16, the subjects were terminated and dissected. Portal blood, arterial blood and tissues were collected for further research purposes. In the current study, only the liver pieces were used for the examinations.

3.2.2 Biochemical Assay Planning

As mentioned above, the first conducted experiment is MTS proliferation assay, serving as the preliminary test. This assay was only performed on the derived cell lines to explore whether the high concentration of carbohydrate feeding would exert a toxic effect on the liver cells per se and whether the different dietary pattens would alter the growth behaviours of hepatocytes.

Lipid quantification assays were then carried out on both cell lines and animal liver tissues to assess the lipid levels resulting from different dietary exposures. The Oil red O staining assay was conducted to spot the neutral triglycerides on three cell lines after 72-h incubation, whereas the histological slides of the rat livers after 16-week feeding were used for the image analysis.

Reagent and protocol details of these two assays are listed below.

3.3 Methodology

3.3.1 Reagents and Materials

3.3.1.1 Experiment Samples

Cell lines: Human Hepatocyte Line 5 (HHL-5) & Human Hepatocyte Line 7 (HHL-7) (generously shared by Professor Arvind Patel, University of Glasgow); Immortalized hepatocyte cell lines: HepG2 cell line (American Type Culture Collection, HB-8065); *Liver tissues*: rat liver pieces (generously shared by Dr Karen Louise Thomsen, Aarhus University);

3.3.1.2 Cell Culture

Eagle's Minimum Essential Medium (EMEM) (Life Technologies, 11095-080); Dulbecco's Modified Eagle Medium (DMEM) (Life Technologies, 31966-021); Penicillin-Streptomycin (P/S) (10.000U/ml) (Life Technologies, 15140-122); Foetal Bovine Serum (FBS) (Life Technologies, 16000-044); Bovine Serum Albumin (BSA) Protease-free Powder (Fisher Scientific, BP9703100); Hanks' Balanced Salt Solution (HBSS) without calcium and magnesium (Life Technologies, 14170-088); Dulbecco's Phosphate Buffered Saline (DPBS) without calcium, chloride and magnesium (Sigma-Aldrich, D8537-500ML), Minimum Essential Medium (MEM) Non-Essential Amino Acids (NEAA) (100×) (Life Technologies, 11140-050); 0.25% Trypsin-Ethylenediaminetetraacetic acid (EDTA) solution (Life Technologies, 25200-072);

3.3.1.3 Carbohydrate Treatments and Positive Lipid Control

DMEM without glucose (Life Technologies, 11966-025); D-(-)-Fructose (VWR chemicals, 103674Y); D-(+)-Glucose (Sigma-Aldrich, G7021); Sucrose (Sigma-Aldrich, S1888-500G); Palmitic acid (Sigma-Aldrich, P5585-10G); Oleic acid (Sigma-Aldrich, O1383-1G); Isopropanol (100%); BSA; FBS;

3.3.1.4 Sample Harvest and Collection

Pierce™ RIPA Lysis and Extraction Buffer (Thermo Fisher, 89900); HEPES (Sigma-Aldrich, H3375); PhosSTOP™ (inhibitor tablets for phosphatase) (Sigma-Aldrich, 4906837001); cOmplete™ ULTRA Tablets, EASYpack Protease Inhibitor Cocktail (Sigma-Aldrich, 5892970001);

3.3.1.5 MTS Proliferation Assay

CellTiter 96 Aqueous One Solution Cell Proliferation Assay (Promega, G3580);

3.3.1.6 Oil Red O Staining Test

Formalin (60%); Isopropanol (100%); Oil red O solution (0.5% in isopropanol) (Sigma-Aldrich, O1391); Haematoxylin (Vector Laboratories, H3404);

3.3.1.7 Measuring Equipment

FLUOstar Omega Filter-based multi-mode microplate reader (BMG Labtech); FluorChem^{TM} M System (Protein Simple) for western blotting; Electron Microscope.

3.3.2 Mechanisms and Protocols

3.3.2.1 Cell Culture

HHL-5 and HHL-7 cells were maintained and grown in 75 cm^2 cell culture flasks in 20ml DMEM containing 10% FBS and 1% MEM NEAA, whereas HepG2 cells were cultivated in 20ml EMEM containing 10% FBS and 100U/ml Penicillin/Streptomycin. The supplement of antibiotics was to diminish potential interference from bacterial contamination. All three cell lines were cultured in a humidified incubator with 37°C and 5% CO_2. Trypsin-EDTA and DPBS were used for routine passaging. For experimental sub-cultivation, the cells were then trypsinized and reseeded in 6-well, 96-well culture plates and 100mm×20mm culture dishes, respectively, at the same density of 26,000 cells/cm^2 for 24 hours before exposing to any experimental treatments. Mycoplasma detection was conducted routinely.

3.3.2.2 Carbohydrate Treatments and Positive Lipid Control

For carbohydrate treatment preparations, fructose, glucose and sucrose powders were dissolved in 50ml glucose-free medium to obtain the stock solutions of 100mM, 100mM and 50mM, respectively. Aliquots were made and stored in -20°C freezer. For positive lipid control, the stock solutions of palmitic acid and oleic acid were prepared in 9.75ml and 8.25ml isopropanol (100%), respectively. Then palmitic acid and oleic acid solutions were mixed at 2:1 to achieve a final concentration of 400mM. This pure free fatty acid (FFA) mixture was aliquoted of 1ml and stored in -20°C for further use, avoiding light and air. Furthermore, one gram of BSA was dissolved in 100ml DPBS and a dilution of free fatty acid cocktail was made in this DPBS solution containing 1% BSA at ratio 1:100. For example, 4mM FFAs cocktail stock solution was made by adding 0.1ml pure free fatty acid mixture to 9.9ml DPBS (1% BSA). All stock solutions were sterilized by 20μm filters before further dilutions. After seeding for 24 hours, all three cell lines were rinsed three times with DPBS before exposing to different treatments.

3.3.2.3 MTS Proliferation Assay

The viability of all three cell lines were quantified by MTS proliferation assay. This assay is based on the mechanism that the MTS tetrazolium compound can be reduced by cells through dehydrogenase enzymes into a coloured formazan product which is soluble and detectable in culture medium (Brunel, 1999). Initially, Cells were seeded in 96-well culture plates at a concentration of 8,000 cells per well. On the next day, numerous carbohydrate treatments were applied to each well, incubating for another 48 hours. At the time points of 24h, 48h, and 72h, assays were conducted by removing 100μl/well medium and directly adding 20μl MTS solution to each well. After incubation at 37°C

with 5% CO_2 for two hours, the absorbance ranging from 350 to 650 was measured with FLUOstar Omega Filter-based multi-mode microplate reader and the absorbance at 490nm was recorded for analysis.

3.3.2.4 Oil Red O Staining Test

The intercellular triglyceride and lipid accumulation in all three cell lines were stained by Oil red O solution. Cells were grown in 6-well plates. The medium was aspirated and the cells were washed for 5 minutes twice with DPBS. To fix the cells, 10% formalin was added to each well for 10 minutes. The formalin was removed and the cells were washed twice with diH2O before incubating for 5 minutes in 60% isopropanol. The isopropanol was aspirated and the cells were incubated for 10 minutes in Oil Red O (ORO) working solution (0.18% ORO in 60% isopropanol, 40% diH2O). Two to five times diH2O washes were performed until the stain was no longer apparent in the water. Then the diH20 was aspirated and one drop of haematoxylin was added to stain the nuclei. Several diH20 rinses were preformed rapidly before imaging.

3.3.2.5 Image Analysis and Data Statistical Analysis

At least triplicate data were collected to calculate means and standard deviations (SD) for all the results in this project. Image analysis was conducted by ImageJ program. Data was analysed through OMEGA-MARS Data Analysis System, Microsoft Excel software and GraphPad Prism 7 software. T-test and one-way ANOVA were operated to compare the disparities between the control group and the experimental groups accordingly. A P-value less than 0.05 was accepted as statistically significant difference.

3.4 Results and Discussion

3.4.1 Animal Sample Characteristics

The data of body weight and liver weight in the animal experiment was recorded to summarise the sample characteristics. The comparison between two groups in body weight as well as in the ratio of liver/body weight are presented in Figure 3-3(A) and (B), respectively. Figure 3-3(C) exhibits the whole liver pieces (one representative from each group) for the visual comparison.

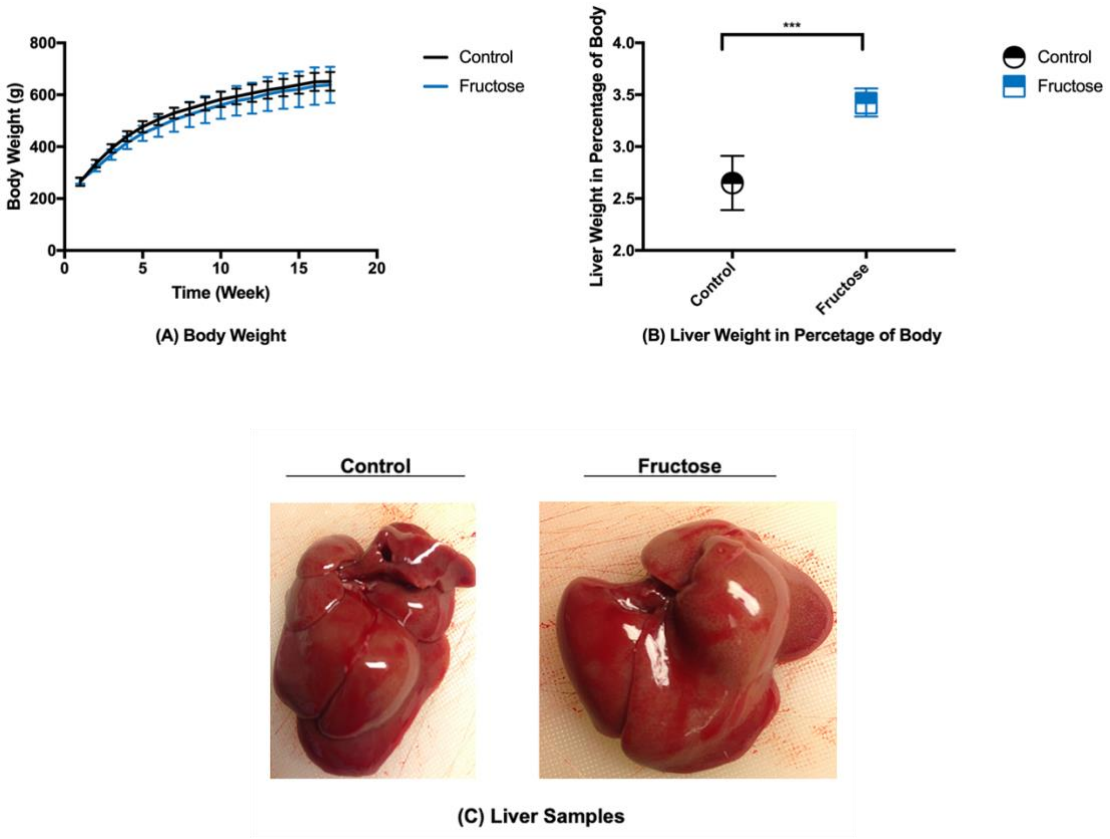

Figure 3-3. Sample characteristics of body weight and liver/body weight ratio

(A and B: Mean ± SD, Control: n=10; Fructose: n=9).

***p < 0.05, **p < 0.01, ***p < 0.001 vs. Control.**

The results show that no significant statistical difference in body weight can be found between the two diet groups. In fact, the average weight of the control rats even is slightly higher than that of the fructose-feeding rats. In contrast, liver weight in the fructose group is remarkably heavier than that in the control group, which can be observed directly from Figure 3-3(C). As a result, the liver/body weight ratio in the fructose group is significantly higher than the other group as shown in Figure 3-3(B), suggesting high fructose consumption leads to hepatic lipid accumulation rather than systemic lipid build up.

3.4.2 The Effect of Different Carbohydrates on Cell Proliferation

To assess the effect of various carbohydrate dose-response treatments on cell viability and proliferation, the MTS assay was conducted.

For experimental setup, four treatments with three different concentrations were exposed to the three cell lines after a 24-hour incubation period. These four treatments are pure fructose, pure glucose, sucrose, and a combination of fructose and glucose in 1:1 ratio. As cell culture medium normally contains approximately 4.5mM glucose, the concentration values introduced to this experiment are 5mM, 10mM and 20mM. A 400μM FFAs cocktail was used as a positive control in this experiment. The viabilities of HHL-5, HHL-7 and HepG2 were reflected by optical density of absorbance spectrum. The outcomes at three time points (24h, 48h and 72h) were recorded for analysis.

The summary of the MTS results is shown in Figure 3-4. As presented in the first row (A1, B1, C1), the cell growth curves of untreated HHLs show exponential tendencies within 72 hours while HepG2 expresses a strong linear regression, providing a general vision of the normal cell behaviours. Under microscope observation, HepG2 cells tend to

expand in a thick massive pattern whereas HHL-5 and HHL-7 cells grow only in monolayer. This explains the higher values of HepG2 growth curve (1.71±0.14 at 24h, 2.28±0.09 at 48h and 2.73±0.12 at 72h) in comparison to HHL-5 (1.33±0.06 at 24h, 1.51±0.04 at 48h and 2.14±0.19 at 72h) and HHL-7 (1.19±0.04 at 24h, 1.56±0.15 at 48h and 2.18±0.08 at 72h).

After exposing to different conditions, Figure 3-4 (A2-4, B2-4, C2-4) summarises the cellular proliferation results of all three cell lines at 48h and 72h time points. In general, it can be observed that HHL-5 and HHL-7 cells shared the same growth and response pattern. To be specific, pure fructose feeding (denoted in brown bars) has a significant inhibitory effect on cell growth at all three concentrations, suggesting HHLs has limited efficiency in fructose uptake. However, when consumed with glucose (denoted in blue bars), it seems that the mixed carbohydrates improve dietary fructose utilisation and attenuate the malabsorption, hence stimulating cell growth dramatically along with the increasing concentrations.

The optical density values of the glucose group are similar to those in the control group at the 5mM condition. As demonstrated in experimental setting, these results are as expected since there are comparable amounts of glucose content in the both groups. As the treated glucose concentration increases, the cell viability enhances.

Similar to the fructose treatment, HHL-5 and HHL-7 hepatocytes incubated with sucrose show a striking decrease in cell proliferation and they remain in a low level at all time points. However, when the cells were treated with 1:1 fructose and glucose mixture as the same components as sucrose, they grew rapidly. Especially for HHL-7 cells, the mixed

treatments induced the highest cell proliferation value under almost every condition at every time point. These results suggest that HHLs cell lines are lacking sucrase, an enzyme that breaks down sucrose to produce glucose and fructose.

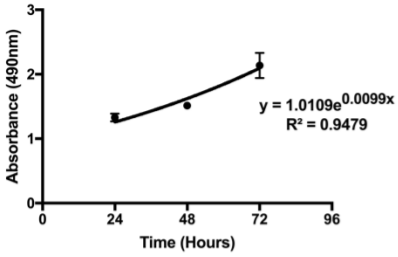

(A1) Control (HHL-5)

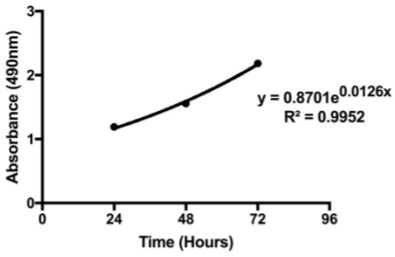

(B1) Control (HHL-7)

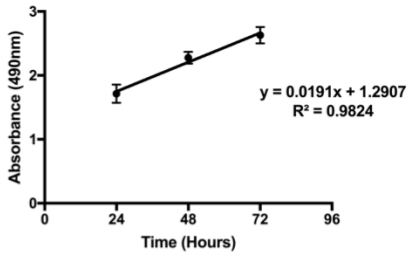

(C1) Control (HepG2)

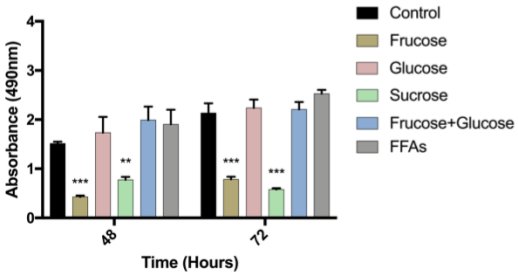

(A2) 5mM Treatment (HHL-5)

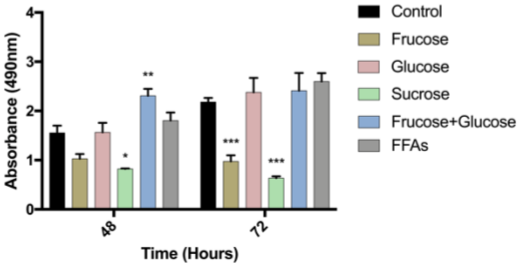

(B2) 5mM Treatment (HHL-7)

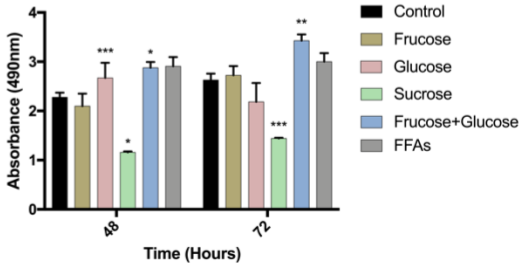

(C2) 5mM Treatment (HepG2)

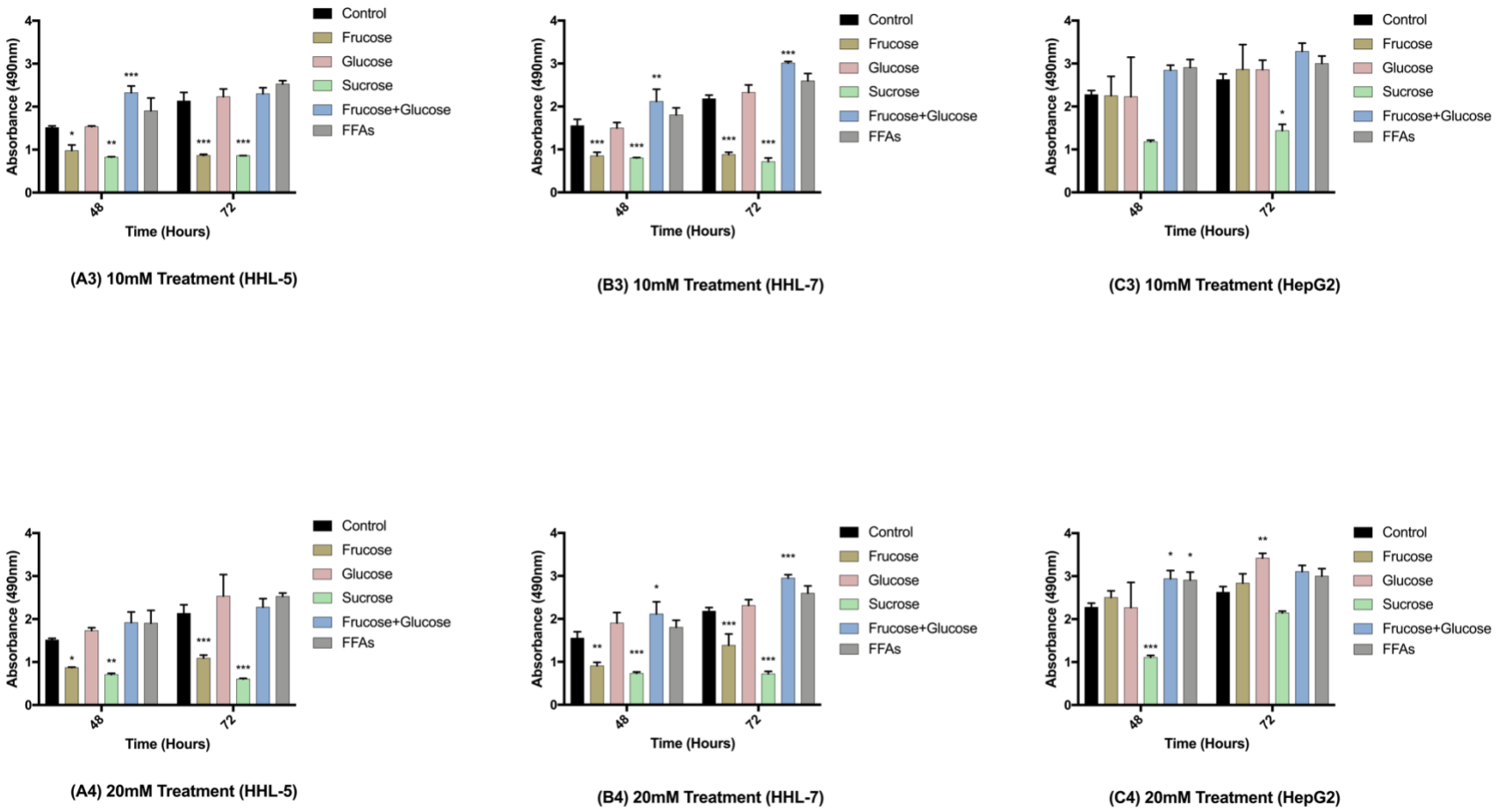

Figure 3-4. The effect of carbohydrate treatment on cell viability and proliferation.

***p < 0.05, **p < 0.01, ***p < 0.001 vs. Control.**

Compared to HHL-5 and HHL-7, it can be seen in Figure 3-4 (C2-4) that HepG2 cells have higher compatibility when it comes to fructose uptake. With longer incubation time, HepG2 hepatocytes in the fructose group even be able to outgrow those in the control group. Same as HHLs, there is no significant statistical difference in cell viability between the glucose group and the control group.

Furthermore, the cells viability was supressed in the sucrose group in comparison to the control group. Sucrose-feeding hepatocytes only managed to achieve a half value of that in the control group. Even though HepG2 cells have higher tolerance with sucrose than HHLs, the sucrose groups still have the lowest cell proliferation numbers among all the conditions. No significant statistical difference can be found between the mixed carbohydrate groups and the free fatty acid group, indicating that the combination of fructose and glucose provides the most suitable environment to boost the cell growth.

To sum up, fructose alone or sucrose alone exerts an inhibitory influence on cell viability and proliferation in the HHLs cell lines. However, it can be observed that consuming fructose and glucose altogether have a synergistic effect on promoting cell growth. HepG2 cells in general are able to take up carbohydrates in a more efficient manner. A high-fructose environment in particular can be tolerated better in HepG2 cells than in HHLs. This might be associated with HepG2's tumorigenic origin and their natural characteristics of high fatty acid content.

3.4.3 The Effect of Different Carbohydrates on Lipid Accumulation

In order to explore the effect of different carbohydrates on cellular lipid accumulation, the Oil red O staining test was performed in the three cell lines after 72 hours incubation.

Same as the MTS assay setting, four kinds of carbohydrate treatments were applied in the experiment. The control group contains 5mM glucose while a condition of 20mM was used in the treated groups in order to simulate a high-concentration environment. Also, the positive control is contributed by a 400μM FFAs cocktail. Under the microscope observation, five visual areas in the same cell culture dish were captured randomly for each condition.

The lipid profile was quantified through ImageJ software by measuring the proportion of the lipid-stained cellular area and by counting the whole-area cell numbers. As a result, the quantity of lipid per cell was calculated by using lipid area to divide cell number. To maintain the objectivity, a blind analysis was performed by masking the labels and shuffling the images. The analytic results are presented in Figure 3-5.

As shown in Figure 3-5 (A), the lipid accumulated pattern of HHL-5 hepatocytes is consistent with its cell growth behaviour. The fructose group and the sucrose group contain lower content of lipid. This phenomenon can be explained by the fact that since it is challenging for the liver cells under these two conditions to seize energy resource on their own, undoubtedly, they have difficulties to produce more fat. The lipid quantity in the glucose group is much higher than that in the control group. It is reasonable considering that their condition setup is in a dose-dependent manner, as 5mM vs. 20mM glucose. In addition, the value in the combination group is slightly higher than that in the glucose group, but lower than that in the fatty acid group. This result suggests that co-uptake of fructose and glucose has a stronger ability to induce lipid deposition.

For HHL-7 cell line, the staining features are quite different in comparison to HHL-5. As presented in Figure 3-5(B), HHL-7 in general was found to produce more lipid despite the various treatments. The hepatocytes in the fructose group managed to generate the largest amount of cellular lipid among the four treated groups. This result indicates that high concentration of fructose modifies lipid metabolism within the cells, possibly through the hepatic *de novo* lipogenesis pathway. Sucrose-treated hepatocytes also make more contribution to lipid deposition in comparison to HHL-5.

In terms of HepG2 cells, no difference can be observed in the cellular lipid level within the carbohydrate treated groups. Again, this might due to the fast proliferation rate of HepG2 cells as stated previously and the fact that they already contain a considerable amount of lipid within the cells.

To conclude, HHL-5 and HHL-7 hepatocytes reacted differently when it comes to lipid deposition even though they have a similar proliferation pattern. Interestingly, HHL-7 cells seem to response more actively to both fructose and sucrose stimulations and generate more lipid than HHL-5 in these two treated groups. The reason that there is no positive correlation can be found between fructose and lipid accumulation except for HHL-7 is because that the enzymes that are associated with fructose metabolism in cell lines are limited. Furthermore, it is difficult to examine the effect of various treatments on cellular lipid accumulation on HepG2 cells as they tend to grow into aggressive spread cell clusters and reserve a mass of fat.

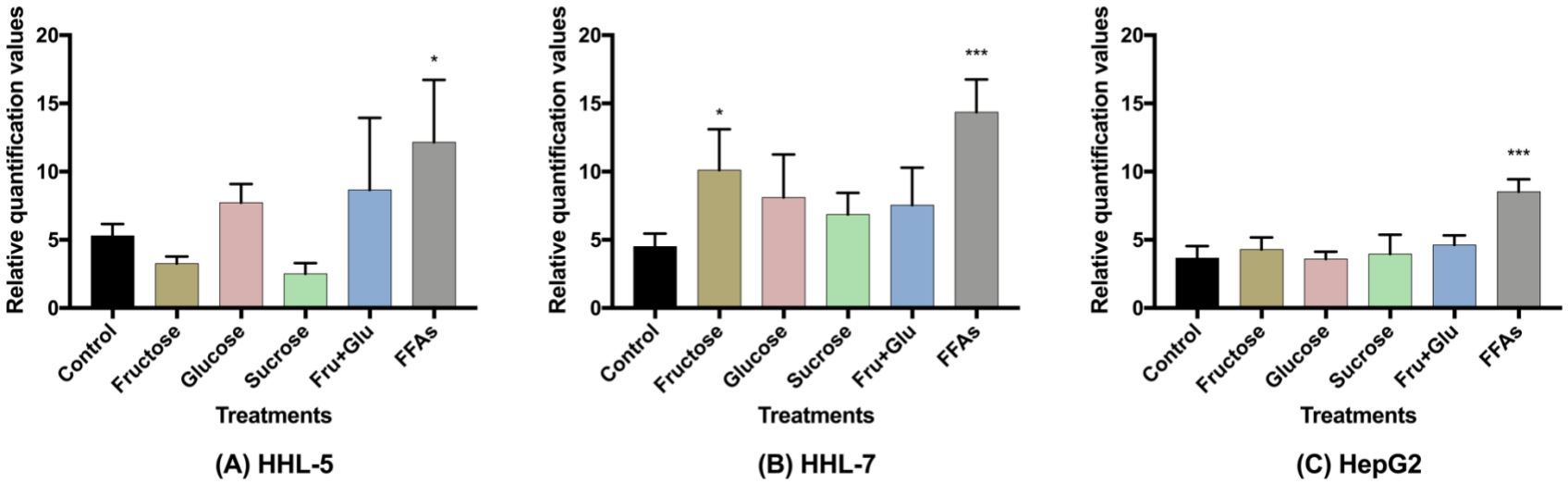

Figure 3-5. The effect of different high-concentration carbohydrates on cellular lipid accumulation.

***p < 0.05, **p < 0.01, ***p < 0.001 vs. Control.**

Apart from the derived hepatocyte cell lines, the rat liver pieces were also employed to investigate the effect of different diets on hepatic lipid build up. A total of 19 hepatic histological slides, including the control group and the fructose group, were analysed by ImageJ software to quantify their lipid area fraction. The results are presented in Figure 3-6.

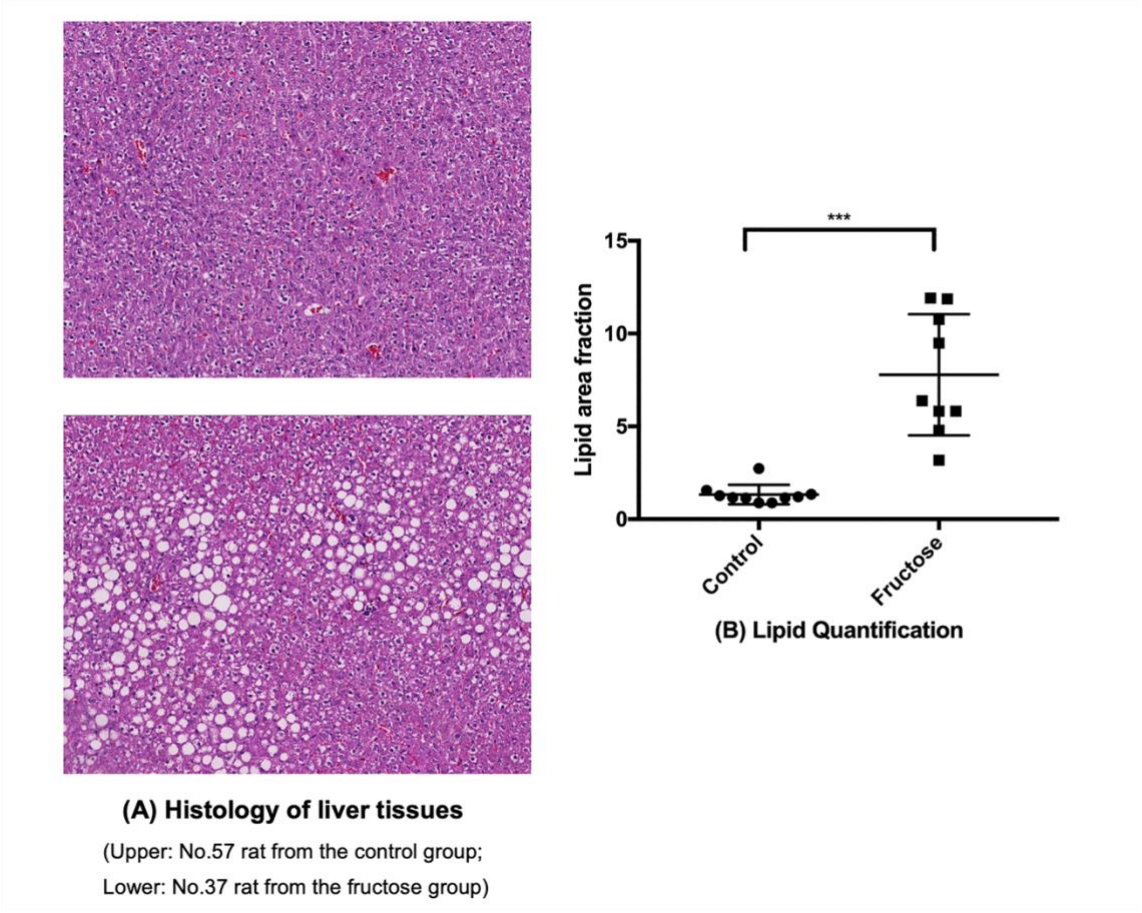

Figure 3-6. Lipid accumulation outcomes stimulated by different diets in the animal experiment.

(B: Scatter plots with single value and means ± SD; Control: n=10; Fructose: n=9).

***p < 0.05, **p < 0.01, ***p < 0.001 vs. Control.**

In Figure 3-6 (A), two histological images were displayed as the representatives: one from the control group and the other one from the fructose group. It is clearly visible that there is a large amount of lipid droplets (white empty spaces) in rat No.37 whereas not much fat can be observed in rat No.57.

The lipid qualification value of each sample (denoted as black dot) and the averages of each group are shown in Figure 3-6 (B), in which 1.33±0.53% of hepatic lipid was accumulated in the rats those fed with normal diet, whereas 7.78±3.27% of fat built up in the fructose-fed ones.

According to the biochemical criteria of hepatic steatosis, the liver is considered to be macroscopic steatosis when it contains more than 5.5% of lipid content histologically (Petäjä and Yki-Järvinen, 2016). Therefore, combined with the sample characteristics in Figure 3-3, a conclusion could be made that the fructose-enriched diet greatly contributes to the development of NAFLD.

3.5 Chapter Conclusions

The *ex vivo* results in this chapter reveal that high fructose consumption does lead to hepatic lipid accumulation in rats and this finding is consistent with the literature conclusions.

In the cell culture model, it is clear that sucrose has an inhibitory effect on their proliferation rates. Furthermore, HHLs cells is unable to process fructose as energy source as well as glucose, but this incapability was not observed in HepG2 cell. Regarding

cellular lipid deposition, HHL7 seems to have a susceptibility to fructose. Therefore, a consensus cannot be reach in liver cell lines whether fructose can facilitate fatty liver.

4 Chapter 4: Model Construction of Fructose Metabolism

4.1 Chapter Introduction

In this chapter, the whole process of the fructose computational model development is presented in details. The process consisted of three stages and these are described: Stage one: model construction of hepatic fructose metabolism, which constructs a single hepatic fructose metabolism section; Stage two: model expansion with fluid flow and cross-membrane transportation, which includes the bloodstream circulation into the model; and Stage three: model combination with glucose metabolism and hormonal regulation, which embraces glucose as an alternative dietary source and combines hormones to mimic homeostasis regulation.

4.2 The Progression of Model Development

4.2.1 Model Description

The kinetic model of the fructose metabolism was developed based on modified Michaelis-Menten and Hill equations. This model comprises approximately 120 parameters, 25 variables and 25 first order differential equations.

As shown in Figure 4-1, variables and equations were divided into three sections representing hepatocytes (SH), hepatic bloodstream (SHB) and bloodstream of the rest of the body (SBC). Hepatic fatty acids (FA) and hepatic triglycerides (TG) were selected to be the major outputs in this model as they are the most important indices reflecting lipid accumulation in the liver. Plasma free fatty acids (FFA) and plasma triglycerides are also

predicted as they are the most directly measurable matching indices recorded in clinical and experimental data. The equations are reported in this section.

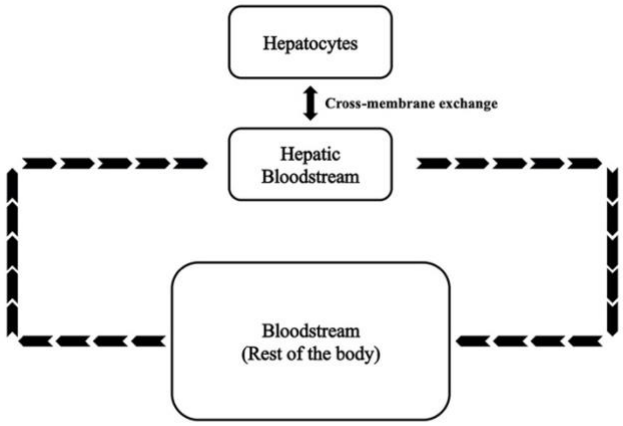

Figure 4-1. Basic framework of the fructose metabolism modelling.

Periodic simulation of the dietary intake (shown below) is based on spiked inputs adapted from Ashworth et al. (2016), which provides three meals a day with four-hour breaks.

$$Dietary\ Input = v_{input} * sin^6\left(\frac{pi}{4(hours)}\right)$$

Equ. 1 Dietary Input

The initial values and parameter settings in the model were presented in Table A-1, Appendix A.

4.2.2 Stage One: Model Construction of Hepatic Fructose Metabolism

4.2.2.1 Hepatocytes - Fructose Metabolism

Since the metabolic activities of fructose mainly take place in the liver parenchyma, hepatocyte metabolism is the primary focus in this study. As mentioned above, the most

common assumption is to link fructose with NAFLD due to its unique metabolic processes. As fructokinase, aldolase B and triokinase are three specialized enzymes for the fructose metabolism, the chemical reactions related to these three enzymes were first included to initiate the model construction.

Substantial evidence leads to the proposition that high fructose consumption is attributable to enhancing *de novo* lipogenesis, suppressing β-oxidation and facilitating triglyceride synthesis (Koo et al., 2008, Lim et al., 2010, Nomura and Yamanouchi, 2012, Tappy and Lê, 2010). The model therefore was developed to incorporate these pathways. However, not every single component in the liver metabolism has been included.

Pyruvate, acetyl-CoA, fatty acids and triglycerides were selected as they are identified as the most common intermediates and ultimate metabolites within the carbohydrate metabolic process associated with lipid deposition (Laughlin, 2014, Mayes, 1993, Sun and Empie, 2012). Also, they are considered to be the key components and they are assessable in clinical experiments, which allows the related parameters be tuned and validated during model development.

Indeed, the reactions between these key metabolites in the human body is more complicated than that which is presented in the model. However, rate-determining enzymes among the biochemical processes were selected to simplify the reactions yet provide adequate details to represent realistic reaction rates.

As a result, Figure 4-2 summarises the biochemical components and reactions identified in the literature that are constructed within the model, including fructolysis, *de novo*

lipogenesis (DNL), beta-oxidation and triglyceride synthesis. Table 4-1 presents the rate equations for the hepatic variables used in this section.

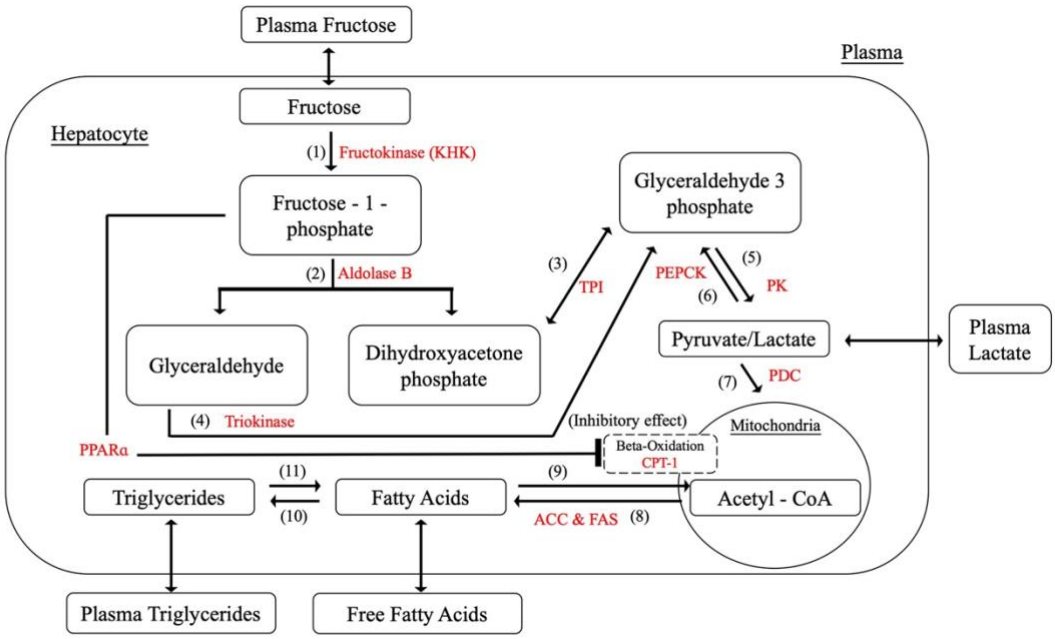

Figure 4-2. Hepatic fructose metabolism

Table 4-1. The rate equations for the hepatic variables in Section Hepatocytes (SH)

Hepatic Variables	Abbreviation	Rate Equations
Fructose	Fru	$\frac{dFru}{dt} = \mathrm{T}_{Fru} - \mathbb{R}_{KHK}$
Fructose-1-Phosphate	F1P	$\frac{dF1P}{dt} = \mathbb{R}_{KHK} - \mathbb{R}_{ald\mathrm{B}}$
Dihydroxyacetone phosphate	DHAP	$\frac{dDHAP}{dt} = \mathbb{R}_{ald\mathrm{B}} - \mathbb{R}_{TPI_{DHAP}} + \mathbb{R}_{TPI_{GA3P}}$
Glyceraldehyde	GA	$\frac{dGA}{dt} = \mathbb{R}_{ald\mathrm{B}} - \mathbb{R}_{Tri}$
Glyceradehyde-3-phosphate	GA3P	$\frac{dGA3P}{dt} = \mathbb{R}_{TPI_{DHAP}} - \mathbb{R}_{TPI_{GA3P}} + \mathbb{R}_{Tri} - \mathbb{R}_{PK} + \mathbb{R}_{PEPCK}$
Pyruvate/Lactate	Pyr	$\frac{dPyr}{dt} = T_{Lac} + \mathbb{R}_{PK} - \mathbb{R}_{PDC} - \mathbb{R}_{PEPCK}$

Acetyl-CoA	ACoA	$\frac{dACoA}{dt} = \mathbb{R}_{PDC} - 8\,\mathbb{R}_{FAS} + 8\,\mathbb{R}_{boxi}$
Fatty Acids (Palmitate)	FA	$\frac{dFA}{dt} = T_{FFA} + \mathbb{R}_{FAS} - \mathbb{R}_{boxi} - 3\,\mathbb{R}_{TGS} + 3\,\mathbb{R}_{Lply}$
Triglycerides	TG	$\frac{dTG}{dt} = T_{TG} + \mathbb{R}_{TGS} - \mathbb{R}_{Lply}$

4.2.2.2 The Distinctive Fructose Metabolic Pathways

Key enzymes and detailed reactions in hepatic fructose metabolism were demonstrated as follows. For (1) to (7), each section is named with reference to the enzyme that catalyses the reaction. The corresponding metabolic functions are listed in Table 4-2.

(1) Hepatic fructokinase (KHK)

$$Fructose + ATP \xrightarrow{KHK} Fructose - 1 - phosphate + ADP$$

Equ. 2 Hepatic Fructokinase

Hepatic fructokinase (KHK, EC 2.7.1.3), one of the three characteristic enzymes in human fructose metabolism, converts fructose into fructose-1-phosphate (F1P) by transferring one phosphate group from adenosine triphosphate (ATP). In contrast to glucose phosphorylation, there is no feedback inhibition for fructose which indicates that the activity of KHK is essentially free of regulatory control. Consequently, when sufficient fructose is available a significant amount of F1P enters subsequent metabolic reactions.

Also, since the Michaelis constant (Km) of KHK is lower than glucokinase, it has been shown that KHK is effectively 10-times faster than glucokinase in substrate phosphorylation (Patel et al., 2015). In terms of energy transport, even though guanosine triphosphate (GTP) can also be utilized in a similar way to ATP for this initial

phosphorylation reaction, it is only responsible for a minor proportion of the total process and the effect of GTP can be ignored in this equation.

(2) Aldolase B

$$Fructose - 1 - phosphate \xrightarrow{Aldolase\ B} Dihydroxyacetone\ phosphate + Glyceraldehyde$$

Equ. 3 Aldolase B

After phosphorylation, fructose-1-phosphate (F1P) undergoes further breakdown into two three-carbon components, namely dihydroxyacetone phosphate (DHAP) and glyceraldehyde (GA) by aldolase B. Aldolase B (E.C.4.1.2.13) is a liver-specific aldolase which can be considered the rate-limiting enzyme of hepatic fructose metabolism. Since little is known about the mechanism of aldolase B regulation, no strong allosteric control has yet been identified for this enzyme.

(3) Triose Phosphate Isomerase (TPI)

$$Dihydroxyacetone\ phosphate \overset{TPI}{\Longleftrightarrow} GA3P$$

Equ. 4 Triose Phosphate Isomerase

DHAP is isomerised to glyceradehyde-3-phosphate (GA3P) by triose phosphate isomerase (TPI) (E.C.5.3.1.1) rapidly and reversibly.

(4) Triokinase

$$Glyceraldehyde + ATP \xrightarrow{Triokinase} GA3P + ADP$$

Equ. 5 Triokinase

The primary pathway for the GA metabolism is through GA3P catalysed by triokinase (E.C.2.7.1.28). This reaction requires one phosphate molecule from ATP, releasing adenosine diphosphate (ADP). The activity of triokinase is allosterically activated by

ATP-Mg^{-2} and inhibited by both ATP and ADP, suggesting that this hepatic triokinase is regulated by the phosphorylation potential in the cytoplasm. Under normal conditions triokinase is fully activated.

(5) Pyruvate Kinase (PK)

$$GA3P + 2ADP + 2Pi \xrightarrow{PK} Pyruvate/Lactate + 2ATP$$

Equ. 6 Pyruvate Kinase

As pyruvate can be converted to lactate swiftly and reversibly, only one variable is used to denote this in the model. The pathways for glucose and fructose metabolism merge at the triose phosphate stage and become the same from this point onwards. GA3P is broken down to pyruvate relying on a series of enzyme reactions. The rate limiting enzyme in this process is pyruvate kinase (PK; E.C.2.7.1.40). Here we simplify the whole six-step conversion of GA3P to pyruvate by using PK. The phosphate in the GA3P and an additional free inorganic phosphate are combined with ADP molecules to produce two ATP molecules in this process. It should be noted that there are two GA3P molecules generated from one fructose molecule in the previous metabolic step, four ATP and two pyruvate molecules are therefore produced in the current reaction. Pyruvate kinase is allosterically controlled by acetyl-CoA.

(6) Phosphoenolpyruvate carboxykinase (PEPCK)

$$Pyruvate/Lactate + 2ATP + GTP \xrightarrow{PEPCK} GA3P + 2ADP + GDP + 2Pi$$

Equ. 7 Phosphoenolpyruvate Carboxykinase

Phosphoenolpyruvate carboxykinase (PEPCK) (E.C.4.1.1.32) is rate limiting in the conversion from pyruvate to GA3P, consuming two ATPs and one GTP. There is no identified allosteric regulation for PEPCK while numerous metabolites, such as insulin and fatty acids, are able to stimulate its production. Over-expression of PEPCK is believed to be associated with high production of glucose and the development of type 2 diabetes (Beale et al., 2007).

(7) Pyruvate Dehydrogenase Complex (PDC)

$$Pyruvate/Lactate + NAD^{+} \xrightarrow{PDC} Acetyl - CoA + NADH$$

Equ. 8 Pyruvate Dehydrogenase Complex

Pyruvate oxidation is regulated by the pyruvate dehydrogenase complex (PDC). This complex contains three enzymes that catalyse the conversion of pyruvate to acetyl-CoA. PDC is allosterically inhibited in a feedback mechanism by acetyl-CoA to prevent its over-production, which could result in mitochondrial stress.

(8) Fatty acid synthesis

$$8\ Acetyl - CoA + 7\ ATP \xrightarrow{ACC\ \&\ FAS} Fatty\ acid\ (Palmitate) + 7\ ADP + 7Pi$$

Equ. 9 Fatty Acid Synthesis

Lipogenesis describes the process of fatty acid synthesis and triglyceride synthesis. With the mediation of acetyl-CoA carboxylase (ACC) (E.C.6.4.1.2) and fatty acid synthase (FAS) (E.C.2.3.1.85), acetyl-CoA is converted into malonyl-CoA. Malonyl-CoA provides the two-carbon structure for producing both short and long chain fatty acids. There are two isoforms of ACC found in the hepatic metabolism as ACC1 contributes to lipogenesis and ACC2 to beta-oxidation. Palmitate (16:0), as the most common saturated fatty acid, has been chosen to represent fatty acids in this model for the purpose of simplification. Thus, eight acetyl-CoA molecules are consumed to synthesize one palmitate molecule. High concentrations of fatty acids are able to suppress this process allosterically.

(9) Beta-Oxidation

$$Fatty\ acid\ (Palmitate) + 2\ ATP \xrightarrow{CPT-1\ (PPAR\alpha)} 8Acetyl - CoA + AMP + ADP + 3Pi$$

Equ. 10 Beta-Oxidation

Hepatic carnitine palmitoyltransferase I (CPT-1) (E.C.2.3.1.21) is the rate-controlling enzyme of beta-oxidation. The metabolic process breaks down fatty acids to generate

acetyl-CoA (Lim et al., 2010). Since malonyl-CoA is the main inhibitor for CPT-1, it supresses beta-oxidation allosterically. To simplify the equation, the inhibitory effect of malonyl-CoA is substituted by acetyl-CoA as the pathway of acetyl-CoA to produce malonyl-CoA is unidirectional. By contrast, it has been discovered recently that peroxisome proliferator-activated receptors (PPARs) promote beta-oxidation by upregulating the expression of CPT1 (Kersten, 2014). However, this regulation can be prevented by the production of fructose-1-phosphate (Nomura and Yamanouchi, 2012). Therefore, fructose-1-phosphate is also considered to be an allosteric inhibitor in the process of beta-oxidation.

(10) Triglyceride Synthesis

$$3\ Fatty\ acids\ (Palmitate) + 3\ ATP \xrightarrow{Glycerol-3-phosphate} Triglyceride + 3AMP + 7Pi$$

Equ. 11 Triglyceride Synthesis

During triglyceride synthesis, three fatty acid molecules and one glycerol backbone from glycerol-3-phosphate are combined to produce triglyceride under the influence of coenzyme A (CoA) and several acyltransferases. Glycerol-3-phosphate is denoted as GA3P due to the rapid exchange rate between these two molecules. Triglyceride synthesis is regulated by insulin and glucagon.

(11) Lipolysis

$$Triglyceride \xrightarrow{Triacylglycerol\ lipase} Glycerol + 3Fatty\ acids\ (Palmitate)$$

Equ. 12 Lipolysis

Three fatty acids are released when one triglyceride breaks down. The rate-determining enzyme during this process is triacylglycerol lipase (E.C.3.1.1.3). The concentration of hepatic triglyceride is regulated by insulin and glucagon under normal circumstances.

Table 4-2. The processes of metabolic reactions and rate functions in the fructose model

	Key Enzymes/Reactions	Abbreviation	Rate Functions
(1)	Fructokinase	KHK	$\mathbb{R}_{KHK} = \mathrm{V}_{KHK} * \frac{Fru^{nf}}{{Km_{KHK}}^{nf} + Fructose^{nf}} * \frac{ATP^{nATP}}{{Km_{ATP}}^{nATP} + ATP^{nATP}}$
(2)	Aldolase B	AldB	$\mathbb{R}_{aldB} = V_{aldB} * \frac{F1P^{nF1P}}{{Km_{F1P}}^{nF1P} + F1P^{nF1P}}$
(3)	Triose phosphate isomerase	TPI	$\mathbb{R}_{TPI\_DHAP} = V_{TPI\_DHAP} * \frac{DHAP^{nDHAP}}{{Km_{DHAP}}^{nDHAP} + DHAP^{nDHAP}}$ $\mathbb{R}_{TPI\_GA3P} = V_{TPI\_GA3P} * \frac{GA3P^{nGA3P}}{{Km_{GA3P\_TPI}}^{nGA3P} + GA3P^{nGA3P}}$
(4)	Triokinase	Tri	$\mathbb{R}_{Tri} = V_{Tri} * \frac{GA^{nGA}}{{Km_{GA}}^{nGA} + GA^{nGA}} * \frac{{ATP_{Mg^{2-}}}^{nATP_{Mg^{2-}}}}{{Km_{ATP_{Mg^{2-}}}}^{nATP_{Mg^{2-}}} + {ATP_{Mg^{2-}}}^{nATP_{Mg^{2-}}}} * \left(1 - \beta_{ATP} \frac{ATP}{K_i^{ATP} + ATP}\right)\left(1 - \beta_{ADP} \frac{ADP}{K_i^{ADP} + ADP}\right)$
(5)	Pyruvate kinase	PK	$\mathbb{R}_{PK} = V_{PK} * \frac{GA3P^{nGA3P}}{{Km_{GA3P}}^{nGA3P} + GA3P^{nGA3P}} * \frac{ADP^{nADPpk}}{{Km_{ADPpk}}^{nADP} + ADP^{nADPpk}} * \left(1 - \beta_{ACoA-PK} \frac{ACoA}{K_i^{ACoA-PK} + ACoA}\right)$
(6)	Phosphoenolpyruvate carboxykinase	PEPCK	$\mathbb{R}_{PEPCK} = V_{PEPCK} * \frac{Pyr}{K_m^{PEPCK} + Pyr} * \frac{ATP}{K_m^{ATPpepck} + ATP} * \frac{GTP}{K_m^{GTP} + GTP}$
(7)	Pyruvate oxidation	PDC	$\mathbb{R}_{PDC} = V_{PDC} * \frac{Pyr}{K_m^{Pyr} + Pyr} * \left(1 - \beta_{ACoA-PDC} \frac{ACoA}{ACoA + k_i^{CoA-pyr}}\right)$

(8)	Fatty acid synthesis	FAS	$\mathbb{R}_{FAS} = V_{FAS} * \frac{ACoA}{K_m^{ACoA} + ACoA} * \frac{ATP}{K_m^{ATPfas} + ATP} * \left(1 - \beta_{FA} \frac{FA}{FA + k_i^{FA-inhib}}\right)$
(9)	Beta-oxidation	boxi	$\mathbb{R}_{boxi} = V_{boxi} * \frac{FA}{K_m^{boxi} + FA} * \frac{ATP}{K_m^{ATPboxi} + ATP} * \left(1 - \beta_{boxi} \frac{ACoA}{ACoA + k_i^{CoA-boxi}}\right) * \left(1 - \beta_{PPAR\alpha} \frac{F1P}{F1P + k_i^{F1P-inhib}}\right)$
(10)	Triglyceride synthesis	TGS	$\mathbb{R}_{TGS} = V_{TGS} * \frac{FA}{K_m^{FA} + FA} * \frac{GA3P}{K_m^{GADP} + GADP}$
(11)	Lipolysis	Lply	$\mathbb{R}_{Lply} = V_{Lply} * \frac{TG}{K_m^{TG} + TG}$

4.2.3 Stage Two: Model Expansion with Fluid Flow and Cross-Membrane Transportation

4.2.3.1 Hepatic Bloodstream – Cross-Membrane Exchange

As previously reviewed in Section 2.1.1 and 2.1.2, the liver receives the inflow from hepatic arteries, portal veins and bile ducts, as seen in Figure 4-3, then drains into central veins, eventually to hepatic veins, which allow hepatocytes to be exposed to nutrients, hormones (insulin and glucagon) and oxygen (Hijmans et al., 2014).

Please noted that Figure 4-3 has been presented once previously in Section 2.1.2.

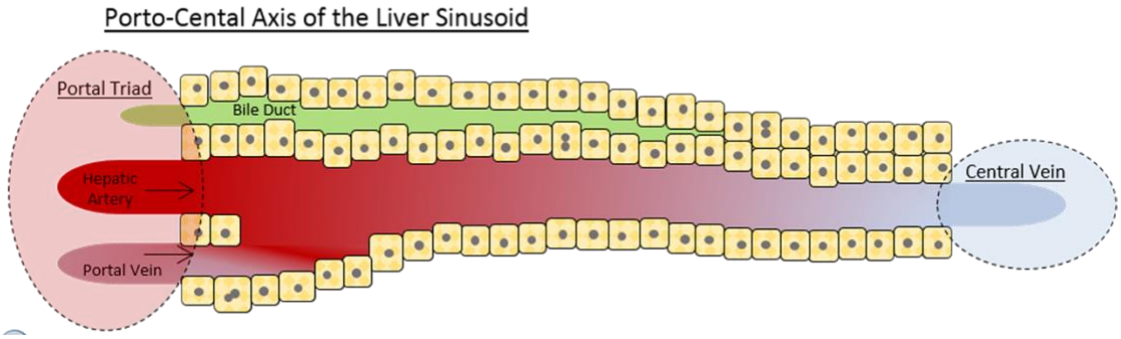

Figure 4-3. The blood flow across the liver sinusoid.

(adopted from Ashworth (2017))

As applied in König et al. (2012) and Ashworth et al. (2016), an altered Michaelis-Menten equation is employed for cross-membrane exchange.

For unidirectional transportation, the model considers the components in the Hepatic Bloodstream as substrates and the corresponding molecules in the hepatocytes as products. For bidirectional exchange the equation for transport (T) is:

$$T_{SHB \rightarrow SH} = \frac{V_{\max(S_{SHB} - S_{SH})}}{K_m + S_{SHB} + S_{SH}}$$

Equ. 13 Bidirectional Exchange for Cross-Membrane Transport

where the (section) Hepatic Bloodstream is denoted as SHB and (section) Hepatocytes denoted as SH.

The transportation and exchange rates of fructose, pyruvate/lactate, fatty acids and triglyceride between SHB and SH are summarised in Table 4-3. The constant R_{HE}= 4 is used to represent the ratio of the total number of hepatocytes to the volume of the hepatic bloodstream as described in Ashworth et al. (2016). The rate equations in SHB are listed in Table 4-4.

Fructose is absorbed from the gut lumen and transported across the brush border membrane into the hepatic portal vein via an energy-dependent process involving GLUT5 and GLUT2, in which GLUT5 has a high specificity to fructose (Douard and Ferraris, 2008).

After fructose uptake from the gut, plasma fructose is observed experimentally to rise only by micromolar levels, implying that hepatocytes have the capacity to uptake the majority of fructose during the first-pass through the liver (Tappy and Lê, 2010). Therefore, both GLUT2 and GLUT5 are included in the model and where the Michaelis-Menten constant of GLUT2 has a lower value than that of GLUT5 as reported previously (Wright et al., 2012).

In addition, glucose transporter 8 (GLUT8) has also been mentioned in terms of hepatic fructose transportation (DeBosch et al., 2014, Manolescu et al., 2007). However, as the

expression of GLUT8 is relatively low in mice in comparison to GLUT5 and GLUT2 even with high-fructose exposure, and the fact that the exact mechanism of this transporter in humans remains largely unknown, the effect of GLUT8 is considered negligible in the current model (Ferraris et al., 2018).

Table 4-3. The Michaelis constants used in the fructose model

Transport Variables	Rate Functions for cross-membrane transportation
Fructose	$T_{Fru} = V_{GLUT2}^{pump} * \frac{Fru_{SHB}}{K_m^{GLUT2-pump} + Fru_{SHB}} + V_{GLUT2}^{ex} * \frac{Fru_{SHB} - Fru_{SH}}{K_m^{GLUT2-ex} + Fru_{SHB} + Fru_{SH}} + V_{GLUT5}^{pump} * \frac{Fru_{SHB}}{K_m^{GLUT5-pump} + Fru_{SHB}} + V_{GLUT5}^{ex} * \frac{Fru_{SHB} - Fru_{SH}}{K_m^{GLUT5-ex} + Fru_{SHB} + Fru_{SH}}$
Pyruvate/Lactate (Simplified from Ashworth et al. (2016))	$T_{Pyr} = V_{Pyr}^{ex} * \frac{Pyr_{SHB} - Pyr_{SH}}{K_m^{Pyr-ex} + Pyr_{SHB} + Pyr_{SH}}$
Fatty acids (Palmitate) (Simplified from Ashworth et al. (2016))	$T_{FA} = V_{FA}^{ex} * \frac{FA_{SHB} - FA_{SH}}{K_m^{FA-ex} + FA_{SHB} + FFA_{SH}} + V_{active} * \frac{FA_{SHB}}{(K_m^{active} + FA_{SHB})}\left(1 + \frac{Ins}{Ins_{ref}^{active}}\right)$
Triglyceride (Simplified from Ashworth et al. (2016))	$T_{TG} = V_{TG}^{ex} * \frac{\left(TG_{SHB} - \frac{TG_{SH}}{TG_{ref}}\right)}{K_m^{TG-ex} + TG_{SHB} + \frac{TG_{SH}}{TG_{ref}}} - V_{out} * \frac{TG_{SH}}{(K_m^{out} + TG_{SH})}$

Table 4-4. The rate equations in Section Hepatic Bloodstream (SHB)

Exchanging Variables	Rate Equations in Section Hepatic Bloodstream (SHB)
Fructose	$\frac{dFru_{SHB}}{dt} = -T_{Fru} * R_{HE} + R_{BS} * (Fru_{SBC} - Fru_{SHB})$
Pyruvate/Lactate (Simplified from Ashworth et al. (2016))	$\frac{dPyr_{SHB}}{dt} = -T_{Pyr} * R_{HE} + R_{BS} * (Pyr_{SBC} - Pyr_{SHB})$
Fatty acids (Palmitate) (Simplified from Ashworth et al. (2016))	$\frac{dFA_{SHB}}{dt} = -T_{FA} * R_{HE} + R_{BS} * (FA_{SBC} - FA_{SHB})$
Triglyceride (Simplified from Ashworth et al. (2016))	$\frac{dTG_{SHB}}{dt} = -T_{TG} * R_{HE} + R_{BS} * (TG_{SBC} - TG_{SHB})$

4.2.3.2 Bloodstream Circulation - Rest of the Body

Since circulation of the bloodstream around the body takes approximately one minute to complete, the rate of blood flow circulation is set to be $R_{BS} = \frac{1}{60} \approx 0.167\ \mathrm{s}^{-1}$. Also, as the blood volume of the whole body and the liver are considered to be approximately 5L and 0.8L, respectively, in an average person, the ratio of the rest of body to the liver R_{RL} is set as: $R_{RL} = 5 - 0.8/0.8 \approx 5.25$ (Ashworth et al., 2016, Eipel et al., 2010, Critchley and Critchley, 1999, Arias, 1994, Davy and Seals, 1994).

As mentioned above (2.1.1), about 75-80% of blood flow in the liver are supplied by the portal vein and the other 20-25% are delivered by the hepatic artery (Sibulesky, 2013). The portal vein is the place where collects the outflows of the spleen, stomach, small and large intestine, gallbladder as well as the pancreas. Passing through the liver, the blood stream then flows out of the liver via hepatic veins to the rest of the body (Eipel et al., 2010). When the liver is impaired and dysfunction, for instance, under the cirrhotic condition, hepatic resistance to portal vein would occur and then result in portal hypertension (Tsochatzis et al., 2014).

The equation representing the blood circulation (C) from (section) Hepatic Bloodstream (SHB) to (section) Bloodstream Circulation (SBC) is in the following form:

$$C_{SBC \to SHB} = \frac{R_{BS} * (C_{SBC} - C_{\mathrm{SHB}})}{R_{RL}}$$

Equ. 14 Bloodstream Circulation

The rate equations in SBC are listed in Table 4-5.

Table 4-5. The rate equations in Section Bloodstream Circulation (SBC)

Exchanging Variables	Rate Equations in Section Bloodstream Circulation (SBC)
Fructose	$\frac{dFru_{SBC}}{dt} = Meal_{Fru} + C_{Fru}$
Pyruvate/Lactate (Simplified from Ashworth et al. (2016))	$\frac{dPyr_{SBC}}{dt} = C_{Pyr}$
Fatty acids (Palmitate) (Simplified from Ashworth et al. (2016))	$\frac{dFA_{SBC}}{dt} = C_{FA} - USE_{FA} + UP_{FA}$
Triglyceride (Simplified from Ashworth et al. (2016))	$\frac{dTG_{SBC}}{dt} = C_{TG} - USE_{TG} + UP_{TG}$

4.2.4 Stage Three: Model Combination with Glucose Metabolism and Hormonal Regulation

4.2.4.1 Additional Dietary Input - Glucose

As demonstrated in Section 2.4.2.1, dietary pattern rarely contains one nutrient (fructose) only. Glucose, as the major energy source, extensively exists in daily intake. Also, after a mixed meal, dietary disaccharides and polysaccharides such as sucrose, HFCS and starches would be broken down into the various proportions of monosaccharides. Therefore, fructose and glucose as the principle simple sugars in diet have been selected as the dietary inputs for the model at this stage. Figure 4-4 shows that glucose was added to the model as an alternative dietary input to fructose.

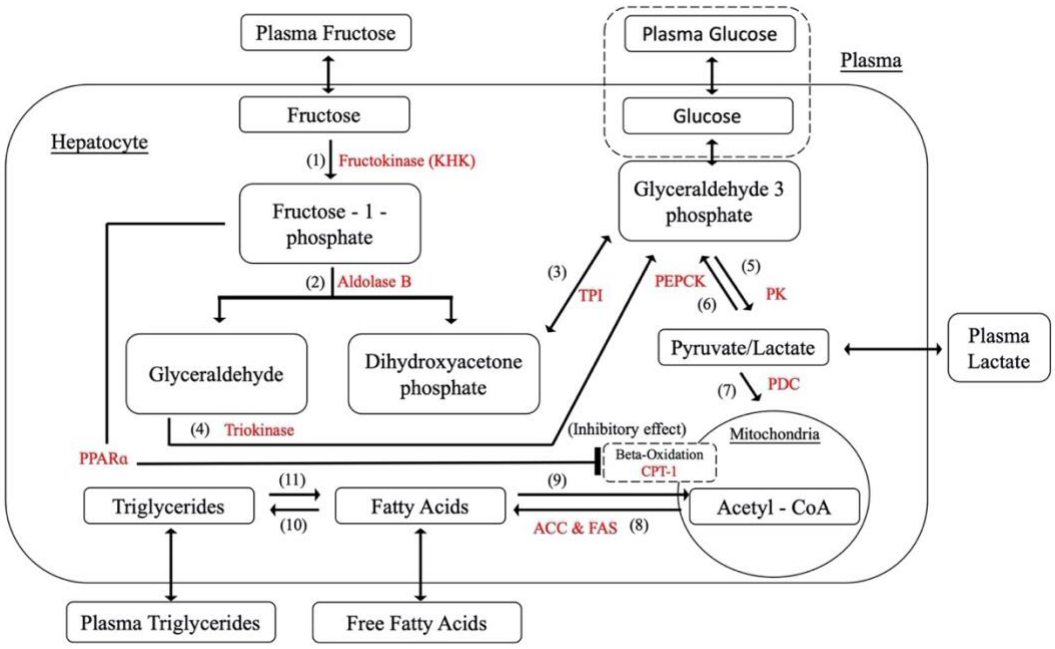

Figure 4-4. Hepatic fructose metabolism with glucose input.

4.2.4.2 Glucose Metabolism Simplification

Hepatic glucose metabolic pathways are exhibited in Figure 4-5. Please noted that this figure has been presented once previously in Section 2.4.2.2.

During glycogenesis, glucose is firstly metabolized into glucose-6-phosphate by glucokinase. Glucose-6-phosphate (G6P) then is converted into glucose-1-phosphate (G1P) by phosphoglucomutase and further evoke glycogen formation. The liver breaks down glycogen into glucose and produce ATP as well as nicotinamide adenine dinucleotide (NADH) via the glycolysis pathway.

After phosphorylation of glucose, G6P is catalysed into fructose-6-phosphate (F6P), further to fructose-1,6-di-phosphate by phosphofructokinase. Then fructose-1,6-di-phosphate is converted into pyruvate and entry into the TCA cycle, which takes place in mitochondrion (Berg et al., 2002).

Relevant equations are simplified from model constructed by Ashworth et al. (2016), as presented in Table 4-6.

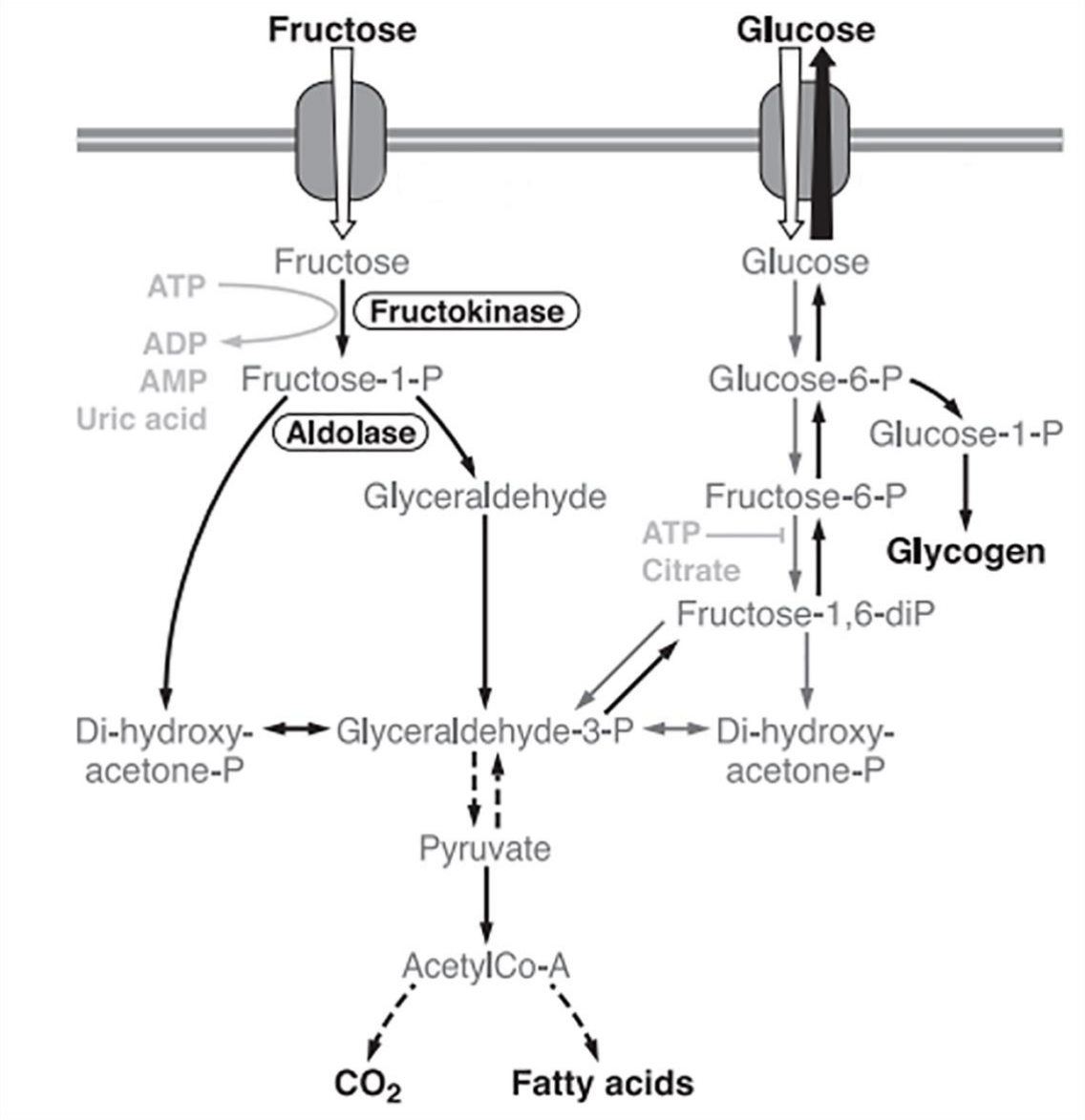

Figure 4-5. Hepatic Fructose VS Glucose metabolism.

(adopted from (Tappy and Lê, 2010))

Table 4-6. The relevant equations of glucose feeding

(Simplified from Ashworth et al. (2016))

Exchanging Variables	**Rate Equations in Section Hepatic Bloodstream (SHB)**
Glucose	$\frac{dGlu_{SHB}}{dt} = -T_{Glu} * R_{HE} + R_{BS} * (\mathrm{Glu}_{SBC} - Glu_{SHB})$
Exchanging Variables	**Rate Equations in Section Bloodstream Circulation (SBC)**
Glucose	$\frac{dGlu_{SBC}}{dt} = Meal_{Glu} + C_{Glu} - USE_{Glu} - UP_{FA} - UP_{TG}$
Hepatic Variables	**Rate Equations**
Glucose (Glu)	$\frac{dGlu}{dt} = \mathrm{T}_{Glu} - \mathbb{R}_{GK} + \mathbb{R}_{G6Pase}$
Glucose-6-phosphate (G6P)	$\frac{dG6P}{dt} = \mathbb{R}_{GK} - \mathbb{R}_{G6Pase} + \mathbb{R}_{FBP} - \mathbb{R}_{PFK}$
Key Enzymes/Reactions	**Rate Functions**
$\mathbf{T_{Glu}}$ - Glucose transportation	$T_{Glu} = V_{GLUTG}^{pump} * \frac{Glu_{SHB}}{K_m^{GLUTG-pump} + Glu_{SHB}} + V_{GLUTG}^{ex} * \frac{Glu_{SHB} - Glu_{SH}}{K_m^{GLUTG-ex} + Glu_{SHB} + Glu_{SH}}$
Glucokinase (GK)	$\mathbb{R}_{GK} = \mathrm{V}_{GK} * \frac{Glu^{nGlu}}{{Km_{Glu}}^{nGlu} + Glu^{nGlu}} * \frac{ATP^{nATP}}{{Km_{ATPgk}}^{nATP} + ATP^{nATP}} * \left(1 - \frac{G6P}{G6P + k_i^{G6P}}\right)$
Glucose-6-phosphatase (G6Pase)	$\mathbb{R}_{G6Pase} = V_{G6Pase} * \frac{G6P}{K_m^{G6Pase} + G6P}$
Fructose-bisphosphatase (FBP)	$\mathbb{R}_{FBP} = V_{FBP} * \frac{GA3P}{K_m^{FBP} + GA3P}$
Phosphofructokinase (PFK)	$\mathbb{R}_{PFK} = V_{PFK} * \frac{G6P}{K_m^{PFK} + G6P} * \frac{ATP}{Km_{ATPpfk} + ATP} * \left(1 - \frac{ATP}{ATP + k_i^{ATPfpk}} * \frac{ADP}{ADP + k_i^{ADPfpk}}\right) * \left(1 - \beta_{PFK} \frac{GA3P}{GA3P + k_i^{GA3Ppfk}}\right)$

4.2.4.3 Hormonal Regulation Simplification

The settings for hormone regulation including insulin and glucagon secretion into the bloodstream (SBC) are based on the model constructed by Hetherington et al. (2012), while the hormonal equations in the liver blood flow (SHB) are simplified from the model built by Ashworth et al. (2016).

4.2.4.4 Additional Settings

In addition to the liver, the amount of each key variable (fructose, glucose, pyruvate/lactate, fatty acid and triglyceride) generated ($USE_{variable}$) and used ($UP_{variable}$) by other body sections such as adipose tissues and muscle tissues are set to be the same as the equations described by Ashworth et al. (2016).

4.3 Model Simulations

Simulations were generated using MATLAB_R2019a (MATLAB, RRID:SCR_001622). Function 'ode45' was used to solve all the ordinary differential equations simultaneously. The default solver setting is listed in Table 4-7. The units of metabolite concentration and reaction rate are presented in micromoles/litre (μM/L) and micromoles/second (μM/s), respectively. The time lengths of the simulations have been set to run over a 12-hour period incorporating 3 meals.

Table 4-7. Function 'ode45' solver setting.

Function	Stage	Order	Solver type	Method
ode45	Six	Fifth	Single-step; Solve non-stiff differential equation	An explicit Runge-Kutta (4,5) formula (the Dormand-Prince pair)

5 Chapter 5: Model Validation and Enhancement

5.1 Chapter Introduction

To validate and improve the fructose model, the modelling results of the whole simulation process consisting of four stages were demonstrated and evaluated as reported in this chapter. These four stages build from a basic fructose metabolism, adding glucose, adding insulin resistance and finally testing potential therapeutic targets.

5.2 Model Testing Design

The first stage presents the basic model behaviour of hepatic fructose metabolism. It is the initial stage that only focuses on Section Hepatocytes (SH) and is used to predict hepatic fatty acids and triglyceride concentrations. This stage was set to test whether the model was functioning properly and generating logical predictions.

As elaborated in previous chapter (4.2.3 and 4.2.4), Stage Two was built and expanded on the basis of Stage One, adding glucose as a separate energy input and two additional sections to mimic body bloodstream circulations. Two scenarios were constructed at this stage for the purpose of model validation. The first predicts lipid concentrations resulting from different dietary consumptions while the second explores the variability of biochemical reaction kinetics rate within the general population.

At Stage Three, model performance with insulin resistance (IR) simulation was delivered. As IR is one of the pathophysiological hallmarks in NAFLD patients, the aim at this stage

is to examine how the model would react to abnormal metabolic conditions and whether it could predict the expected lipid deposition patterns under the effects of isocaloric and hypercaloric diets. Additionally, one of the simulations at Stage Three would be applied in the following stage, showing a representation of a simple pre-steatosis condition (early stage of NAFLD) for further potential treatment explorations.

Finally, Stage Four investigates the impacts of potential interventional targets, pyruvate kinase (PK), fructokinase (KHK) and peroxisome proliferator-activated receptors alpha (PPARα), as well as the synergistic effect of these three foci. The pairwise comparisons between these three targets were conducted accordingly. Both moderate and severe IR conditions were simulated to discover the interventional outcomes. This stage is to explore the effectiveness and robustness of current model in novel therapy design.

Some figures in this chapter, mainly at Stage Two, along with several descriptions of text were published in Liao et al. (2020).

5.3 Results and Discussion

5.3.1 Stage One: Basic Model Behaviour of Hepatic Fructose Metabolism

Corresponding to Section 4.2.2 in the model construction chapter, the results of Stage One presented the initial model behaviour of fructose metabolism within the liver section. The simulations were conducted under the assumption that there is no further demand from utilisation or transportation of metabolites outside the liver. The main purpose at this first stage was to test whether the model was functioning properly and whether it was able to

generate rational predictions, rather than matching the exact numbers with clinical or experimental data.

Only nine hepatic variables which were considered as distinctive components in the fructose pathways were included at this stage. Three meals with an equal quantity of pure fructose were simulated at time points 8:00, 12:00 and 16:00, respectively. An arbitrary number was assigned to fructose input since the range of fructose concentrations in clinical and experimental data can vary largely in magnitude depending on different detection methods: from 0.008 to 16mM (Douard and Ferraris, 2013, Patel et al., 2015). Also, the effect of varying fructose intake on hepatic fatty acids and triglycerides was explored as a part of the model presentations. Three diets were simulated: a baseline diet, a high fructose diet (with a 25% increase compared to baseline) and a very high fructose diet (with a 50% increase compared to baseline). The initial values of all variables were set to zero.

The plots of the nine key variables are displayed in Figure 5-1, representing the basic model performance of hepatic fructose metabolism in response to fructose consumption. As shown in Figure 5-1, the black line shows that each input cycle takes two hours to digest a fructose meal and to reach the peak value of hepatic fructose concentration. This behaviour is slightly different from the clinical data (Chong et al., 2007, Low et al., 2018), which achieves a summit in around one hour and has a longer steadier decreasing tail after one meal. The discrepancy is caused by the simplification of dietary input, which was set as a high-power sine equation. However, this simplification is acceptable as it does not affect the subsequent model behaviours in lipid profiles.

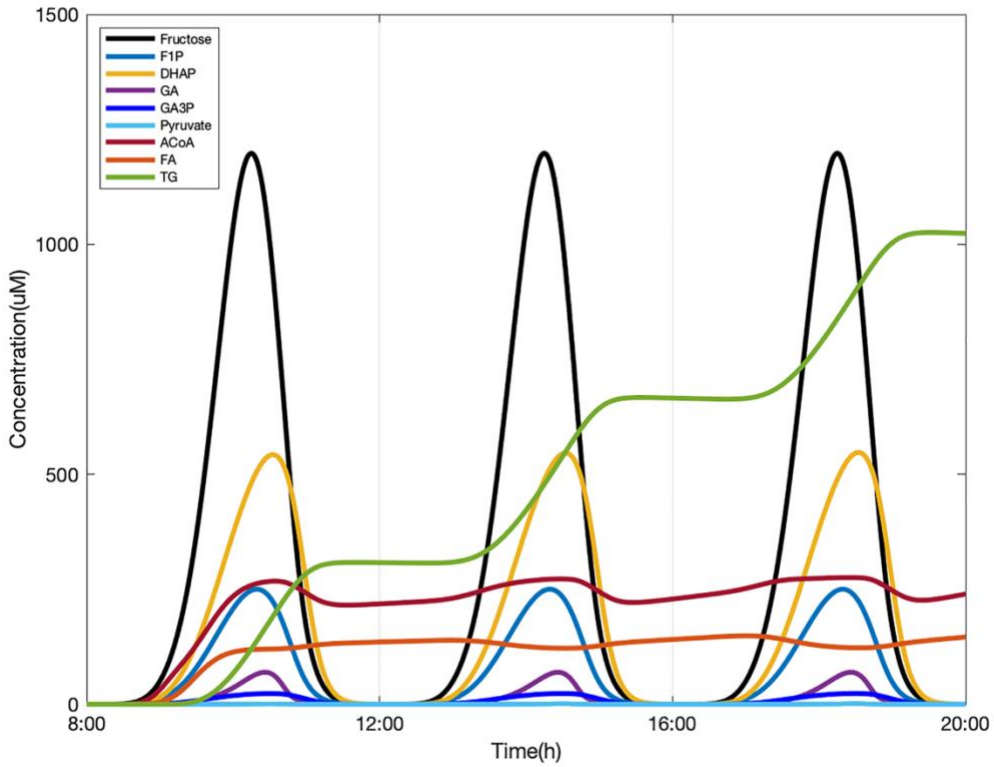

Figure 5-1. Baseline model behaviour of hepatic fructose metabolism.

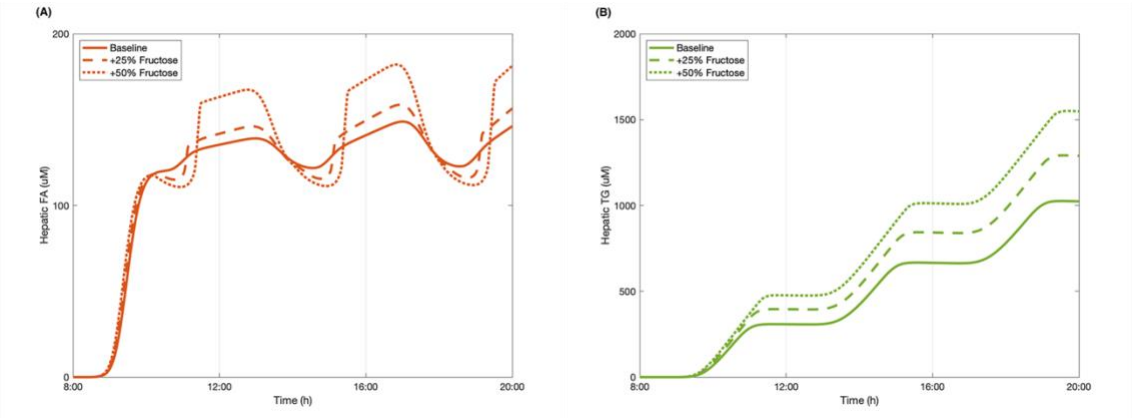

Figure 5-2. The change of hepatic lipid concentration after different fructose intakes.

(A) Hepatic FA and (B) Hepatic TG.

Apart from acetyl-CoA, fatty acids and triglycerides, the concentrations of the other variables increased gradually after the meals and then dropped back to baseline along the time axis. For acetyl-CoA and fatty acids, their postprandial values were raised after breakfast and then fluctuated periodically within a certain range after lunch and dinner. These behaviours suggest that neither acetyl-CoA nor fatty acids were consumed completely by the liver after fructose feeding. However, they showed a tendency that they were able to reach an equilibrium state after three meals. Additionally, triglycerides presented a stable growth pattern with constant accumulations. This plot indicates that fructose input has been converted into triglycerides over three meals.

In addition, the results of hepatic lipid accumulation after inducing fructose diets are presented in Figure 5-2. As shown in Figure 5-2A, when fructose exposure is increased by 25% and 50% per meal, the levels of hepatic fatty acids rise and fall more dramatically. Higher fructose intake results in more erratic fluctuations. In terms of hepatic triglycerides, Figure 5-2B reveals that this product accumulates in a dose-dependent manner.

The results of this stage suggest that the kinetic equations are constructed properly and the model is performing logically and is obeying the law of conservation of mass.

5.3.2 Stage Two: Scenario Construction and Validation after Model Combination

5.3.2.1 Scenario One: The Effect of Varying Carbohydrate Intake on Lipid Accumulation

After feeding, carbohydrates are processed in the digestive system and enter the hepatic portal system. According to the Dietary Guideline for Americans (2015-2020) (Health and Services, 2015), daily caloric intake of a healthy adult is in the range of 1600kcal to

3000kcal, of which, 45-65% are derived from carbohydrates. Therefore, in this scenario where we explore dietary inputs, we set up the baseline to reflect a midpoint caloric consumption of 2400kcal per day and 50% of this energy source to be obtained from carbohydrates. A total amount of 300g/day carbohydrates (4kcal/g) was set to be taken up into the body from the diet. The remaining calorie intake would be comprised of proteins and fats. However, as this scenario has been set to examine the effects of carbohydrates in the liver, protein and fat inputs are not considered in this section.

As described above, a dietary setup was created in which 100g of carbohydrates were consumed by healthy subjects for each meal (3/day). Here we tested the effect of three different diets on lipid deposition, including: a 100% fructose meal, a mixed meal (50:50 fructose and glucose), and a 100% glucose meal, representing two extreme conditions and one more realistic setting. The results of these simulations are presented in Figure 5-3. The levels of hepatic fatty acids (FA), triglycerides (TG), plasma free fatty acids (FFA), triglycerides, as well as blood glucose were predicted after three meals. The model takes approximately an hour for the initial transient phase before establishing a set of consistent predictions.

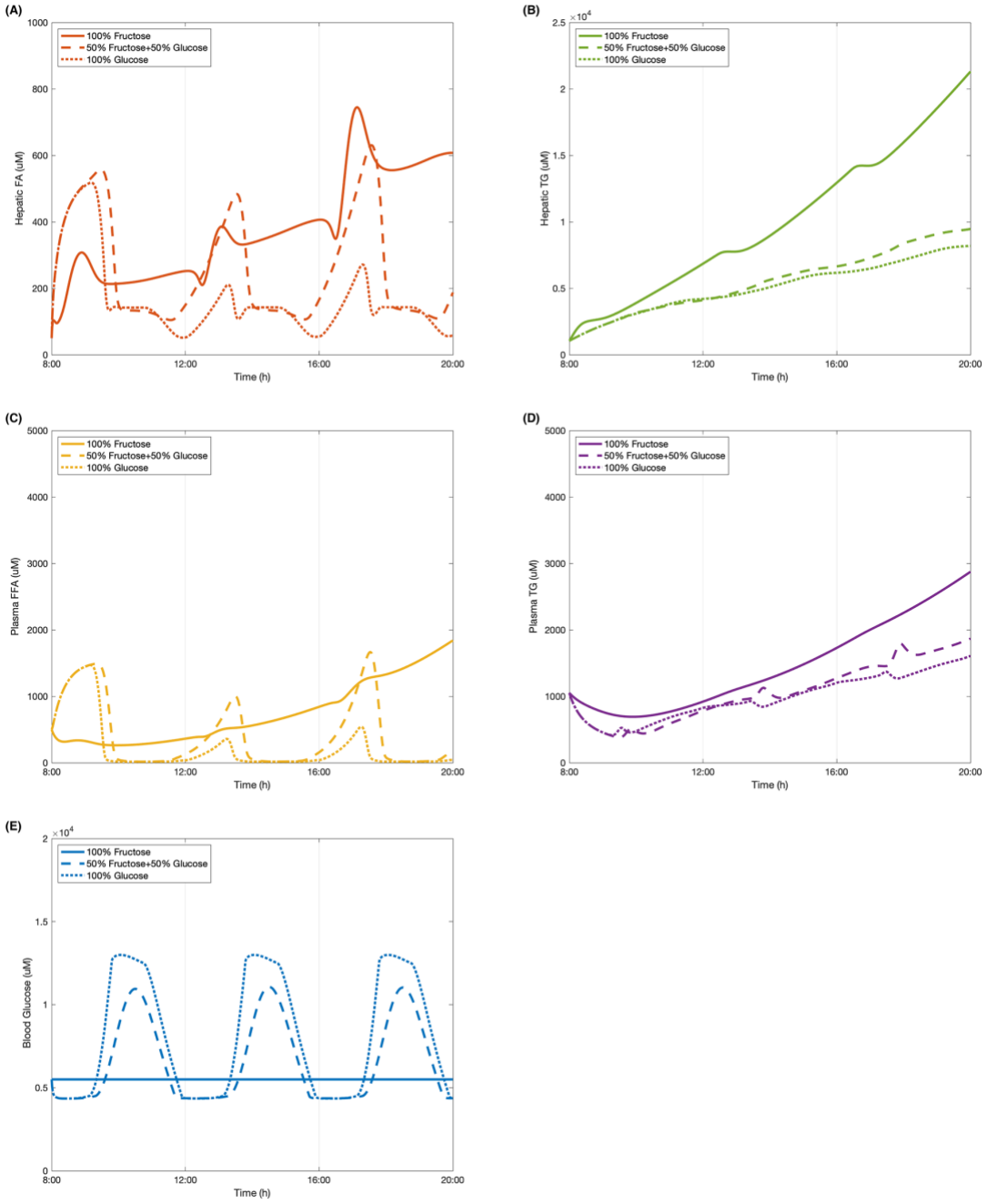

Figure 5-3. The change of lipid accumulation after different dietary intakes.

(A) Hepatic FA, (B) Hepatic TG, (C) Plasma FFA, (D) Plasma TG, and (E) Blood Glucose.

As shown in Figure 5-3A, hepatic fatty acids started decreasing after the first meal and reached a peak at around 13:00 in the fructose feeding group and approximately 13:30 in both glucose and the mixed diet subjects. These decreasing patterns are due to the mechanism that three fatty acids are required to generate one triglyceride after meals during the triglyceride synthetic process. After the second meal, the subsequent peak time of fatty acid levels stimulated by all three diets was observed between 17:00-18:00, and again the fructose group took slightly less time to achieve the peak value. As stated in Section 2.4.2.2, this phenomenon could be explained by the mechanism that fructose has the capability to bypass the key rate-controlling regulatory enzyme of glycolysis in the glucose metabolism.

Even though the consumption of 50% glucose and 50% fructose resulted in the highest level of hepatic fatty acids for the first peak, a significantly higher concentration was induced by the fructose diet after the second meal. The glucose feeding group was found to have the lowest levels of fatty acids over the observation period. The concentration of hepatic FA in the mixed-meal feeding group displayed stronger periodic behaviour than in the other two extreme conditions. These phenomena occurred because of the hormonal regulation settings: fructose does not react to insulin regulation; the mixed meal responses slower to hormonal control than the pure glucose diet as it contains lower glucose content; hence the mixed meal has highest value at the beginning of the model simulations and also have the strongest periodic behaviour among three groups.

In terms of hepatic triglyceride (Figure 5-3B), the plots of the glucose group and the mixed-carbohydrate group overlapped for several hours after breakfast. From around 13:00, the mix group started accumulating larger amounts of hepatic triglycerides than

that of the glucose group. After consumption of the fructose-only diet, triglyceride concentration presents a relatively dramatic increasing growth trend leading to the highest levels observed. These plots suggest that, in an isocaloric diet, fructose tends to exacerbate lipid accumulation in the liver.

In addition to hepatic lipid concentrations, Figure 5-3C and Figure 5-3D show the plasma levels of free fatty acids and triglycerides respectively. Similar to the periodic patterns of hepatic fatty acids, free fatty acids in the plasma declined over several hours before developing the first peak. For both mixed-sugar feeding and glucose only groups, the levels of free fatty acids then returned to baseline after about 30 minutes. The second peaks of these two groups generated slightly higher values than the first peaks before again reducing to the baseline. Regarding the 100% fructose model, this showed a smaller fluctuation than the other two diets and presented a flattened profile, and was not seen to drop back to the baseline level. Consistent with hepatic FA observations, plasma FFA peaked earlier in the fructose group than the others. Again, these plots reflect that fructose metabolism could not be regulated by hormonal secretion. Therefore, fructose was absorbed and digested faster to produced lipid profiles, in comparison with glucose.

Considering plasma triglyceride levels (Figure 5-3D), the fructose diet produced the highest concentrations throughout the model simulation. After breakfast, the glucose group contributed to greater triglyceride production than that induced by the mixed group. However, this phenomenon shifted over during the 12:00-13:00 period where the mixed sugar group outgrew the glucose meal and continued increasing plasma triglyceride levels after second meal exposure. The reason for this change is due to the insulin regulation of glucose homeostasis.

Blood glucose levels were also simulated after consuming different proportions of monosaccharides. A baseline normal blood glucose level was established within the model and the effects of the meals examined in addition to this. As presented in Figure 5-3E, the predicted peak values for each diet model throughout the period were equal in magnitude since the three meals were divided and induced equally. After pure fructose meals, blood glucose stayed relatively constant along the time period, while for the pure glucose group and the mixed-sugar group, both of them caused dynamic periodic oscillations. It is apparent that blood glucose responded more strongly to the pure glucose diet than the mixed diet. As the models were considering healthy individuals, the effects of insulin in mediating cellular glucose uptake from the blood became more apparent once levels exceeded upper normal values (>1.2mmol), which can be observed as a blunting of the peak glucose levels in the figure.

Overall, it can be observed that it took approximately 5 hours on average to digest dietary meals containing 100g carbohydrates to subsequently achieve peak values in lipid profiles. Compared to fatty acids, triglycerides in the liver and plasma progressively accumulated. The rate of accumulation was greater in the fructose diet than that of the mixed or glucose only models. For both fatty acids and triglyceride concentrations, glucose meals were observed to result in the lowest levels over the study period. Additionally, for the 50/50 glucose/fructose model, the fatty acid curves fluctuated more dramatically in comparison to the other dietary inputs.

Clinical data from Abraha et al. (1998), Chong et al. (2007) and Stanhope et al. (2008) were used to compare the model predictions. The comparison of plasma TG between model simulations and literature data is presented in Figure 5-4.

The research carried out by Chong et al. (2007) recruited 14 healthy individuals to have one test meal either containing 0.75g/kg body weight fructose or glucose. Plasma composition was recorded over 6 hours to investigate the acute effect of high-carbohydrate diets.

In the study by Stanhope et al. (2008), a larger sample size and a larger time scale were applied with more abundant dietary carbohydrate forms. A total of 34 subjects were provided with three meals with sucrose or high fructose corn syrup (HFCS) drinks. For this study 8 men also participated in a sub-study that included pure glucose and pure fructose consumption. Blood samples of all participants were collected regularly during a 24-hour period.

In contrast to these two studies, Abraha et al. (1998) also included diabetic patients as subjects of an investigation to explore the effect of fructose on postprandial lipid profiles. Six healthy individuals and six diabetic individuals were provided a test meal with a fructose-enriched drink or starch-enriched bread. Plasma metabolites for both groups were recorded for 6 hours.

These data were chosen as they covered varying dietary carbohydrate compositions in both healthy and diabetic subjects, which were considerably suitable for testing the compatibility of the constructed model. It should be noted that since diabetic and NAFLD patients are considered to have similar insulin responses when inducing high-carbohydrate meals, the clinical values measured in these diabetic subjects were regarded as reference indices. Also, as hepatic lipid levels are difficult to measure in clinical

studies, only plasma lipid profiles were employed to make comparisons with the data from the selected studies.

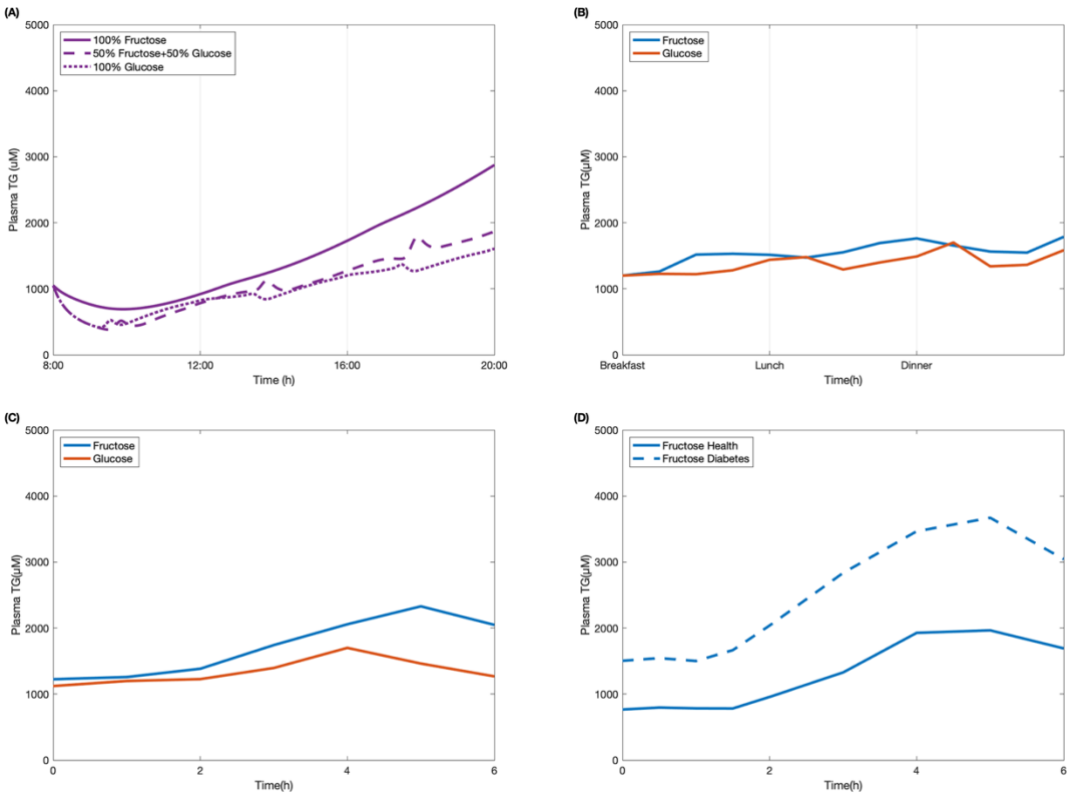

Figure 5-4. The comparison of plasma TG between model simulations and literature data.

(A) Model simulations, (B) Experimental data from (Stanhope et al., 2008), (C) Experimental data from (Chong et al., 2007), (D) Experimental data from (Abraha et al., 1998).

(Please note: A and B include 3 meals in a 12-hour period, while C and D present a 6-hour period after only one meal).

Our model concurred with the findings from these studies in the following ways.

Model predictions and literature data took roughly the same time to process meal inputs and to produce lipid profiles (both plasma FA and TG). Specifically, the plasma FFA

concentrations in the simulated data dropped for roughly 90 minutes before they rose to reach a peak after approximately 5 hours.

Also, consistent with results from these experimentally measured data, in healthy subjects the incremental plasma triglyceride concentration was higher after pure fructose meals than the other meal plans (as shown in Figure 5-4). The simulated results show that consumption of pure glucose can be attributed to the lowest triglyceride levels for the various diets, which is in keeping with the findings in Stanhope et al. (2008). Another consistency can be observed in Figure 5-4A and Figure 5-4B is that the plots of the pure fructose group always have flattened but steady accumulated tendency in lipid production, in comparisons with the other two groups.

Additionally, even though it is relatively difficult for computational models to make predictions matching the exact values of clinical measured data, the plasma triglyceride concentrations the model simulated here (seen in Figure 5-4A) fitted within the range of 1000-2000μmol for both glucose and mix-sugar feeding groups in the healthy subjects. Despite pure fructose exposure producing values as high as 3000μmol plasma TG in the model predictions, this level was still lower than the plasma TG measured in the diabetic individuals after a fructose test meal (around 3800 μmol), as presented in Figure 5-4A and Figure 5-4D. This result suggests that the model predictions are indicative of the normal range of plasma TG levels in a healthy population, even when considering two extreme conditions. Blood glucose predictions were also in agreement with the literature findings above.

Furthermore, there are some discrepancies between the experimental figures and simulated numbers. We note that the peaks of plasma FFA induced by consumption of the mixed diet were higher than that of pure fructose diet. This is caused by the mechanism whereby fructose is not regulated by insulin and glucagon in the model setting. However, in the reality, this feature could also occur and could be explained by the concept that dietary fructose is able to enhance hepatic glucose uptake, hence indicating a synergistic effect of fructose and glucose in fatty acid synthesis.

In this scenario, the model has been tested by three different diets and the simulated results are compared with clinical data. This computational model of fructose metabolism displays its capacity of reproducing significant metabolic features of experimental findings.

5.3.2.2 Scenario Two: The Effect of Varying Reaction Rate Constants on the Hepatic Metabolic Process and Simulations of Individuals

Rate constants indicate the maximum capacity of the enzymes in metabolic reactions, which are affected by numerous factors, e.g., age, diet, life style and genetic predisposition. To explore the variability of these rate constants in the hepatic metabolic processes, an OAT (one at a time) sensitivity analysis was conducted by changing 11 key rate constants in the fructose pathway within the Section Hepatocytes (SH). Since the normal range for healthy liver function can vary substantially between individuals, possibly by as much as 25% according to dye clearance measures designed to assess detoxification function (Vos et al., 2014), a mid-point 10% variation one at a time was applied to each rate constant to reflect the expected metabolically differences among healthy subjects. It is reasonable to choose this value as it is large enough to produce

obvious changes on lipid levels that allow us to recognise the relative importance of metabolic reactions, but small enough to maintain within a healthy range.

Building on the above setting, 20 individuals were simulated with random rate constants within the ±10 % variation. The averages and standard deviations (SD) of selected lipid contents were calculated and compared to the baseline condition.

A 50/50 fructose/glucose diet was set as the standard input and the simulations were run for twelve hours for acute effect consideration. Both hepatic and plasma concentrations of fatty acids and triglycerides were recorded as the end points for the analysis.

The results of the sensitivity analysis are displayed in Table 5-1. Hepatic TG levels were the most sensitive to the reaction rate associated with pyruvate kinase, the rate-limiting enzyme that converts triose phosphate product GA3P to pyruvate for both fructose and glucose. Increasing the enzymatic activity of pyruvate kinase by 10% resulted in +320.09μmol (+3.38%) accumulation of hepatic TG and +74.51μmol (+3.99%) of plasma TG while decreasing this rate by 10% caused a decline of 357.91μmol (-3.78%) and 83.11μmol (-4.45%) in hepatic and plasma TG concentration, respectively.

Secondly, an increase of 281.15μmol (2.97%) in hepatic TG and 42.43μmol (2.27%) in plasma TG levels were observed as the result of increasing the activity rate of KHK by 10%. A decrease of 325.16μmol (-3.44%) in hepatic TG and 49.38 μmol (-2.64%) was found when KHK was inhibited by 10%. The reason that the changes in hepatic TGs were greater than that of plasma TGs is because there is around 5% of body lipid stored in the liver under normal conditions, as such the triglyceride level in the liver is ordinarily higher than that in the plasma.

The two significant variations of PK and KHK activity suggest that they are likely to be the key determinants of individual responsiveness to the progression of simple lipid deposition in the liver. These predictions are consistent with the biological evidence as: PK is the rate limiting enzyme in the glycolysis process engaging in the merging pathway of fructose and glucose metabolism; while KHK is the significant enzyme that exclusively contributes to fructose metabolism, known as bypassing the crucial regulatory control of phosphorylation in glucose metabolism.

Therefore, these two enzymes are of interest for further investigation in potential therapeutic testing Section 5.3.4. Apart from PK and KHK, PEPCK, PDC and FAS also expressed with high sensitivity to lipid levels, especially to hepatic TG concentrations.

Table 5-1. Results for sensitivity analysis of rate constants in Section Hepatocytes (SH).

	Key Enzymes/Reactions	Abbreviation	Δ Hepatic Fatty Acids (μmol)		Δ Hepatic Triglyceride (μmol)		Δ Plasma Fatty Acids (μmol)		Δ Plasma Triglyceride (μmol)	
			+10%	-10%	+10%	-10%	+10%	-10%	+10%	-10%
(1)	Fructokinase	KHK	3.44 (1.84%)	-5.07 (-2.71%)	281.15 (2.97%)	-325.16 (-3.44%)	22.24 (11.16%)	-25.85 (-12.97%)	42.43 (2.27%)	-49.38 (-2.64%)
(2)	Aldolase B	aldB	-18.87 (-10.08%)	17.80 (9.51%)	152.01 (1.61%)	-211.55 (-2.24%)	-6.23 (-3.13%)	1.98 (0.99%)	13.24 (0.71%)	-22.06 (-1.18%)
(3)	Triose phosphate isomerase	TPI	0.00 (0.00%)	0.00 (0.00%)	0.78 (0.01%)	-0.94 (-0.01%)	0.00 (0.00%)	-0.01 (-0.01%)	0.18 (0.01%)	-0.19 (-0.01%)
(4)	Triokinase	Tri	0.00 (0.00%)	0.00 (0.00%)	0.03 (0.00%)	-0.05 (0.00%)	0.00 (0.00%)	0.00 (0.00%)	0.01 (0.00%)	-0.01 (0.00%)
(5)	Pyruvate kinase	PK	25.27 (13.50%)	-25.88 (-13.83%)	320.09 (3.38%)	-357.91 (-3.78%)	38.59 (19.37%)	-37.67 (-18.90%)	74.51 (3.99%)	-83.11 (-4.45%)
(6)	Phosphoenolpyruvate carboxykinase	PEPCK	-16.05 (-8.57%)	18.33 (9.79%)	-222.74 (-2.35%)	241.06 (2.55%)	-22.97 (-11.53%)	27.00 (13.55%)	-52.58 (-2.82%)	57.29 (3.07%)
(7)	Pyruvate oxidation	PDC	15.61 (8.34%)	-16.73 (-8.94%)	217.04 (2.29%)	-244.18 (-2.58%)	22.66 (11.37%)	-23.67 (-11.88%)	52.77 (2.83%)	-58.74 (-3.15%)
(8)	Fatty acid synthesis	FAS	12.14 (6.49%)	-13.14 (-7.02%)	168.42 (1.78%)	-190.44 (-2.01%)	19.23 (9.65%)	-20.28 (-10.18%)	38.78 (2.08%)	-43.83 (-2.35%)

(9)	**Beta-oxidation**	**boxi**	**-0.45 (-0.24%)**	**0.47 (0.25%)**	**-19.09 (-0.20%)**	**20.71 (0.22%)**	**-0.64 (-0.32%)**	**0.68 (0.34%)**	**-4.41 (-0.24%)**	**4.77 (0.26%)**
(10)	**Triglyceride synthesis**	**TGS**	**-7.18 (-3.84%)**	**7.36 (3.93%)**	**96.77 (1.02%)**	**-112.67 (-1.19%)**	**1.07 (0.54%)**	**-1.90 (-0.95%)**	**-25.38 (-1.36%)**	**26.82 (1.44%)**
(11)	**Lipolysis**	**Lply**	**0.37 (0.20%)**	**-0.36 (-0.19%)**	**-0.88 (-0.01%)**	**0.87 (0.01%)**	**0.13 (0.07%)**	**-0.12 (-0.06%)**	**0.71 (0.04%)**	**-0.71 (-0.04%)**

Table 5-2. The random rate constants for the 20 simulated individuals.

Simulated Individuals	Rate Constants of Key Enzymes/Reactions										
	KHK	aldB	TPI	Tri	PK	PEPCK	PDC	FAS	boxi	TGS	Lply
1	4.45	1.69	2.63	7.12	94.21	36.23	16.43	4.28	3.54	9.46	0.080
2	4.73	1.68	2.94	6.74	91.92	37.83	13.61	3.80	3.43	9.72	0.087
3	4.59	1.72	2.44	6.96	83.44	37.86	14.48	4.07	3.45	9.41	0.078
4	4.75	1.80	2.88	6.31	80.94	36.73	16.42	4.35	3.40	8.83	0.085
5	4.15	1.77	2.77	6.76	93.05	33.32	14.60	3.64	3.31	9.79	0.091
6	4.93	1.83	2.72	6.97	91.96	36.33	14.43	3.64	3.19	8.56	0.092
7	4.81	1.55	2.78	7.31	83.01	32.42	13.86	3.62	3.41	9.06	0.085
8	4.10	1.60	2.82	6.63	82.26	32.36	16.25	4.15	3.05	9.82	0.081
9	4.47	1.69	2.48	6.14	83.89	32.84	13.91	4.08	3.07	8.58	0.088
10	4.34	1.86	2.90	6.11	92.73	32.52	14.50	3.69	2.98	8.55	0.092
11	4.62	1.80	2.44	6.87	92.61	35.60	16.19	4.24	3.61	9.77	0.085
12	4.26	1.68	2.59	7.10	88.23	32.01	15.00	4.09	3.61	8.22	0.093
13	4.57	1.64	2.53	6.96	88.25	37.26	15.35	3.66	3.05	8.64	0.080
14	4.59	1.55	2.93	6.49	83.28	36.56	15.25	3.66	3.28	9.16	0.078

15	4.59	1.78	2.47	7.30	90.46	37.98	15.59	3.71	3.40	8.47	0.082
16	4.45	1.70	2.74	6.73	92.15	34.95	13.59	4.23	3.16	9.24	0.083
17	4.08	1.60	2.77	7.31	85.98	36.08	15.08	3.67	3.47	9.54	0.084
18	4.51	1.68	2.78	6.13	86.06	37.73	13.60	3.79	3.34	9.00	0.082
19	4.42	1.59	2.90	6.31	86.40	35.27	15.98	3.79	3.25	9.27	0.088
20	4.15	1.79	2.46	7.07	83.16	33.48	14.52	3.68	3.15	9.53	0.078

Furthermore, a total of 20 subjects were simulated by the model. Table 5-2 lists all the parameter values that were generated randomly within the range. Figure 5-5 presents the scatter plots of lipid products for each subject as well as the mean values and standard deviations. The comparisons of four lipid contents between baseline condition and individual simulation averages were also exhibited, seen in Figure 5-6.

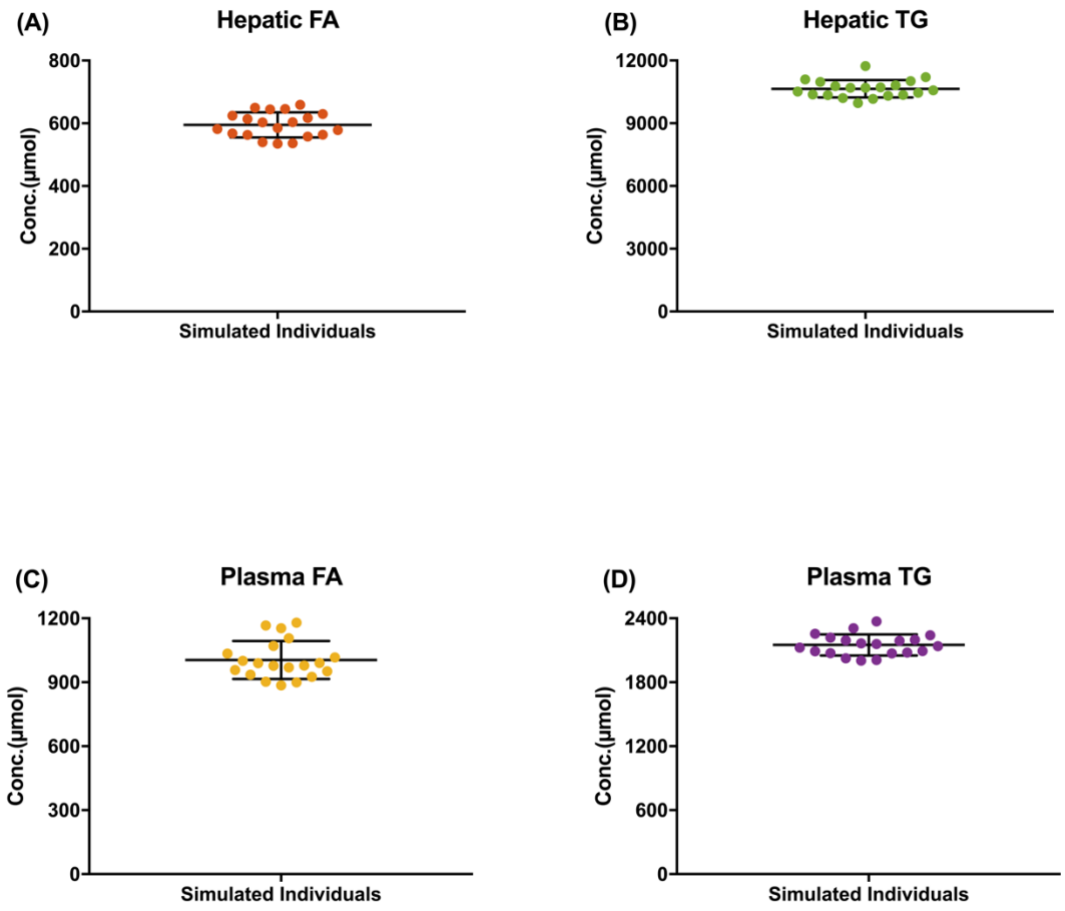

Figure 5-5. The concentrations of lipid compositions for the 20 simulated individuals.

(Scatter plots with single value and means ± SD)

Hepatic FA, (B) Hepatic TG, (C) Plasma FFA, and (D) Plasma TG.

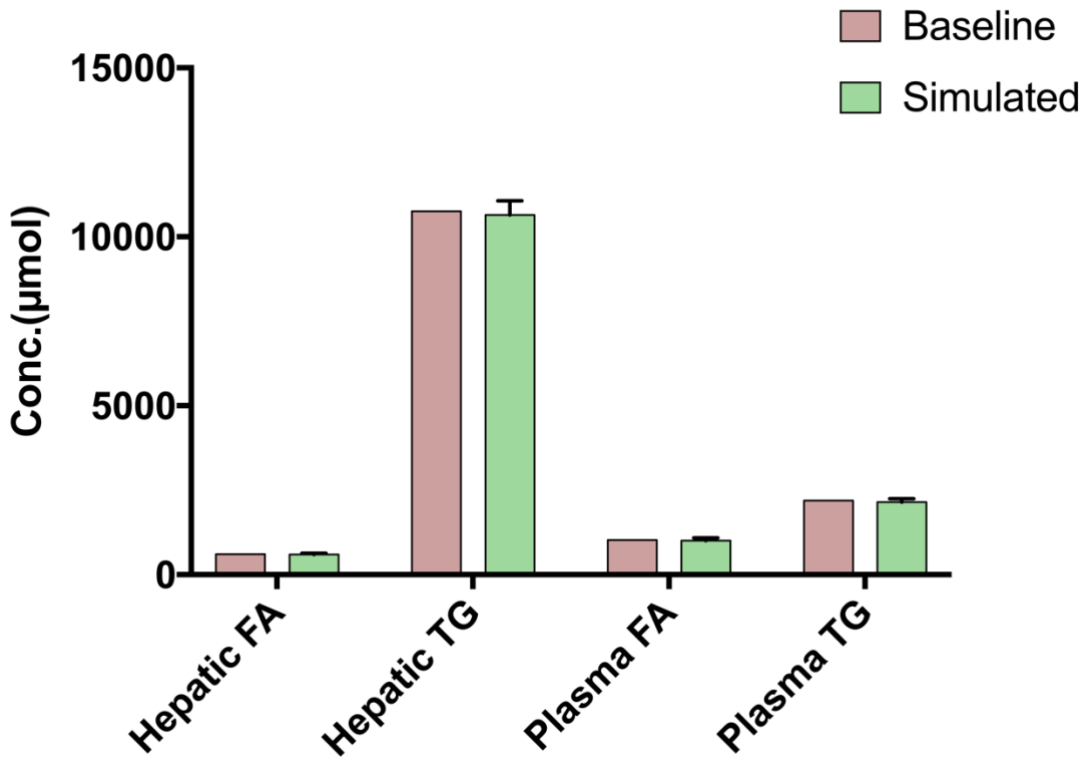

Figure 5-6. The comparisons of four lipid contents between baseline condition and simulated individual average.

As shown in Figure 5-5, the concentration ranges for hepatic fatty acids, hepatic triglycerides, plasma fatty acids, and plasma triglycerides fell between 500µmol and 700 µmol, 9000µmol and 12000µmol, 800µmol and 1200µmol, 2000µmol and 2400µmol, respectively. A more discrete distribution pattern was observed in both hepatic and plasma fatty acids, in comparison with both triglyceride contents. In Figure 5-6, the mean values of four kinds of lipids generated by the 20 simulated individuals are similar to the values produced using baseline parameter values. However, a slightly lower average on hepatic triglycerides could be spotted for the simulated subjects, compared to the value emitted by standard parameters. Overall, for four kinds of lipid profiles, very little variation was

observed between the concentrations generated by baseline values and simulated individuals.

In this scenario, a sensitivity analysis and individual simulations were performed to assess the robustness of the model and to explore the correlations between input and output variables. The predicted outcomes suggest the model is rational and solid.

To conclude, the constructed model has been validated at this stage by clinical data and the uncertainty in the output has been explored by sensitivity analysis. The results at the current stage elucidate that the model is capable of replicating hepatic fructose metabolism and making reasonable predictions of its effect on lipid production under the healthy status, suggesting the model is valid and sound. It is suitable for the model to be tested under abnormal conditions and be further employed to investigate the relationship between fructose consumption and NAFLD.

5.3.3 Stage Three: Model Performance with Insulin Resistance Simulation

At Stage Three, the model was evaluated under abnormal metabolic conditions. Insulin resistance (IR) is one of the common pathophysiological features of NAFLD, even in non-obese patients. Subjects with an insulin resistant condition are considered to be the high-risk population that are predisposed to NAFLD. Using the model, IR conditions were triggered by multiplying an IR constant with a value of less than one. The values of IR=0.5 and IR=0.25 were assigned to represent moderate IR and severe IR at this stage. The peak values of both hepatic and plasma concentrations of fatty acids and triglycerides were recorded for further analysis and validation.

Before constructing any scenarios, model performance under both normal and abnormal metabolic status were undertaken and are presented in Figure 5-7. As described in Section 5.3.2.1, a 50/50 fructose/glucose diet was set as the standard input and the simulations were run for twelve hours for acute effect consideration. It can be observed that higher concentrations of lipid contents were produced under IR environments, compared to healthy status. Blood glucose level is also higher under IR conditions, consistent with the mechanism that impaired insulin sensitivity often fails to regulate glucose homeostasis. Meanwhile, when the worse IR condition occurs, a more severe lipid deposition would develop, especially reflected in hepatic TG and plasma FA. These phenomena imply that severe insulin resistance has the tendency to induce simple lipid accumulation, leading to the early stages of NAFLD.

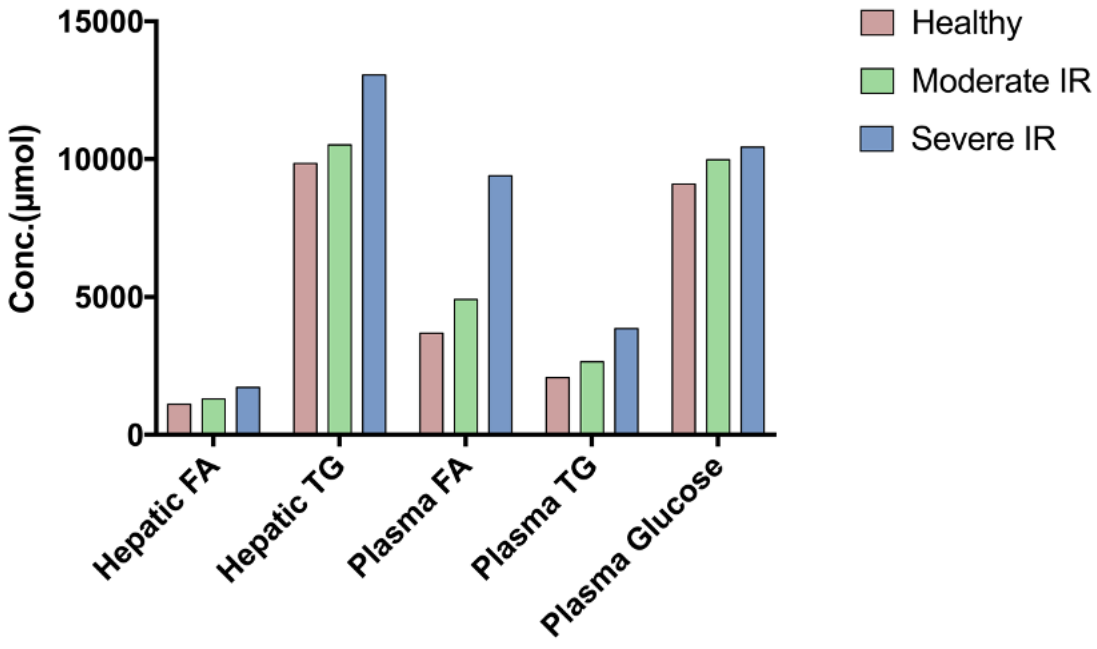

Figure 5-7. Lipid deposition after moderate IR and severe IR simulation.

To further test model performance under impaired insulin sensitivity situations, two scenarios were created. Different kinds of compositions for dietary design were simulated accordingly, mimicking isocaloric carbohydrate intake and hypercaloric fructose intake.

5.3.3.1 Scenario one: Isocaloric Carbohydrate Intake with Impaired Insulin Sensitivity

In this scenario, the isocaloric meals comprising different combinations of monosaccharides (50:50 or 60:40 for fructose and glucose) were introduced as the dietary inputs. These two specific diets represent sucrose and high fructose corn syrup (HFCS), respectively. The reason for these input choices is because they are often considered as the most common forms of fructose consumption. The simplification was made that sucrose breaks down into fructose and glucose directly in 1:1 proportion, excluding the digestive process of sucrose. Therefore, the data in Figure 5-7 is used to denote sucrose consumption in Figure 5-8. A total of 100g of carbohydrates were introduced in each cycle. The changes in lipid profiles as well as in blood glucose level are summarised in Figure 5-8.

Under the healthy status, the HFCS feeding group managed to produce higher concentrations of both hepatic and plasma FA than the sucrose feeding group. For TG profiles, little variation was seen between the sucrose consuming group and the HFCS feeding group. These predictions are in accordance with the findings reported by Stanhope et al. (2008) and Stanhope et al. (2009), suggesting HFCS is likely to enhance hepatic *de novo* lipogenesis as it contains 10% more fructose than sucrose.

When insulin sensitivity is damaged, a similar pattern was observed in FA profiles, which is consistent with the outcomes presented by Abraha et al. (1998). In terms of the TG

levels, it can be seen that HFCS, in comparison to sucrose, contributes to a higher hepatic TG production but a lower plasma TG secretion under the moderate IR condition. This suggests that consuming high fructose content tends to cause hepatic lipid deposition but not systemic fat accumulation.

It is worth mentioning that some surprising results were spotted when the IR condition become more critical. Theoretically, HFCS group is expected to generate higher triglyceride level than sucrose group as HFCS has higher proportion of fructose. However, as shown in Figure 5-8(B) and Figure 5-8(D), the model predictions display that less hepatic TG was generated in the HFCS group compared to the sucrose group and the exacerbated difference between the two groups was observed in plasma TG level. These unexpected behaviours can be explained by the insulin regulation setup in the model. During model development, insulin resistance is considered having a larger effect on glucose metabolism but fructose is effectively insulin-independent. Therefore, when a large amount of insulin is released under severe IR condition, the glucose components are affected to a greater extent relative to fructose, causing higher TG production in the sucrose group.

For blood glucose, sucrose consumption induces a higher level than HFCS for both healthy and unhealthy status. The results are as expected since insulin secretion are often considered not to be triggered by fructose intakes.

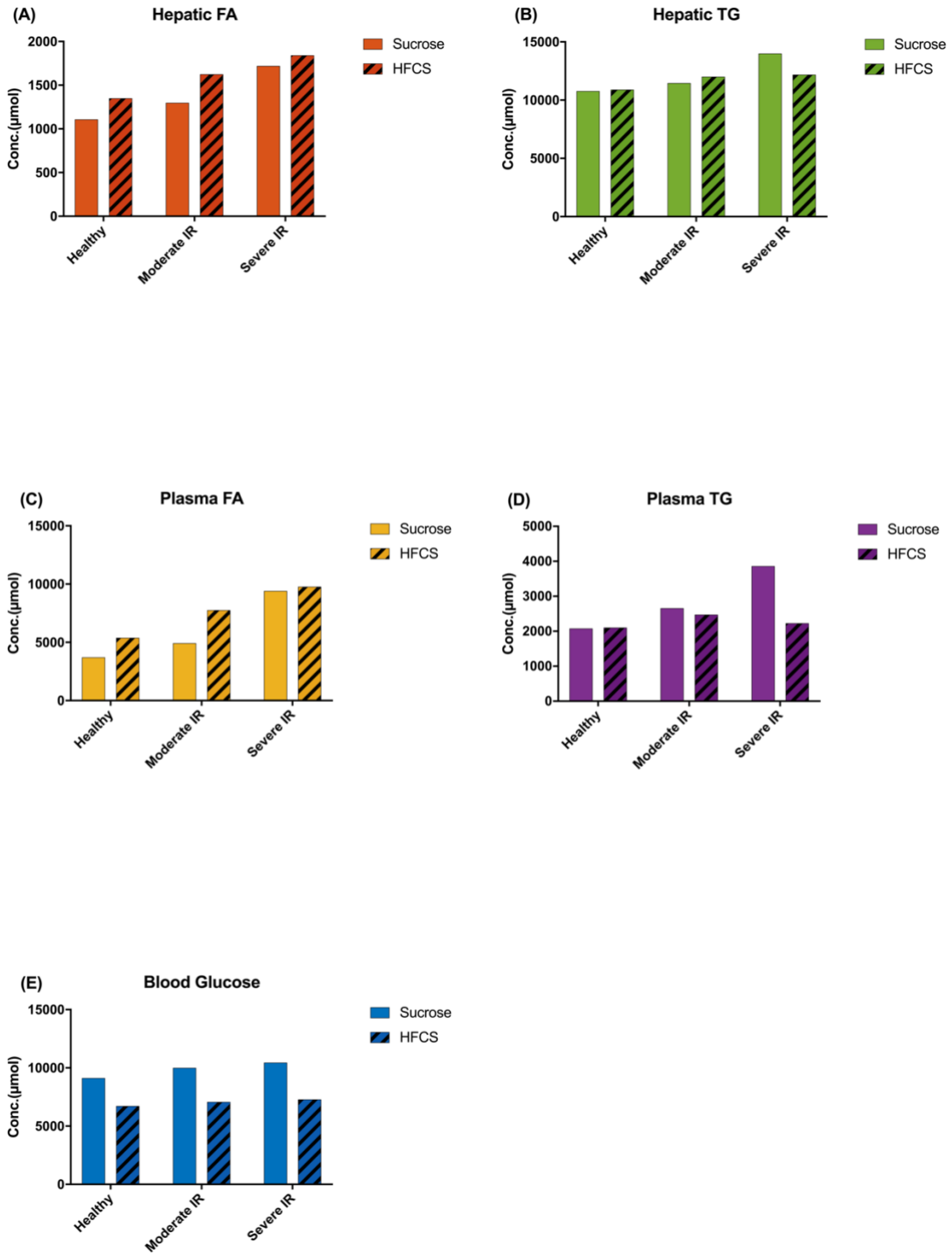

Figure 5-8. The changes of lipid profiles after different dietary intakes combined with IR.

(A) Hepatic FA, (B) Hepatic TG, (C) Plasma FFA, (D) Plasma TG, and (E) Blood Glucose.

*** The data shown above in Figure 5-7 is included here as Sucrose for comparison with HFCS.**

To sum up, the effect of isocaloric carbohydrate intake combined with impaired insulin sensitivity on lipid production was assessed in the current scenario. The results indicate that the model is capable of making rational predictions under abnormal metabolic conditions. However, the performance under severe IR simulation is limited.

5.3.3.2 Scenario Two: Hypercaloric Fructose Intake with Impaired Insulin Sensitivity

In order to test the model extremity, a hypercaloric fructose intake scenario combined with impaired insulin sensitivity was created to represent the worst scenario. In reality, it is against the no-harm policy and experimental ethics to replace all carbohydrate source with fructose in terms of clinical experimental design. However, computational modelling has its own advantage in being able to simulate the unrealistic, excessive amount of fructose exposure without any ethical concerns.

Considering fructose is naturally consumed with glucose, the hypercaloric fructose diets were set with an addition of 50g glucose per meal. The three simulated diets are: a baseline diet (50g fructose per meal), a high fructose diet (a 12.5% increase in fructose) and a very high fructose diet (a 25% increase in fructose). Same as in Section 5.3.3.1, both moderate and severe IR environments were included.

The effects of these hypercaloric fructose consumptions on lipid accumulations combined with IR conditions are presented in Figure 5-9. As shown in the figure, concentrations of all four kinds of lipids increase in a dose-dependent manner. Furthermore, as the IR condition that the model simulates worsens, more severe fat deposition was observed.

It should be noted that the high fructose diet was selected to represent a simple pro-steatosis condition (the early phrase in NAFLD development), in which 7.5% and 26.1%

increases in hepatic triglycerides was observed under moderate and severe IR status, respectively. This setting fitted in the criteria of mild steatosis (Petäjä and Yki-Järvinen, 2016). Therefore, this high fructose diet (62.5g fructose+50g glucose/meal) combined with IR conditions was applied to induce pro-steatosis circumstance for potential treatment exploration in the following stage.

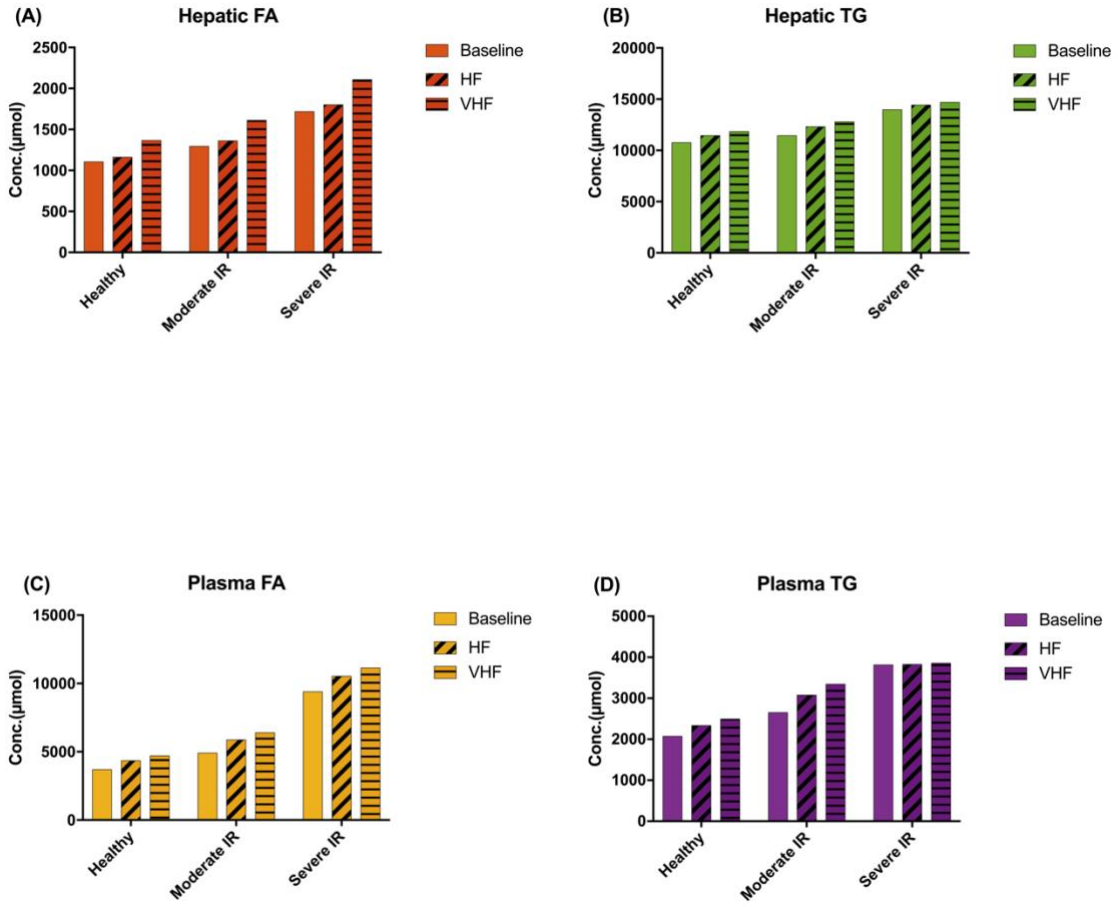

Figure 5-9. The change of lipid accumulation after different fructose intakes combined with IR.

HF: A high fructose diet; VHF: a very high fructose diet.

(A) Hepatic FA, (B) Hepatic TG, (C) Plasma FFA, and (D) Plasma TG.

Overall, two scenarios have been applied at this stage to examine whether the constructed model has the capability to make solid predictions under pathological conditions. In the following section, the proposals for synergistic drug treatments are explored.

5.3.4 Stage Four: Model Based NAFLD Analysis and Synergistic Treatment Exploration

The current stage mainly focuses on the effects of potential interventional targets on early stage of NAFLD, which is featured as simple lipid deposition. As shown in Figure 5-10, pyruvate kinase (PK), fructokinase (KHK) and PPARα are selected as the three potential therapeutic points. The reason for choosing them is that they are three significant components in the metabolic regulations.

To be specific, after glucose and fructose metabolism merging at glyceraldehyde 3 phosphate (GA3P), PK is the rate limiting enzyme to break down GA3P to pyruvate, releasing essential substrates for lipid synthesis. Therefore, inhibiting PK at this point is considered to be a potential intervention which can productively reduce fatty acid synthesis.

As for KHK, KHK is not limited by adenosine triphosphate (ATP) or citrate availability (as is the case of glucokinase in the glycolytic pathway) as part of the fructose phosphorylation process. Since this reaction is the first step in the fructose metabolism within the liver and it is exclusively contributing to the fructose metabolic pathway, suppressing this process should prevent fructose-induced lipid accumulation effectively.

In terms of PPARα, recent research has shed a new light on it but its role in NAFLD still remains unclear. It has been reported that the expression of PPARα might be inhibited by

high production of fructose-1-phosphate, leading to the decrease of beta-oxidation activity. As a result, the clearance capacity of lipid contents would be impaired, contributing to the development of NAFLD. Therefore, PPARα activation is considered as a promising intervention to protect the liver from developing NAFLD after fructose over-consumption.

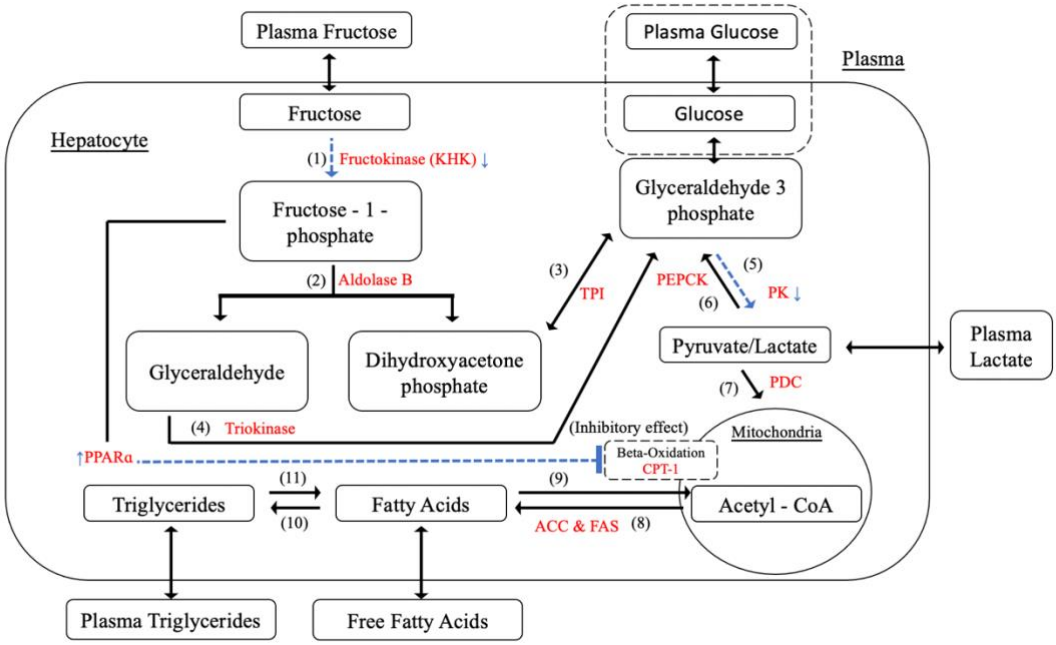

Figure 5-10. Hepatic fructose metabolism with interventional treatments

(The blue dash lines indicate reaction reduction)

As stated above, a total of 62.5g fructose with an addition of 50g glucose was employed for each meal as dietary setting, representing high fructose feeding scenario. In addition, two abnormal conditions including moderate and severe IR were simulated to represent the two degrees of pro-steatosis conditions. Three practical interventions are introduced, including 50% suppression of PK, 50% inhibition of KHK and 50% activation of PPARα.

The synergistic effects of these interventions have also been assessed. The pairwise comparisons were conducted in order between the three potential targets. This stage is to explore the effectiveness and robustness of current model in novel therapy design.

The results of the pairwise comparisons between three interventions are shown in Figure 5-11 to Figure 5-14, presenting hepatic fatty acids, hepatic triglycerides, plasma free fatty acids and plasma triglycerides, respectively. It should be noted that the plots of PPARα activation and PPARα + PK overlap completely in panel (F) of these four figures.

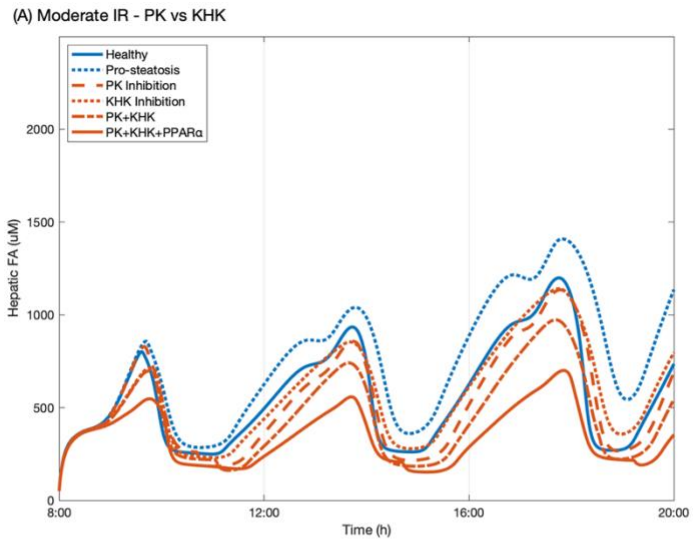
(A) Moderate IR - PK vs KHK
Healthy
Pro-steatosis
PK Inhibition
KHK Inhibition
PK+KHK
PK+KHK+PPARα
Hepatic FA (uM)
0
500
1000
1500
2000
8:00
12:00
16:00
20:00
Time (h)

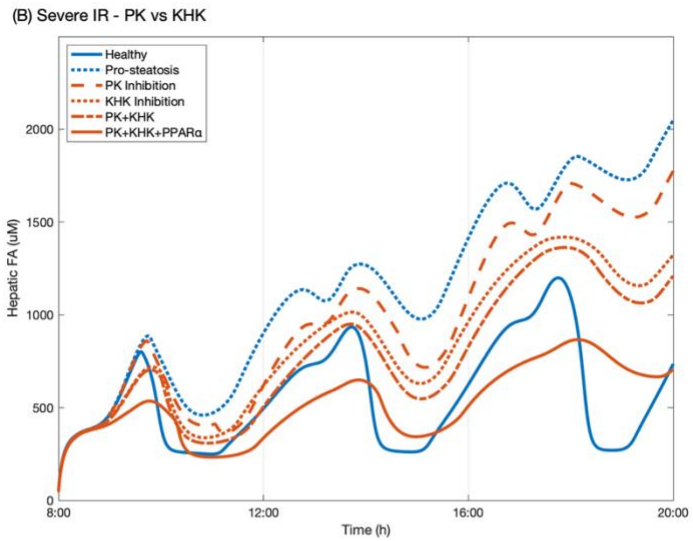
(B) Severe IR - PK vs KHK
Healthy
Pro-steatosis
PK Inhibition
KHK Inhibition
PK+KHK
PK+KHK+PPARα
Hepatic FA (uM)
0
500
1000
1500
2000
8:00
12:00
16:00
20:00
Time (h)

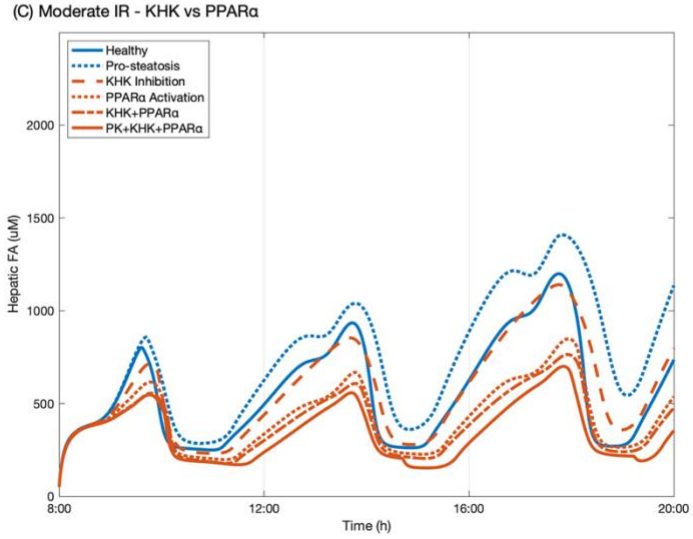
(C) Moderate IR - KHK vs PPARα
Healthy
Pro-steatosis
KHK Inhibition
PPARα Activation
KHK+PPARα
PK+KHK+PPARα
Hepatic FA (uM)
0
500
1000
1500
2000
8:00
12:00
16:00
20:00
Time (h)

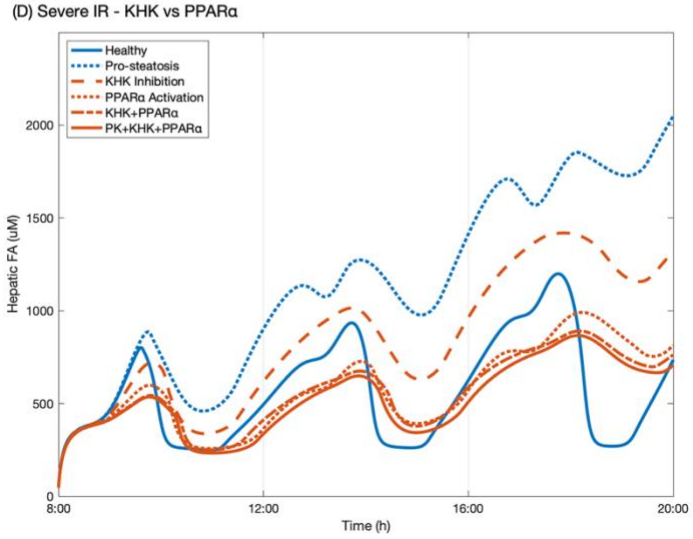
(D) Severe IR - KHK vs PPARα
Healthy
Pro-steatosis
KHK Inhibition
PPARα Activation
KHK+PPARα
PK+KHK+PPARα
Hepatic FA (uM)
0
500
1000
1500
2000
8:00
12:00
16:00
20:00
Time (h)

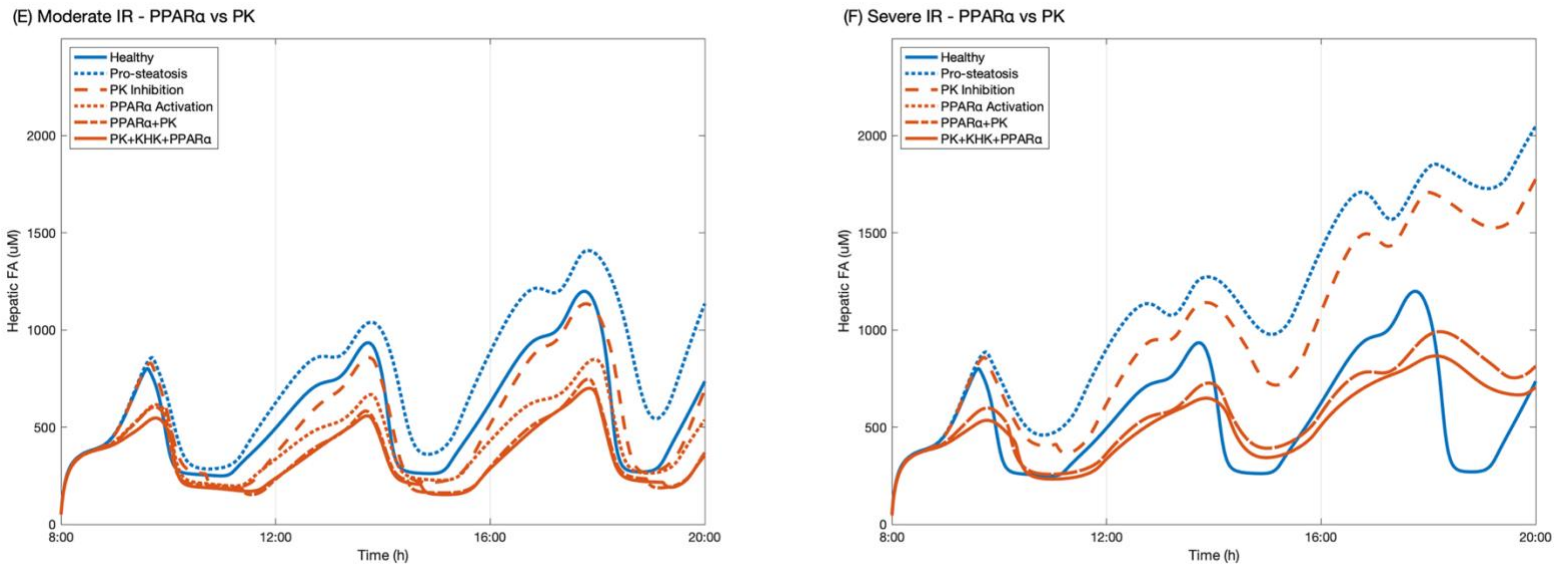

Figure 5-11. The effects of three potential therapeutic targets on hepatic fatty acids.

Pairwise comparisons: (A) (B) PK vs KHK, (C) (D) KHK vs PPAR*α*, (E) (F) PPAR*α* vs PK.

In Figure 5-11, it can be seen from panel (A) that inhibiting PK by 50% is able to reverse the hepatic fatty acid build-up condition back to a healthy level when insulin sensitivity is impaired mildly. Compared to PK, KHK suppression exerted a similar effect on protecting from fatty acid synthesis. Lower level was induced as a result of dual inhibition of PK and KHK. As insulin resistance progressed to a more severe condition in Figure 5-11 (B), suppressing KHK seems more effective than inhibiting PK on decreasing fatty acid concentration. However, even applying PK and KHK intervention simultaneously, the fatty acid level can hardly return to normal.

In addition, as shown in panel (C) to (E), the outcome of 50% PPARα activation on controlling fatty acid level is outstanding, regardless of the severity degree of insulin resistance. Enhancing PPARα expression enables a decrease in hepatic fatty acid accumulation significantly. Under moderate IR condition, the synergistic effect of PPARα and PK is practically as effective as the combination of three treatment, suggesting that KHK is the least efficient interventional targets among those three. When severe IR was simulated, the situation is slightly different as the least impact was observed after supressing PK activity.

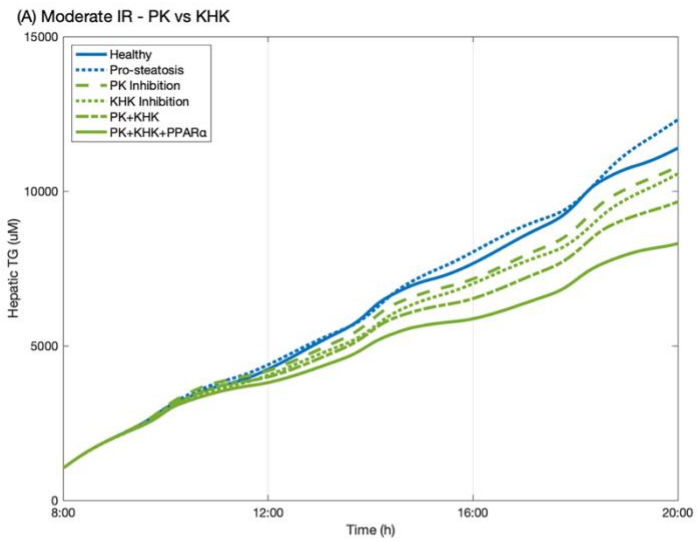
(A) Moderate IR - PK vs KHK
Healthy
Pro-steatosis
PK Inhibition
KHK Inhibition
PK+KHK
PK+KHK+PPARα
Hepatic TG (uM)
Time (h)
15000
10000
5000
0
8:00
12:00
16:00
20:00

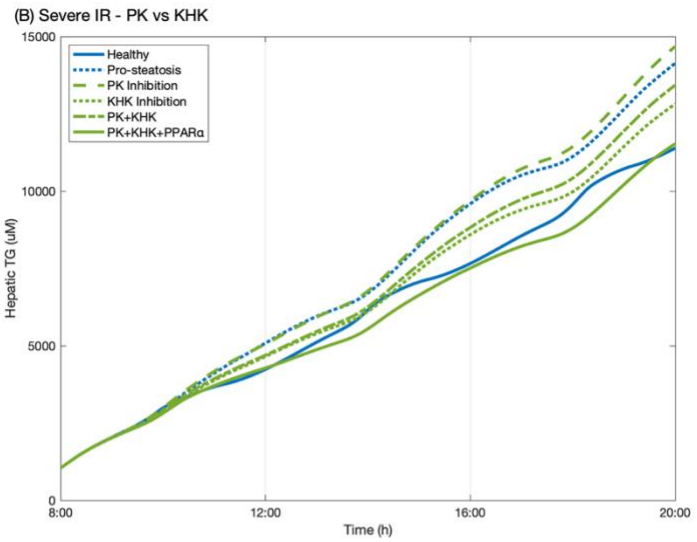
(B) Severe IR - PK vs KHK
Healthy
Pro-steatosis
PK Inhibition
KHK Inhibition
PK+KHK
PK+KHK+PPARα
Hepatic TG (uM)
Time (h)
15000
10000
5000
0
8:00
12:00
16:00
20:00

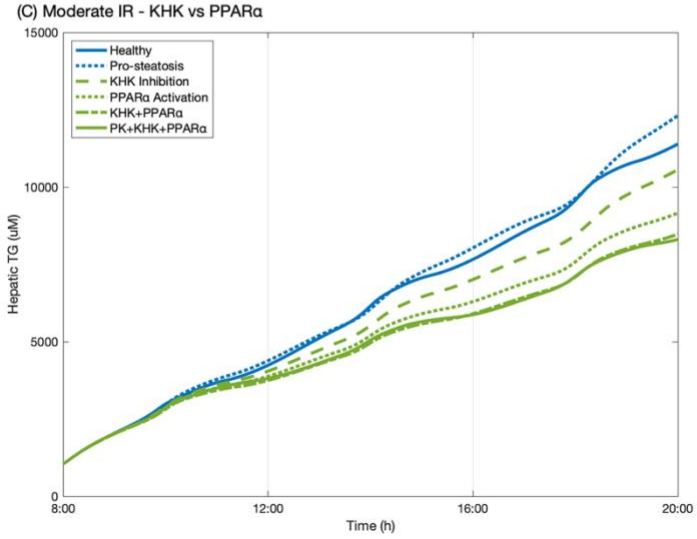
(C) Moderate IR - KHK vs PPARα
Healthy
Pro-steatosis
KHK Inhibition
PPARα Activation
KHK+PPARα
PK+KHK+PPARα
Hepatic TG (uM)
Time (h)
15000
10000
5000
0
8:00
12:00
16:00
20:00

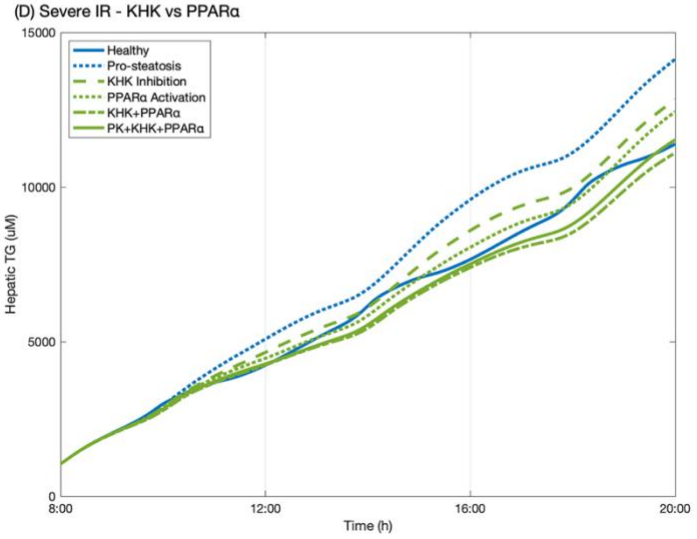
(D) Severe IR - KHK vs PPARα
Healthy
Pro-steatosis
KHK Inhibition
PPARα Activation
KHK+PPARα
PK+KHK+PPARα
Hepatic TG (uM)
Time (h)
15000
10000
5000
0
8:00
12:00
16:00
20:00

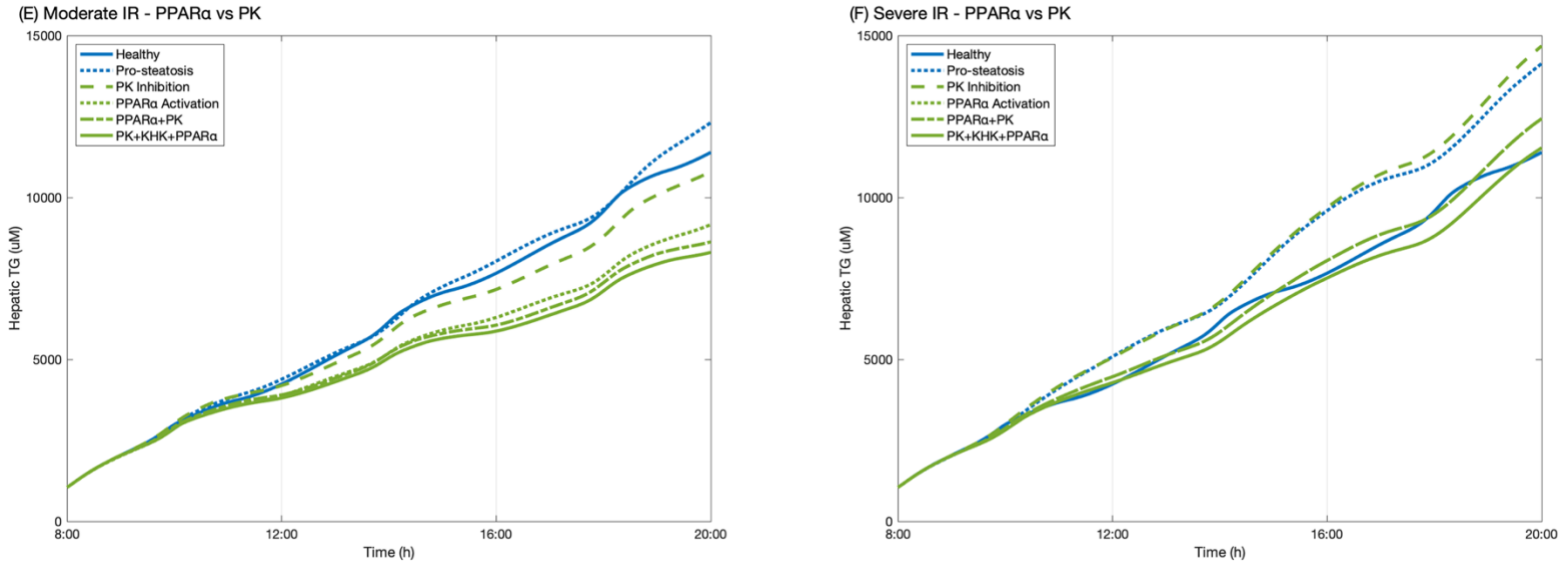

Figure 5-12. The effects of three potential therapeutic targets on hepatic triglycerides.

Pairwise comparisons: (A) (B) PK vs KHK, (C) (D) KHK vs PPARα (E) (F) PPARα vs PK.

In terms of hepatic triglyceride, the similar reverse patterns can be perceived under moderate IR condition, as shown in Figure 5-12 (A), (C) and (E). However, the results are rather interesting when insulin resistance is worsening. It can be observed from Figure 5-12(B) that inhibiting PK tends to boost triglyceride production in the liver, instead of decreasing it as expected. The triglyceride level after PK treatment is even higher than that under the pro-steatosis condition.

Conceptually, this feature can be explained by a particular phenomenon called the Warburg Effect. This metabolic alteration eludes catabolic oxidation deliberately to redirect the carbon substrate to generate lipid, protein or other biomass, resulting in the acceleration of cell growth and proliferation (Liberti and Locasale, 2016). However, the model was built in a less complicated manner that it does not include the feedback mechanisms such as the Warburg Effect.

At the model construction level, the reason why PK suppression surprisingly leads to triglyceride accumulation can be elucidated by Figure 5-10 and Equ. 11. As highlighted in Figure 5-10, when PK is inhibited, the amount of GA3P would increase and subsequent metabolites after pyruvate are supposed to decrease. However, excess GA3P are then used to synthesize triglyceride as in Equ. 11, causing triglyceride over-production.

Furthermore, as shown in Figure 5-13 and Figure 5-14, the effects of three interventional treatments on plasma free fatty acids and triglycerides share similar trends as they perform in the hepatic lipid profiles. However, as three potential targets act on fructose metabolic pathway in the liver, a slight damping effect caused by blood circulation was observed in the plasma lipid levels, especially under critical IR condition.

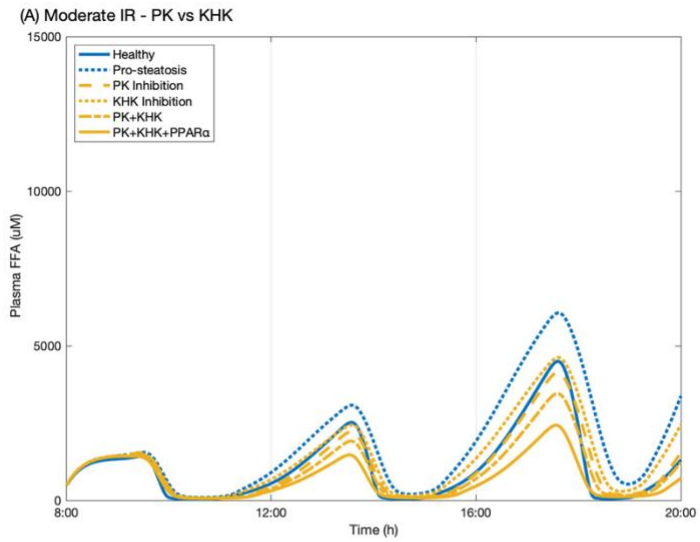
(A) Moderate IR - PK vs KHK
Healthy
Pro-steatosis
PK Inhibition
KHK Inhibition
PK+KHK
PK+KHK+PPARα
Plasma FFA (uM)
Time (h)
15000
10000
5000
0
8:00
12:00
16:00
20:00

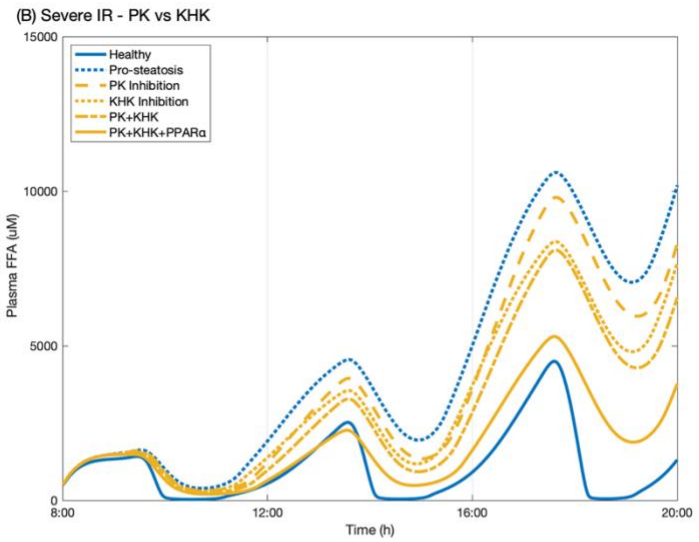
(B) Severe IR - PK vs KHK
Healthy
Pro-steatosis
PK Inhibition
KHK Inhibition
PK+KHK
PK+KHK+PPARα
Plasma FFA (uM)
Time (h)
15000
10000
5000
0
8:00
12:00
16:00
20:00

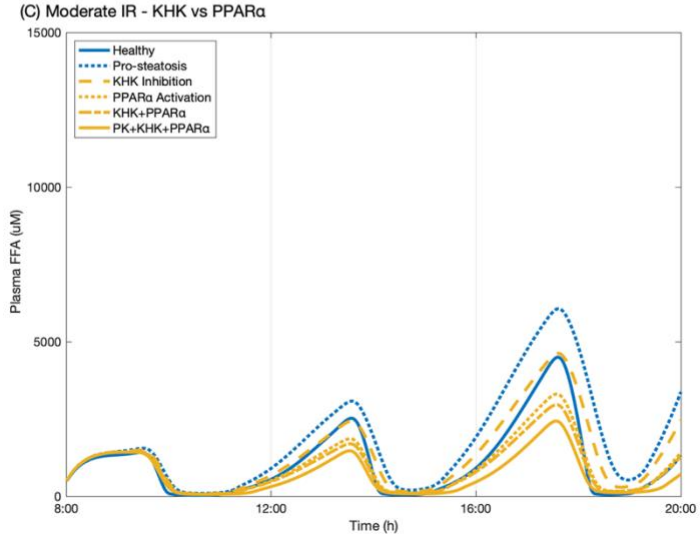
(C) Moderate IR - KHK vs PPARα
Healthy
Pro-steatosis
KHK Inhibition
PPARα Activation
KHK+PPARα
PK+KHK+PPARα
Plasma FFA (uM)
Time (h)
15000
10000
5000
0
8:00
12:00
16:00
20:00

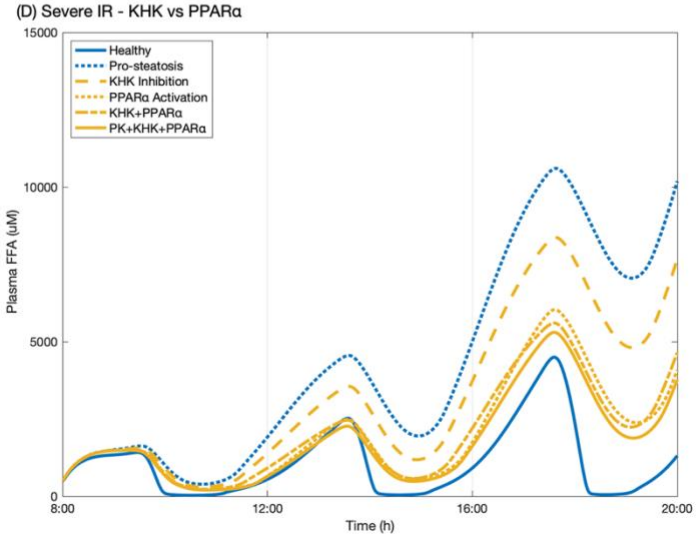
(D) Severe IR - KHK vs PPARα
Healthy
Pro-steatosis
KHK Inhibition
PPARα Activation
KHK+PPARα
PK+KHK+PPARα
Plasma FFA (uM)
Time (h)
15000
10000
5000
0
8:00
12:00
16:00
20:00

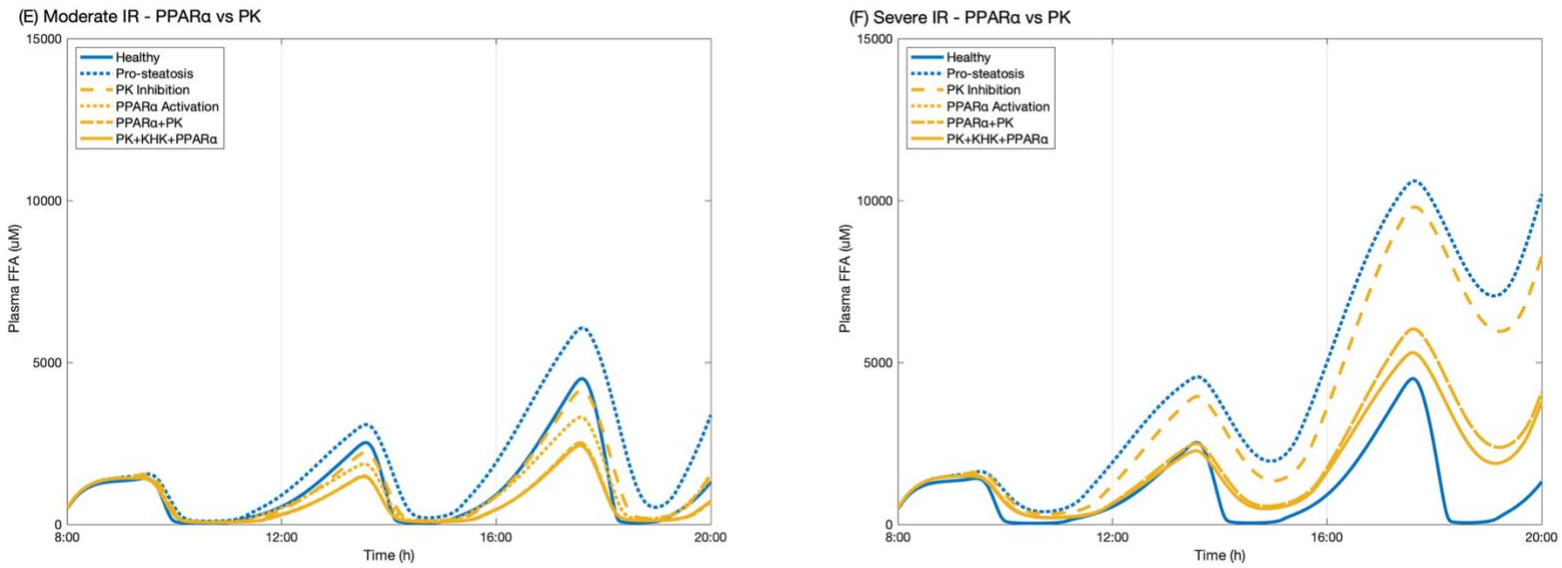

Figure 5-13. The effects of three potential therapeutic targets on plasma free fatty acids.

Pairwise comparisons: (A) (B) PK vs KHK, (C) (D) KHK vs PPARα, (D) (E) PPARα vs PK.

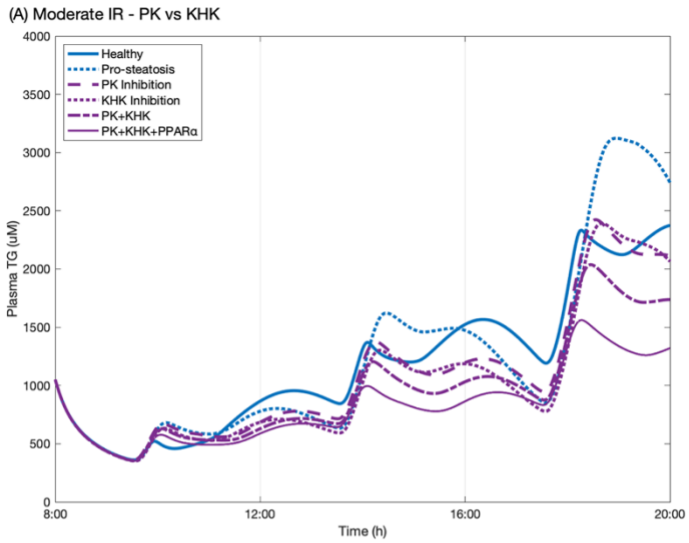
(A) Moderate IR - PK vs KHK
Healthy
Pro-steatosis
PK Inhibition
KHK Inhibition
PK+KHK
PK+KHK+PPARα
Plasma TG (uM)
Time (h)
8:00
12:00
16:00
20:00
0
500
1000
1500
2000
2500
3000
3500
4000

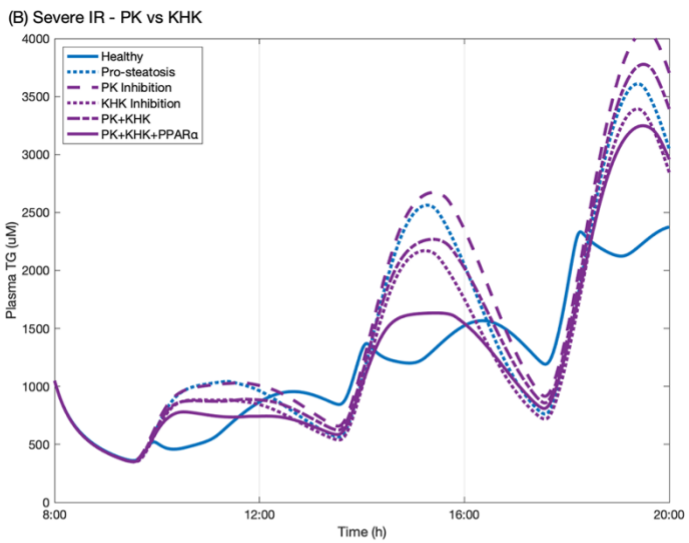
(B) Severe IR - PK vs KHK
Healthy
Pro-steatosis
PK Inhibition
KHK Inhibition
PK+KHK
PK+KHK+PPARα
Plasma TG (uM)
Time (h)
8:00
12:00
16:00
20:00
0
500
1000
1500
2000
2500
3000
3500
4000

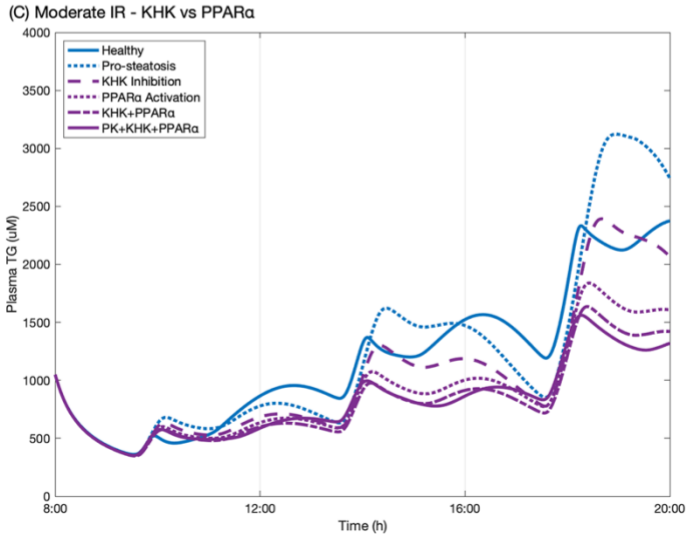
(C) Moderate IR - KHK vs PPARα
Healthy
Pro-steatosis
KHK Inhibition
PPARα Activation
KHK+PPARα
PK+KHK+PPARα
Plasma TG (uM)
Time (h)
8:00
12:00
16:00
20:00
0
500
1000
1500
2000
2500
3000
3500
4000

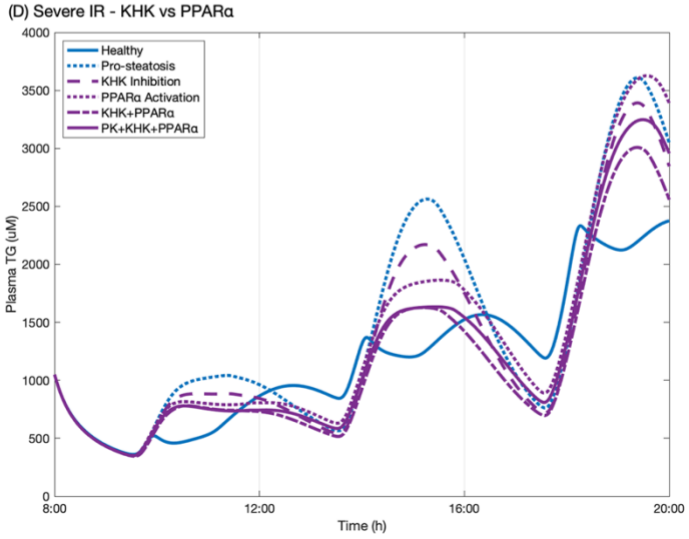
(D) Severe IR - KHK vs PPARα
Healthy
Pro-steatosis
KHK Inhibition
PPARα Activation
KHK+PPARα
PK+KHK+PPARα
Plasma TG (uM)
Time (h)
8:00
12:00
16:00
20:00
0
500
1000
1500
2000
2500
3000
3500
4000

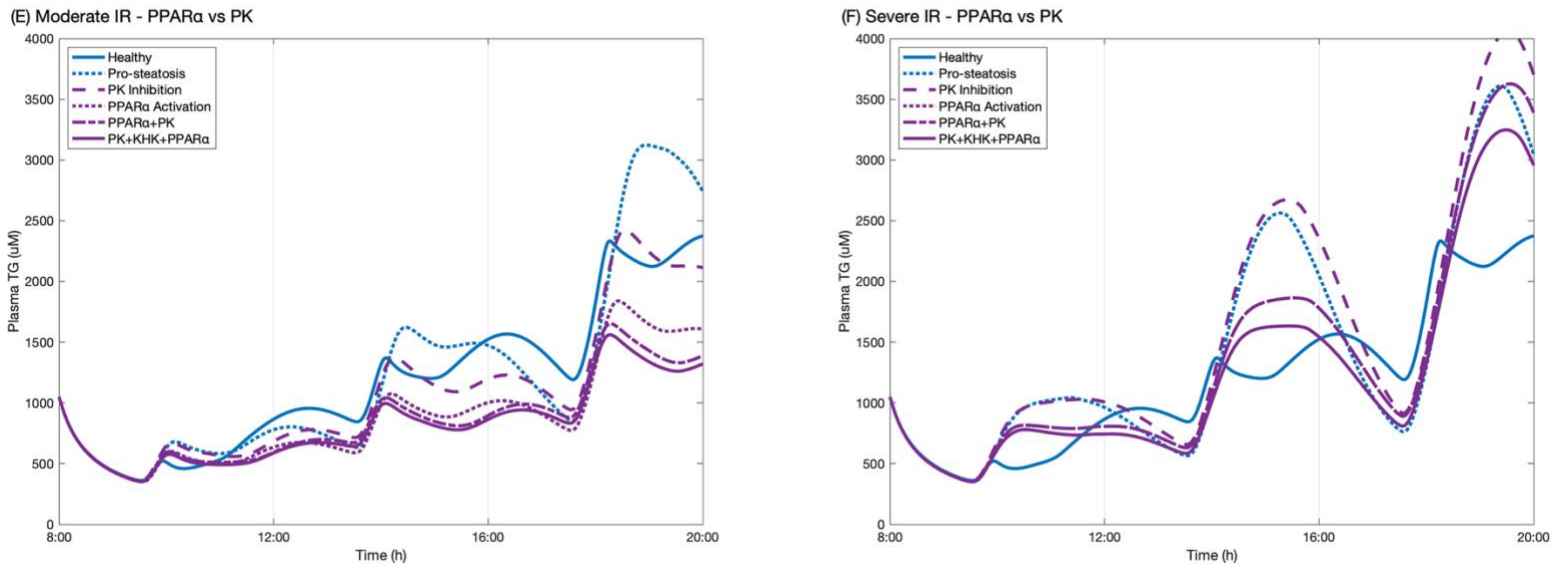

Figure 5-14. The effects of three potential therapeutic targets on plasma triglycerides.

Pairwise comparisons: (A) (B) PK vs KHK, (C) (D) KHK vs PPAR*α*, (E) (F) PPAR*α* vs PK.

Overall, based on the model predictions, all three interventional approaches have the capability to recover from fatty acid deposition under moderate IR condition. PPARα activation is the most stable treatment that would not be affected by the degree of insulin sensitivity impairments and plays a dominating role in the combination treatments.

5.4 Chapter Conclusions

The simulations in the four stages above suggest that the model is robust and it has sufficient detail to present the kinetic relationship between fructose and lipid in the liver under both healthy and insulin-resistant conditions. Synergistic interventions of PK, KHK and PPAR has been tested as the most effective treatment to reduce the production of both fatty acids and triglycerides under both moderate and severe IR conditions. However, it should be noted that PPARα is considered as the most suitable therapeutic target according to its dominant and consistent behaviour during the simulation.

6 Chapter 6: Experimental Assessment and Validation

6.1 Chapter Introduction

As demonstrated previously in Section 5.3.4, PK, KHK and PPARα are the three interested interventional targets. Given the model is built on protein level, proteins are the priority in the following experimental setting. Therefore, two experiments were employed to evaluate whether the expression levels and activity rates of these potential points were altered by different carbohydrate diets.

6.2 Biochemical Assay Planning

In the following two assays, the required protein samples were only provided by the liver tissues of rats, because there was no adequate amount of proteins can be harvested from cell lysates. Therefore, to set up the test, the targeted proteins were extracted from the liver pieces in the animal experiment. Sample collection method is the same as description in Section 3.2.1 and the dietary treatments are the normal chow and the fructose-enriched diet as stated previously.

Firstly, western blotting was operated to measure the protein expression levels of KHK and PPARα. The aim of this assay is to quantify the amount of KHK and PPARα in order to test whether fructose feeding would upregulate or downregulate the expression of these two key targets in the fructose metabolic pathways.

Apart from protein expression level, activity rate has also been taken into consideration in this chapter. As a result, the enzymatic activity assays of PK and KHK were performed

to explore whether the reaction rates of these two crucial enzymes would be affected by high fructose consumption.

The results of Western blotting and enzymatic activity assay are exploited to provide another insight of whether it is reasonable to select PK, KHK and PPARα as the potential treatments.

6.3 Methodology

6.3.1 Reagents and Materials

6.3.1.1 Micro BCA Protein Assay and BCA Protein Assay

Micro BCA Protein Assay Kit (Thermo Fisher, 23235); BCA Protein Assay Kit (Thermo Fisher, 23225);

6.3.1.2 Western Blotting

Sample preparation: Bolt Sample Reducing Agent (10×) (Thermo Fisher, B0009); Bolt LDS Sample buffer (4×) (Thermo Fisher, B0007); *Markers:* Novex Sharp Pre-Stained Protein Standard (Thermo Fisher, LC5800); MagicMark XP Western Protein Standard (Thermo Fisher, LC5602); *Electrophoresis:* Bolt 4-12% Bis-Tris Plus Gels (Thermo Fisher, NW04122BOX); Bolt Antioxidant (Thermo Fisher, BT0005); Bolt MOPS SDS Running Buffer (20×) (Thermo Fisher, B0001); *Transfer:* NuPAGE Transfer Buffer (20×) (Thermo Fisher, NP0006-1); Western blotting membranes (Sigma-Aldrich, GE10600096); NuPAGE Antioxidant (Thermo Fisher, NP0005); Filter Paper (Thermo Fisher, 88605); *Staining:* Ponceau S solution (Sigma-Aldrich, P7170); *Primary antibodies:* Ketohexokinase (KHK) Antibody (1D8) (Monoclonal, Mouse) (Novus

Biologicals, NBP2-02639); Anti-KHK antibody (Polyclonal, Rabbit) (Sigma-Aldrich, HPA007040-100UL); PPARα Antibody (H-2) (Monoclonal, Mouse) (Santa Cruz, SC398394); PPARα Antibody (Monoclonal, Mouse) (Novus Biologicals, NB300-537); *Secondary antibodies:* Donkey anti-Mouse IgG (H+L) Highly Cross-Adsorbed Secondary Antibody, HRP (Thermo Fisher, A16017); Goat anti-Rabbit IgG-HRP (Santa Cruz, SC-2054); *Positive control (KHK):* Ketohexokinase Overexpression Lysate (Native) (Novus Biologicals, NBL1-12232); *Stripping and loading control:* Restore PLUS western blot stripping buffer (Thermo Fisher, 46430); Anti-beta Tubulin antibody (Abcam, ab6046); *Imaging:* Immobilon Western Chemiluminescent HRP Substrate (Merck, WBKLS0050);

6.3.1.3 Pyruvate Kinase Activity Assay

HEPES buffer (pH 7.1); Imidazole·HCl buffer (pH 7.6) (Sigma-Aldrich, I3386): containing Potassium chloride (KCl) (Sigma-Aldrich, P9333), and Magnesium sulfate heptahydrate ($MgSO_4 \cdot 7H_2O$) (Sigma-Aldrich, M1880); Phosphoenolpyruvate (PEP) acid trisodium salt hydrate (Sigma-Aldrich, P7002-250MG); Adenosine 5′-diphosphate sodium salt (ADP) (Sigma-Aldrich, A2754); β-NADH; Lactate dehydrogenase;

6.3.1.4 Fructokinase Activity Assay

HEPES buffer (pH 7.1): containing KCl (Sigma-Aldrich, P9333), DL-Dithiothreitol (DTT) (Sigma-Aldrich, D9779) and EDTA (Sigma-Aldrich, E6758); Magnesium chloride ($MgCl_2$) (Sigma-Aldrich, M8266); Sodium fluoride (NaF) (BDH Reagents & Chemicals, 102464T); D-(-)-Fructose; PEP acid trisodium salt hydrate (Sigma-Aldrich, P7002-250MG); Pyruvate kinase from rabbit muscle (Sigma-Aldrich, P7768); β-Nicotinamide

adenine dinucleotide, reduced disodium salt hydrate (β-NADH) (Roche, 10128023001); Lactate dehydrogenase from rabbit muscle (Merck, 427217); N-acetyl-D-glucosamine (Sigma-Aldrich, A3286-5G); Adenosine 5'-triphosphate (ATP) (Sigma-Aldrich, A6419);

6.3.1.5 Measuring Equipment

FLUOstar Omega Filter-based multi-mode microplate reader (BMG Labtech); FluorChem^{TM} M System (Protein Simple) for western blotting; Electron Microscope.

6.3.2 Mechanisms and Protocols

6.3.2.1 Micro BCA Protein Assay and BCA Protein Assay

The BCA protein assays are one of the most commonly used measurements for total protein quantification. The difference between Micro BCA assay and BCA assay is their sensitivity. The micro one has the linear working range from 0.5 to 20μg/ml while the normal BCA assay covers the working range of 20-2000μg/ml. These two tests utilise bicinchoninic acid (BCA) as the detection reagent for Cu^{+1}. In an alkaline environment, Cu^{+2} is known to be reduced by protein to generate Cu^{+1} (Smith et al., 1985).

To prepare the standard solutions, one bovine serum albumin (BSA) ampule (2mg) was diluted to obtain a gradient of 200 - 0μg/ml for Micro BCA and 2000-0μg/ml for BCA, respectively. Placing on ice to defrost slowly, samples were suspended evenly before pipetting into the 96-well plates. For Micro BCA assay, each well contained 150μl of standard solutions or the unknown samples and 150μl of working reagents. For BCA assay, 25μl of standard solutions or the unknown samples and 200μl of working reagents were added to each well. The plates were mixed thoroughly and then incubated at 37°C for either 2 hours (Micro BCA) or 30 minutes (BCA). After the incubation and cool down

period, the absorbance ranging from 350 to 650 was measured with the plate reader and the absorbance at 562nm was recorded for further analysis.

Three replicates were performed for both standard solutions and the unknown samples. The standard curves were then calculated and used to estimate the protein concentrations of the samples.

6.3.2.2 Western Blotting

Sample preparation: Before heating at 70°C for 10 minutes, a 24µl sample mixture for each well was prepared by adding loading buffer, reducing agent, distilled water and a pre-calculated amount of sample contacting 24µg proteins. Electrophoresis: The sharp pre-stained protein and MagicMarker mixture was used as the molecular weight makers and 10µl of it was loaded into the first well of the gels. The other eleven wells were filled with the heated samples in a total volume of 20µl. Proteins were separated along with electrophoresis at 160V for an hour, infiltrating in running buffer (1×). Transfer: While the electrophoresis was processing, one litre transfer buffer was prepared contacting 10% methanol, 30ml transfer buffer (20×) and 510ml distilled water. The proteins were then transferred from the gel to the membrane by assembling the transfer sandwich at a constant voltage of 30V for one hour. Staining: To examine the transfer conveniently and rapidly, the membranes were stained with ponceau S solution for 3-5 minutes then rinsed completely with running water. Blocking: The washing buffer was prepared to contain 0.1% tween in 1× tri-buffered saline, stored at room temperature. The blocking buffer then was made for blocking by dissolving 2.5 gram of BSA in 50ml washing buffer, whereas the antibody buffer was prepared by adding 2% BSA in 50ml washing buffer. Each membrane was wrapped into a tube filled with 10ml blocking buffer and rolled for

one hour at room temperature. Antibody incubation: After blocking, the membranes were incubated with the primary antibodies at 4°C overnight, followed by the incubation with secondary antibody for an hour at room temperature. Images were then developed with chemiluminescent substrate and detected by FluorChem™ M System.

6.3.2.3 Pyruvate Kinase Activity Assay

The pyruvate kinase activity was determined by the following reaction:

$$Phosphoenolpyruvate\ (PEP)\ +\ ADP \xrightarrow{Pyruvate\ kinase} Pyruvate + ATP$$

Equ. 15 Pyruvate Kinase Activity 1

$$NADH + Pyruvate \longrightarrow Lactate + NAD^{+}$$

Equ. 16 Pyruvate Kinase Activity 2

The reduction in absorbance resulting from the oxidation of NADH was what this assay exactly measured (Ainsworth and Macfarlane, 1973). Quantified by BCA assay in advance, the diluted proteins at a concentration of 1mg/ml were obtained from the collected protein extracts of the rat liver tissues, served as the enzyme substrate in this test. To make the 0.05M imidazole·HCl buffer, 0.52g imidazole hydrochloride, 0.89g potassium chloride (KCl) and 1.5 magnesium sulphate heptahydrate (MgSO4·7H2O) were dissolved in 80ml distilled water. With stirring, added a small amount of potassium hydroxide (KOH) solution to the mixture in order to achieve a pH value of 7.6. The mixed solution was then diluted to 100ml, transferred and stored at room temperature. An experimental cocktail was mixed by 90% of 0.05M imidazole·HCl buffer, 0.3% 45mM ADP, 0.3% 45Mm PEP and 0.03% 1350 units/ml lactate dehydrogenase. In order to avoid enzyme activated, all extracts were placed on ice during the whole procedure. Each

experimental well of the 96-well plates contained 20µl samples and 200µl reagent cocktail. It should be noted that 10µl/well of NADH have to be added in the wells exactly before the measurement. The plate reader was set to mix well for 2 seconds before starting 60 cycles (equal to 38min21s) assay at the absorbance ranging from 300nm to 650nm. Cycle1 to cycle60 of the absorbance at 340nm were selected for further analysis.

Calculation: The extinction coefficient for NADH is equal to 6220 ($L \cdot mol^{-1} \cdot cm^{-1}$). The pyruvate kinase activity was then calculated for statistical analysis by using the below equation:

$$Pyruvate\ kinase\ activity\ (\text{IU}) = \frac{\Delta A340_{nm} * Reaction\ Volume(\mu l)}{t(\text{min}) * 6220 * Sample\ Volume\ (\mu l)}$$

Equ. 17 Pyruvate Kinase Activity Calculation

Where,

$\Delta A340_{\text{nm}} = \Delta A340_{Initial} - \Delta A340_{Final}$;

$t = duration\ of\ incubation.$

6.3.2.4 Fructokinase Activity Assay

The activity rate of fructokinase was estimated by the enzyme-coupled reaction as shown in Figure 6-1. The rate of decreasing NADH is directly proportional to the rate of production of lactate and thus to the KHK activity (Groisillier and Tonon, 2015). The solution of the sample buffer contains 25mM HEPES buffer (pH 7.1), 100mM KCl, 1mM DTT and 0.1mM EDTA. The tablets for phosphatase and protease were also adding into the sample buffer to prevent targeted enzymes from dephosphorylation. Rat liver tissues

were then homogenized in the sample buffer by the homogenizer. The reaction mixture was made to comprise 25mM HEPES (pH 7.1), 6mM MgCl2, 25mM KCl, 10mM NaF, 5mM D-fructose, 0.2mM NADH, 1mM phosphoenolpyruvate, 40U/ml pyruvate kinase, 40U/ml lactate dehydrogenase, and 50mM N-acetyl-D-glucosamine. The role of N-acetyl-D-glucosamine is to supress hexokinase but maintain fructokinase activity. In order to avoid enzyme activated, all extracts were placed on ice during the whole procedure. Each experimental well of the 96-well plates was adding 20µl sample (containing 50µg protein) and 200µl reaction mix. It should be noted that 10µl/well of ATP have to be added in the wells exactly before the measurement. The plate reader was set to mix well for 2 seconds before starting 60 cycles (equal to 24min34s) assay at the absorbance ranging from 300nm to 650nm. Cycle1 to cycle60 of the absorbance at 340nm were selected for further analysis.

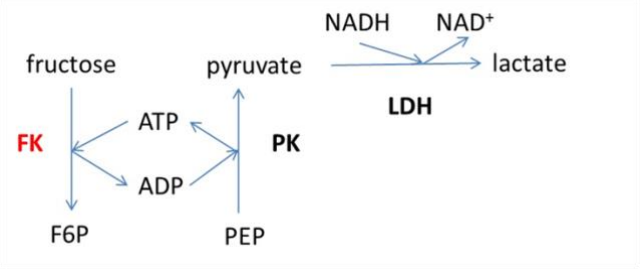

Figure 6-1. The enzyme-coupled reaction of fructokinase activity assay

(adapted from Groisillier and Tonon (2015))

Calculation: The extinction coefficient for NADH is equal to 6220 ($L \cdot mol^{-1} \cdot cm^{-1}$). The fructokinase activity was calculated for statistical analysis by using the below equation:

$$Fructokinase\ activity\ (\text{IU}) = \frac{\Delta A340_{nm} * Reaction\ Volume(\mu l)}{t(\text{min}) * 6220 * Sample\ Volume\ (\mu l)}$$

Equ. 18 Fructokinase Activity Calculation

Where,

$\Delta A340_{\text{nm}} = \Delta A340_{Initial} - \Delta A340_{Final}$;

$t = duration\ of\ incubation.$

6.3.2.5 Image Analysis and Data Statistical Analysis

At least triplicate data were collected to calculate means and standard deviations (SD) for all the results in this project. Image analysis was conducted by ImageJ program. Data was analysed through OMEGA-MARS Data Analysis System, Microsoft Excel software and GraphPad Prism 7 software. T-test and one-way ANOVA were operated to compare the disparities between the control group and the experimental groups accordingly. A P-value less than 0.05 was accepted as statistically significant difference.

6.4 Results and Discussion

6.4.1 The Effect of Different Carbohydrates on KHK and PPARα Expressions

To evaluate whether the high fructose diet could alter protein expression of KHK and PPARα, the Western blotting technique was performed. Since KHK and PPARα are considered to be the more fructose-specific components, only these two kinds of proteins were assessed in the current section.

Two questions would be answered here: whether fructose has the capability to trigger more KHK expression, converting itself to fructose-1-phosphate and delivering abundant substrates for subsequent lipogenesis reactions; and whether fructose has an inhibitory effect on PPARα that results in less β-oxidation and more lipid deposition.

The signal ß-Tubulin was used as the loading control to normalise the expression value. The protein expression level is detected by chemiluminescent method and quantified by its optical density. The results are presented in Figure 6-2.

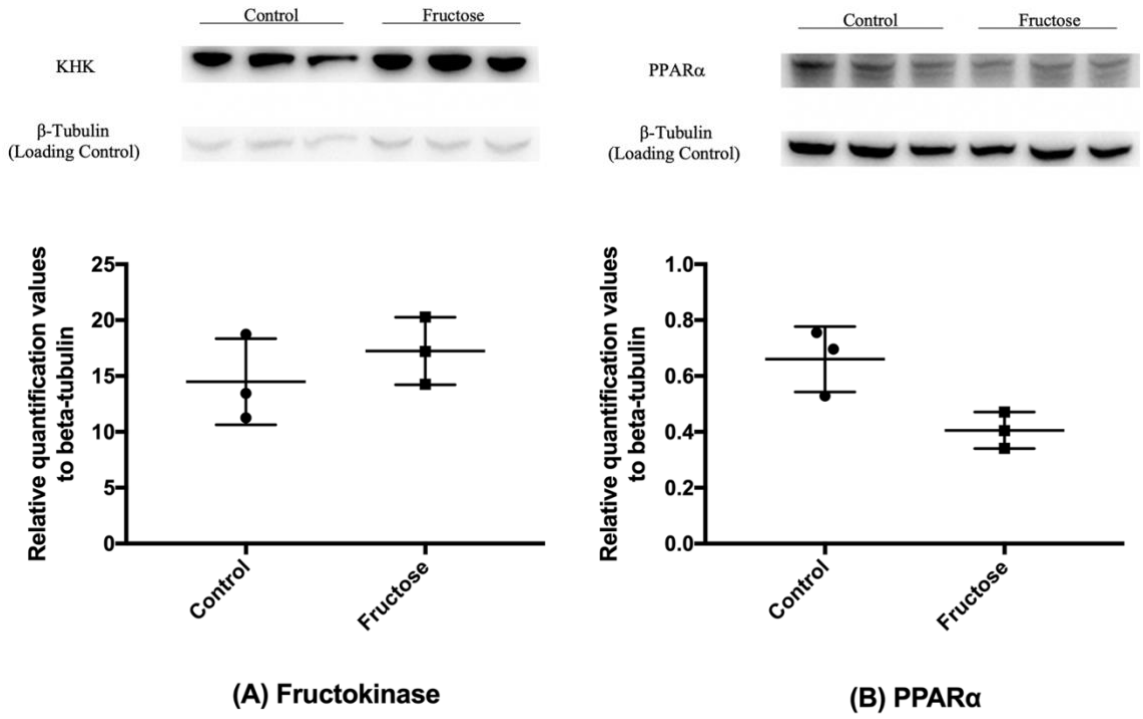

Figure 6-2. The effect of different diets on KHK and PPARα expression.

(The upper figure shows the KHK and PPARα bands. The amount of protein loaded was confirmed by the loading control in each lane; The bottom scatter plots shows the relative protein levels of KHK and PPARα in the liver samples. Control: n=3; Fructose: n=3).

Although no statistical difference was found between the control group and the fructose group in neither KHK nor PPARα expression, it could be seen that KHK was up-regulated in the livers of rats fed with the high-fructose diet while hepatic PPARα was down-regulated in the fructose group. These results are in accordance with other studies in terms of KHK (Della Casa et al., 2016, Ishimoto et al., 2012, Roncal-Jimenez et al., 2011) and

in PPARα (Schultz et al., 2015, Schmilovitz-Weiss et al., 2013, Roglans et al., 2007), suggesting that high-fructose consumption enhances KHK expression and supresses PPARα expression.

6.4.2 The Effect of High-Fructose Diet on Enzymatic Activities of PK and KHK

After measuring the protein expression by Western blot, the activity rates of two enzymes PK and KHK are examined through enzymatic activity assays. PPARα is excluded here because it is a receptor instead of an enzyme, which means it is unable to catalyse any chemical reactions. This assay is to identify whether there are any effects on changing reaction rates of PK and KHK metabolically after consuming a fructose-enriched diet.

A total of 60 cycles of absorbance values were recorded during approximately 30 minutes. The decrease of optical density at 340nm were measured quantitatively to reflect the reaction rates of the targeting subjects. However, only the values in time period of 6-8min for PK and 2-4min for KHK were further analysed. The reason for this selection is that the values within these periods are considered as the maximum rates of reactions as they shown in the first parts of the curves, before the reactions slowed down and ended up with the lacks of substrate availability. The detail equations based on the Beer-Lambert law that used to calculate reaction rate can be found in Section 6.3.2.3 and 6.3.2.4. The results are presented in Figure 6-3.

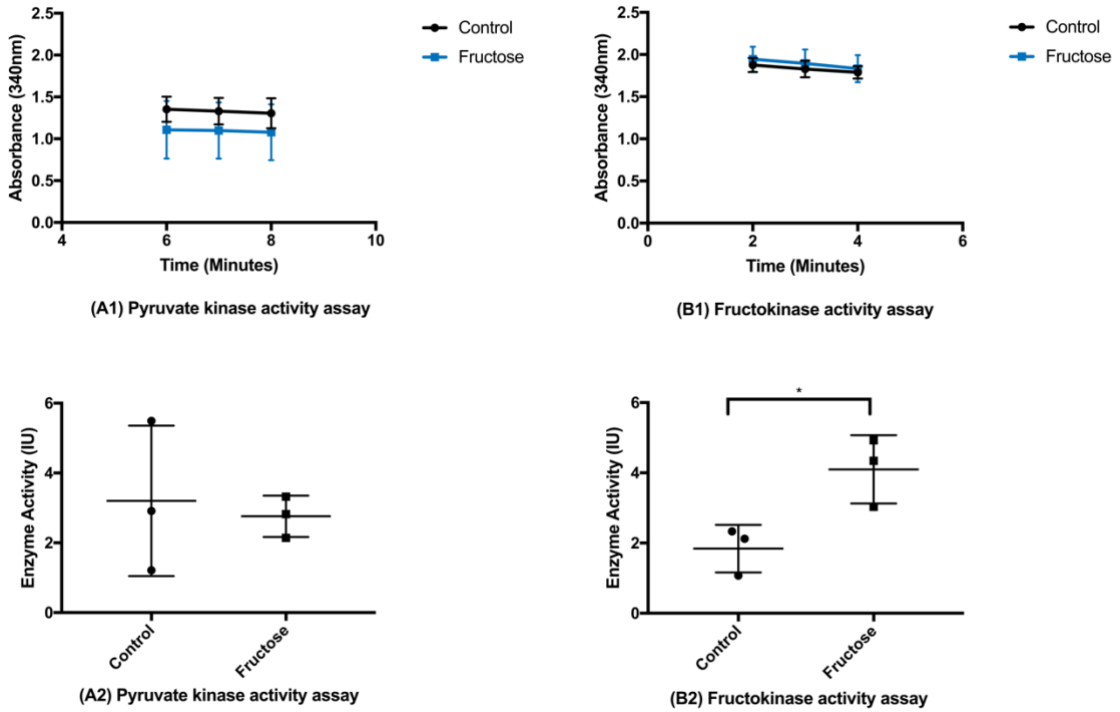

Figure 6-3. The effect of different diets on PK and KHK activities.

(A1 and B1 shows the optical density values in means ± SD of PK and KHK within the time periods; A2 and B2 are the scatter plots with single value and means ± SD, representing the average reaction rates of PK and KHK after calculation. Control: n=3; Fructose: n=3).

***p < 0.05, **p < 0.01, ***p < 0.001 vs. Control. IU: µmol/min/litre**

In terms of PK activity, the slopes of the lines for each group as shown in Figure 6-3(A1) are quite similar, despite the values in the control group is higher than that in the fructose group in parallel. After the calculation, the averages of PK reaction rates presented in Figure 6-3(A2) are 3.20±1.24IU and 2.76±0.34IU for normal and fructose-fed rats, respectively.

Similar to PK, the slopes of KHK activity in both groups are seen to be very alike in Figure 6-3(B1). However, the slope of the fructose group is slightly more inclined than

that of the control one, suggesting the reaction rate of KHK is faster in the fructose group. With further analysis, it can be observed in Figure 6-3(B2) that the KHK activity rate is significantly higher in the rats exposed to the high-fructose diet than those fed with the normal chow, as in 4.1±0.56IU vs. 1.84±0.39IU.

These results indicate that high-fructose consumption has no effect on PK activity but has the capacity to accelerate KHK reaction rate significantly. Combined with the results from Western blotting in Figure 6-2(B), it can be concluded that the fructose-enriched diet induces fatty liver not only through up-regulating the protein expression level, but also increasing the reaction rates in the related metabolic pathway.

6.5 Chapter Conclusions

Stimulating KHK secretion and activity as well as suppress PPARα expression was confirmed in the high fructose feeding rats with the fatty livers. The experimental results in the current chapter are supporting the model predictions on interventional targets in Section 5.3.4.

7 Chapter 7: Conclusions and Future work

7.1 Overview

In this thesis, a systems biology approach has been adopted to explore the metabolic mechanisms whereby fructose consumption can induce dyslipidaemia associated with NAFLD and to explore whether the pathological conditions can be reversed during the early stages of disease.

The primary goal has been achieved as we presented a computational model of the hepatic fructose metabolism. This kinetic model is able to recapture the key features of NAFLD and point out a qualitative correct direction for further studies.

Secondly, the constructed model is robust and it has sufficient detail to predict the kinetic relationship between fructose and fatty liver under both healthy and insulin resistance conditions, which fulfils the second objective of the current project.

Combined the model simulation and experimental results, identification and evaluation of potential interventional targets for treating fructose-induced fatty liver have also been conducted matching the final goal.

The most significant remark is that the results support the hypothesis statement, fructose over-consumption does have a significant influence on the development of NAFLD. Throughout the first experimental attempt, we also eliminate the confounded factors of excessive calorie intake and fat.

Another finding is high-fructose intake combined with insulin resistance would greatly deteriorate hepatic lipid accumulation. This finding is not only consistent with the

proposed mechanism, but also allow the constructed model to serve as a tool to identify the potential interventional targets.

Last but not least, with three regulatory points being assessed in computational simulation, arousing KHK secretion and activity as well as suppress PPARα expression was confirmed in the high fructose feeding rats with the fatty livers, suggesting that they are suitable candidates for synergistic therapeutic treatment.

Although we have confidence in the model, we recognise that further validation work is necessary in order to improve and expanded the model. The major issue is that, at the current stage, the model is incapable of generating accurate quantitative prediction. Secondly, the actual dietary intake is more complicated than introduced in this model. The model is designed to give only the response to carbohydrate input. Thirdly, only acute effects of different carbohydrate diet could be represented by the current model. Simulation over a long period may result in cumulative errors. Last but not least, the structure of the liver is complex and the current simulations consider liver as a lumped model that neglects zonation across the liver plate.

Therefore, there are a few works could be done in the future.

7.2 Future work

The most urgent task is to further adjust and refine the model in order to narrow the gap between model prediction and clinical validation, which allows the model to match its simulation with the experimental data as accurate as possible.

In the short term, more experimental conductions should be processed in the *in vitro* models to further validate the constructed model by inhibiting KHK, activating PPARα and a combination of both.

Additionally, protein and fat can be added into the model as dietary inputs, in which a more realistic dietary pattern can be reproduced. Corresponding metabolic pathways of dietary protein and fat should then be included in the model. The effect of varying macronutrient distributions can be tested subsequently. Also, the current model simulated identical meal sizes for all three meals and the input simulation is rapid and simple. Therefore, a passage of food digestive process through the body should be considered to be added to the model, in order to simulate a more realistic liver uptake rate.

In the mediate term, the inflammatory and mitochondrial oxidative stress pathways should be included into the model to gain a better understanding of 'multiple-hit' mechanism of NAFLD. A threshold of lipid contents can be set to trigger the release of cytokines. The interactions between fructose metabolic pathways, insulin resistance and innate immune system should be added. Oxygen concentration should also be taken into account regarding oxidative stress. In addition, metabolism in adipose tissue and muscle tissue can also be integrated to simulate a multi-organ biological network.

In the long term, more comprehensive insight and more accurate information would be provided if the model could be further refined and expanded to include zonated effects. Furthermore, as the development of NAFLD can be multifactorial and multisystem-involved, other diseases such as diabetes, chronic kidney disease as well as cardiovascular

diseases should also be taken into consideration to construct a more sophisticated interaction system.

We believe that organ modelling *in silico* model systems will have numerous applications in developing future therapeutic strategies and represent a future growth area for disease modelling using the quantitative approaches applied by engineers to complex problems. These systems biology studies need to involve collaborations between engineers and clinical colleagues.

Appendix A. Initial Values and Parameter Values Setting

Table A-1. Initial values of variables and parameter values used in the model

Hepatocytes (SH)	Rate Equations	Initial values (uM), organism and references
Fructose	$\frac{dFru}{dt} = \mathrm{T}_{Fru} - \mathbb{R}_{KHK}$	$[Fru] = 30$; Human; (Sengupta et al., 2015)
Fructose-1-Phosphate	$\frac{dF1P}{dt} = \mathbb{R}_{KHK} - \mathbb{R}_{ald\mathrm{B}}$	$[F1P] = 0.2$; Human; (Sengupta et al., 2015, Rodrigues et al., 2014)
Glucose (Glu)	$\frac{dGlu}{dt} = \mathrm{T}_{Glu} - \mathbb{R}_{GK} + \mathbb{R}_{G6Pase}$	$[Glu] = 5500$; Human; (Ashworth et al., 2016)
Glucose-6-phosphate (G6P)	$\frac{dG6P}{dt} = \mathbb{R}_{GK} - \mathbb{R}_{G6Pase} + \mathbb{R}_{FBP} - \mathbb{R}_{PFK}$	$[G6P] = 102$; Human; (Ashworth et al., 2016)
Dihydroxyacetone phosphate	$\frac{dDHAP}{dt} = \mathbb{R}_{ald\mathrm{B}} - \mathbb{R}_{TPI_{DHAP}} + \mathbb{R}_{TPI_{GA3P}}$	$[DHAP] = 15$; Human; (Sengupta et al., 2015)
Glyceraldehyde	$\frac{dGA}{dt} = \mathbb{R}_{ald\mathrm{B}} - \mathbb{R}_{Tri}$	$[GA] = 1500$; Human; (Sengupta et al., 2015)
Glyceradehyde-3-phosphate	$\frac{dGA3P}{dt} = \mathbb{R}_{TPI_{DHAP}} - \mathbb{R}_{TPI_{GA3P}} + \mathbb{R}_{Tri} - \mathbb{R}_{PK} + \mathbb{R}_{PEPCK} - \mathbb{R}_{FBP} + \mathbb{R}_{PFK}$	$[GA3P] = 480$; Human; (Sengupta et al., 2015, Ashworth et al., 2016)
Pyruvate/Lactate	$\frac{dPyr}{dt} = T_{Lac} + \mathbb{R}_{PK} - \mathbb{R}_{PDC} - \mathbb{R}_{PEPCK}$	$[Pyr] = 1200$; Human; (Sengupta et

		al., 2015, Ashworth et al., 2016)
Acetyl-CoA	$\frac{dACoA}{dt} = \mathbb{R}_{PDC} - 8\,\mathbb{R}_{FAS} + 8\,\mathbb{R}_{boxi}$	$[ACoA] = 40$; Human; (Sengupta et al., 2015, Ashworth et al., 2016)
Fatty Acids (Palmitate)	$\frac{dFA}{dt} = T_{FFA} + \mathbb{R}_{FAS} - \mathbb{R}_{boxi} - 3\,\mathbb{R}_{TGS} + 3\,\mathbb{R}_{Lply}$	$[FA] = 50$; Human; (Sengupta et al., 2015, Ashworth et al., 2016)
Triglycerides	$\frac{dTG}{dt} = T_{TG} + \mathbb{R}_{TGS} - \mathbb{R}_{Lply}$	$[TG] = 1050$; Human; (Sengupta et al., 2015, Ashworth et al., 2016)
Hepatic Bloodstream (SHB)	**Rate Equations**	**Initial values (uM), organism and references**
Fructose	$\frac{dFru_{SHB}}{dt} = -T_{Fru} * R_{HE} + R_{BS} * (Fru_{SBC} - Fru_{SHB})$	$[Fru_{SHB}] = 50$; Human; (Sengupta et al., 2015, Ashworth et al., 2016)
Glucose (Simplified from (Ashworth et al., 2016))	$\frac{dGlu_{SHB}}{dt} = -T_{Glu} * R_{HE} + R_{BS} * (Glu_{SBC} - Glu_{SHB})$	$[Glu_{SHB}] = 5500$; Human; (Sengupta et al., 2015, Ashworth et al., 2016)
Pyruvate/Lactate (Simplified from (Ashworth et al., 2016))	$\frac{dPyr_{SHB}}{dt} = -T_{Pyr} * R_{HE} + R_{BS} * (Pyr_{SBC} - Pyr_{SHB})$	$[Pyr_{SHB}] = 1000$; Human; (Sengupta et al., 2015, Ashworth et al., 2016)

Fatty acids (Palmitate) **(Simplified from (2016))**	$\frac{dFA_{SHB}}{dt} = -T_{FA} * R_{HE} + R_{BS} * (FA_{SBC} - FA_{SHB})$	$[FA_{SHB}] = 500$; Human; (Sengupta et al., 2015, Ashworth et al., 2016)
Triglyceride **(Simplified from (Ashworth et al., 2016))**	$\frac{dTG_{SHB}}{dt} = -T_{TG} * R_{HE} + R_{BS} * (TG_{SBC} - TG_{SHB})$	$[TG_{SHB}] = 1050$; Human; (Sengupta et al., 2015, Ashworth et al., 2016)
Section Bloodstream Circulation (SBC)	**Rate Equations**	**Initial values (uM), organism and references**
Fructose	$\frac{dFru_{SBC}}{dt} = Meal_{Fru} + C_{Fru}$	$[Fru_{SBC}] = 50$; Human; (Sengupta et al., 2015, Ashworth et al., 2016)
Glucose **(Simplified from (Ashworth et al., 2016))**	$\frac{dGlu_{SBC}}{dt} = Meal_{Glu} + C_{Glu} - USE_{Glu} - UP_{FA} - UP_{TG}$	$[Glu_{SBC}] = 5500$; Human; (Sengupta et al., 2015, Ashworth et al., 2016)
Pyruvate/Lactate **(Simplified from (Ashworth et al., 2016))**	$\frac{dPyr_{SBC}}{dt} = C_{Pyr}$	$[Pyr_{SBC}] = 1000$; Human; (Sengupta et al., 2015, Ashworth et al., 2016)
Fatty acids (Palmitate) **(Simplified from (2016))**	$\frac{dFA_{SBC}}{dt} = C_{FA} - USE_{FA} + UP_{FA}$	$[FA_{SBC}] = 500$; Human; (Sengupta et al., 2015, Ashworth et al., 2016)

Triglyceride **(Simplified from (Ashworth et al., 2016))**	$\frac{dTG_{SBC}}{dt} = C_{TG} - USE_{TG} + UP_{TG}$	$[TG_{SBC}] = 1050$; Human; (Sengupta et al., 2015, Ashworth et al., 2016)
Hepatic Enzymes /Reactions in SH	**Rate Functions**	**Parameter values, organism and references (Km unit: μM; Reaction rate unit: μM/s)**
Fructokinase	$\mathbb{R}_{KHK} = \mathrm{V}_{KHK} * \frac{Fru^{nf}}{Km_{KHK}{}^{nf} + Fructose^{nf}} * \frac{ATP^{nATP}}{Km_{ATP}{}^{nATP} + ATP^{nATP}}$	$Km_{KHK} = 800$; Human; (Bais et al., 1985) $Km_{ATP} = 1430$; Rat; (Phillips and Davies, 1985) $\mathrm{V}_{KHK} = 4.5$; Human; (Asipu et al., 2003)
Aldolase B	$\mathbb{R}_{aldB} = V_{aldB} * \frac{F1P^{nF1P}}{Km_{F1P}{}^{nF1P} + F1P^{nF1P}}$	$Km_{F1P} = 230$; Human; (Doyle and Tolan, 1995) $V_{aldB} = 1.7$; Human; (Malay et al., 2002)
Triose phosphate isomerase	$\mathbb{R}_{TPI_{DHAP}} = V_{TPI_{DHAP}} * \frac{DHAP^{nDHAP}}{Km_{DHAP}{}^{nDHAP} + DHAP^{nDHAP}}$	$Km_{DHAP} = 590$; Human; (Yuan et al., 1979, Gracy, 1975, Snyder and Lee, 1975)

	$\mathbb{R}_{TPI_{GA3P}} = V_{TPI_{GA3P}} * \frac{GA3P^{nGA3P}}{Km_{GA3P_{TPI}}{}^{nGA3P} + GA3P^{nGA3P}}$	$Km_{GA3P_{TPI}} = 400$; Human; (Snyder and Lee, 1975) $V_{TPI_{DHAP}} = 2.7$; Human; (Yuan et al., 1979, Gracy, 1975, Snyder and Lee, 1975) $V_{TPI_{GA3P}} = 0.05$; Human; (Yuan et al., 1979, Gracy, 1975, Snyder and Lee, 1975)
Triokinase	$\mathbb{R}_{Tri} = V_{Tri} * \frac{GA^{nGA}}{Km_{GA}{}^{nGA} + GA^{nGA}} * \frac{ATP_{Mg^{2-}}{}^{nATP_{Mg^{2-}}}}{Km_{ATP_{Mg^{2-}}}{}^{nATP_{Mg^{2-}}} + ATP_{Mg^{2-}}{}^{nATP_{Mg^{2-}}}} * \left(1 - \beta_{ATP} \frac{ATP}{K_i^{ATP} + ATP}\right)\left(1 - \beta_{ADP} \frac{ADP}{K_i^{ADP} + ADP}\right)$	$Km_{GA} = 18$; Rat; (Sillero et al., 1969) $Km_{ATP_{Mg^{2-}}} = 770$; Rat; (Frandsen and Grunnet, 1971) $K_i^{ATP} = 380$; Rat; (Frandsen and Grunnet, 1971) $K_i^{ADP} = 1100$; Rat; (Frandsen and Grunnet, 1971) $V_{Tri} = 6.7$; Rat; (Sillero et al., 1969)
Pyruvate kinase	$\mathbb{R}_{PK} = V_{PK} * \frac{GA3P^{nGA3P}}{Km_{GA3P}{}^{nGA3P} + GA3P^{nGA3P}} * \frac{ADP^{nADPpk}}{Km_{ADPpk}{}^{nADP} + ADP^{nADPpk}} * \left(1 - \beta_{ACoA-PK} \frac{ACoA}{K_i^{ACoA-PK} + ACoA}\right)$	$Km_{GA3P} = 250$; Human; (Daly et al., 1998, Albe et al., 1990, Taylor et al., 1996)

		$Km_{ADPpk} = 240$; Human; (Dombrauckas et al., 2005) $K_i^{ACoA-PK} = 30$; Rat; (Weber et al., 1967) $\beta_{ACoA-PK} = 0.8$; Rat; (Weber et al., 1967) $V_{PK} = 87$; Human; (Ashworth et al., 2016)
Phosphoenolpyruvate carboxykinase	$\mathbb{R}_{PEPCK} = V_{PEPCK} * \frac{Pyr}{K_m^{PEPCK}+Pyr} * \frac{ATP}{K_m^{ATPpepck}+ATP} * \frac{GTP}{K_m^{GTP}+GTP}$	$K_m^{PEPCK} = 500$; Human; (Daly et al., 1998, Albe et al., 1990, Taylor et al., 1996) $K_m^{ATPpepck} = 10$; Estimated; (Ashworth et al., 2016) $K_m^{GTP} = 64$; Human; (Dharmarajan et al., 2008) $V_{PEPCK} = 35$; Human; (Ashworth et al., 2016)
Pyruvate oxidation	$\mathbb{R}_{PDC} = V_{PDC} * \frac{Pyr}{K_m^{Pyr}+Pyr} * \left(1 - \beta_{ACoA-PDC} \frac{ACoA}{ACoA+k_i^{CoA-pyr}}\right)$	$K_m^{Pyr} = 540$; Human; (Daly et al., 1998, Albe et al., 1990, Taylor et al., 1996, Ainscow and Brand, 1999) $k_i^{CoA-pyr} = 35$; Human; (Kiselevsky et al., 1990)

		$\beta_{ACoA-PDC} = 1$; Human; (Kiselevsky et al., 1990) $V_{PDC} = 15$; Human; (Ashworth et al., 2016)
Fatty acid synthesis	$\mathbb{R}_{FAS} = V_{FAS} * \frac{ACoA}{K_m^{ACoA}+ACoA} * \frac{ATP}{K_m^{ATPfas}+ATP} * \left(1 - \beta_{FA} \frac{FA}{FA+k_i^{FA-inhib}}\right)$	$K_m^{ACoA} = 58$; Human; (Cheng et al., 2007) $K_m^{ATPfas} = 120$; Human; (Cheng et al., 2007) $\beta_{FA} = 1$; Human; (Reaven et al., 1988) $k_i^{FA-inhib} = 300$; Human; (Reaven et al., 1988) $V_{FAS} = 4$; Human; (Ashworth et al., 2016)
Beta-oxidation	$\mathbb{R}_{boxi} = V_{boxi} * \frac{FA}{K_m^{boxi}+FA} * \frac{ATP}{K_m^{ATPboxi}+ATP} * \left(1 - \beta_{boxi} \frac{ACoA}{ACoA+k_i^{CoA-boxi}}\right) * \left(1 - \beta_{PPAR\alpha} \frac{F1P}{F1P+k_i^{F1P-inhib}}\right)$	$K_m^{boxi} = 5$; Rat; (Kim et al., 2001, Van Horn et al., 2005, Marcel and Suzue, 1972) $K_m^{ATPboxi} = 87$; Rat; (Stinnett et al., 2007) $k_i^{CoA-boxi} = 47.8$; Human; (Zierz and Engel, 1987)

		$k_i^{F1P-inhib} = 100$; Rat; (Nomura and Yamanouchi, 2012) $\beta_{boxi} = 0.4$; Human; (Zierz and Engel, 1987) $\beta_{PPAR\alpha} = 1$; Rat; (Nomura and Yamanouchi, 2012) $V_{boxi} = 3.3$; Human; (Ashworth et al., 2016)
Triglyceride synthesis	$\mathbb{R}_{TGS} = V_{TGS} * \frac{FA}{K_m^{FA}+FA} * \frac{GA3P}{K_m^{GADP}+GADP}$	$K_m^{FA} = 645$; Rat; (Kim et al., 2001, Van Horn et al., 2005, Marcel and Suzue, 1972) $K_m^{GADP} = 460$; (Vancura and Haldar, 1994) $V_{TGS} = 10$; Human; (Ashworth et al., 2016)
Lipolysis	$\mathbb{R}_{Lply} = V_{Lply} * \frac{TG}{K_m^{TG} + TG}$	$K_m^{TG} = 50715$; Non-human; (KAPLAN and Teng, 1971, Chakraborty and Raj, 2008) $V_{Lply} = 0.085$; Human; (Ashworth et al., 2016)

Transport Variables in SHB	Rate Functions for cross-membrane transportation	Parameter values, organism and references (Km unit: μM; Reaction rate unit: μM/s)
Fructose	$T_{Fru} = V_{GLUT2}^{pump} * \frac{Fru_{SHB}}{K_m^{GLUT2-pump} + Fru_{SHB}} + V_{GLUT2}^{ex} * \frac{Fru_{SHB} - Fru_{SH}}{K_m^{GLUT2-ex} + Fru_{SHB} + Fru_{SH}}$ $V_{GLUT5}^{pump} * \frac{Fru_{SHB}}{K_m^{GLUT5-pump} + Fru_{SHB}} + V_{GLUT5}^{ex} * \frac{Fru_{SHB} - Fru_{SH}}{K_m^{GLUT5-ex} + Fru_{SHB} + Fru_{SH}}$	$K_M^{GLUT2-pump} = 76000$; Cell culture; (Zhao and Keating, 2007) $K_m^{GLUT2-ex} = 76000$; Cell culture; (Zhao and Keating, 2007) $K_m^{GLUT5-pump} = 6000$; (Burant et al., 1992, Zhao and Keating, 2007, Karim et al., 2012) $K_m^{GLUT5-ex} = 6000$; Human & Cell culture; (Burant et al., 1992, Zhao and Keating, 2007, Karim et al., 2012) $V_{GLUT2}^{pump} = 10$; Cell culture; (Zhao and Keating, 2007) $V_{GLUT2}^{ex} = 30$; Cell culture; (Zhao and Keating, 2007) $V_{GLUT5}^{pump} = 20$; Human & Cell culture; (Burant

		et al., 1992, Zhao and Keating, 2007, Karim et al., 2012) $V_{GLUT5}^{ex} = 60$; Human & Cell culture; (Burant et al., 1992, Zhao and Keating, 2007, Karim et al., 2012)
Glucose	$T_{Glu} = V_{GLUTG}^{pump} * \frac{Glu_{SHB}}{K_m^{GLUTG-pump} + Glu_{SHB}} + V_{GLUTG}^{ex} * \frac{Glu_{SHB} - Glu_{SH}}{K_m^{GLUTG-ex} + Glu_{SHB} + Glu_{SH}}$	$K_m^{GLUTG-pump} = 17000$; Human & Cell culture; (Thorens, 1992, Zhao and Keating, 2007, Laughlin, 2014) $K_m^{GLUTG-ex} = 17000$; Human & Cell culture; (Thorens, 1992, Zhao and Keating, 2007, Laughlin, 2014) $V_{GLUTG}^{pump} = 118$; Human; (Ashworth et al., 2016) $V_{GLUTG}^{ex} = 224$; Human; (Ashworth et al., 2016)
Pyruvate/Lactate	$T_{Pyr} = V_{Pyr}^{ex} * \frac{Pyr_{SHB} - Pyr_{SH}}{K_m^{Pyr-ex} + Pyr_{SHB} + Pyr_{SH}}$	K_m^{Pyr-ex} =1200; Human; (Ashworth et al., 2016) $V_{Pyr}^{ex} = 200$; Human; (Ashworth et al., 2016)

Fatty acids (Palmitate)	$T_{FA} = V_{FA}^{ex} * \frac{FA_{SHB} - FA_{SH}}{K_m^{FA-ex} + FA_{SHB} + FFA_{SH}} + V_{active} * \frac{FA_{SHB}}{(K_m^{active} + FA_{SHB})} \left(1 + \frac{Ins}{Ins_{ref}^{active}}\right)$	$K_m^{FA-ex} = 200$; Human; (Ashworth et al., 2016) $K_m^{active} = 2$; Human; (Ashworth et al., 2016) $V_{FA}^{ex} = 1.45$; Human; (Ashworth et al., 2016) $V_{active} = 0.08$; Human; (Ashworth et al., 2016)
Triglyceride	$T_{TG} = V_{TG}^{ex} * \frac{\left(TG_{SHB} - \frac{TG_{SH}}{TG_{ref}}\right)}{K_m^{TG-ex} + TG_{SHB} + \frac{TG_{SH}}{TG_{ref}}} - V_{out} * \frac{TG_{SH}}{(K_m^{out} + TG_{SH})}$	$K_m^{TG-ex} = 1000$; Human; (Ashworth et al., 2016) $K_m^{out} = 33810$; Human; (Ashworth et al., 2016) $V_{TG}^{ex} = 0.6$; Human; (Ashworth et al., 2016) $V_{out} = 0.3$; Human; (Ashworth et al., 2016)
Glucose input variables **(Simplified from (Ashworth et al., 2016))**	**Rate Functions**	**Parameter values, organism and references (Km unit: μM; Reaction rate unit: μM/s)**

Glucokinase	$\mathbb{R}_{GK} = \mathrm{V}_{GK} * \frac{Glu^{nGlu}}{Km_{Glu}{}^{nGlu} + Glu^{nGlu}} * \frac{ATP^{nATP}}{Km_{ATPgk}{}^{nATP} + ATP^{nATP}} * \left(1 - \frac{G6P}{G6P + k_i^{G6P}}\right)$	$Km_{Glu} = 7500$; Human; (Ashworth et al., 2016) $Km_{ATPgk} = 240$; Human; (Ashworth et al., 2016) $k_i^{G6P} = 240$; Human; (Ashworth et al., 2016) $\mathrm{V}_{GK} = 132.16$; Human; (Ashworth et al., 2016)
Glucose-6-phosphatase	$\mathbb{R}_{G6Pase} = V_{G6Pase} * \frac{G6P}{K_m^{G6Pase} + G6P}$	$K_m^{G6Pase} = 2410$; Human; (Ashworth et al., 2016) $V_{G6Pase} = 370$; Human; (Ashworth et al., 2016)
Fructose-bisphosphatase	$\mathbb{R}_{FBP} = V_{FBP} * \frac{GA3P}{K_m^{FBP} + GA3P}$	$K_m^{FBP} = 250$; Human; (Ashworth et al., 2016) $V_{FBP} = 68$; Human; (Ashworth et al., 2016)
Phosphofructokinase	$\mathbb{R}_{PFK} = V_{PFK} * \frac{G6P}{K_m^{PFK} + G6P} * \frac{ATP}{Km_{ATPpfk} + ATP} * \left(1 - \frac{ATP}{ATP + k_i^{ATPfpk}} * \frac{ADP}{ADP + k_i^{ADPfpk}}\right) * \left(1 - \beta_{PFK} \frac{GA3P}{GA3P + k_i^{GA3Ppfk}}\right)$	$K_m^{PFK} = 5$; Human; (Ashworth et al., 2016) $Km_{ATPpfk} = 42.5$; Human; (Ashworth et al., 2016)

		$k_i^{ATPfpk} = 2100$; Human; (Ashworth et al., 2016) $k_i^{ADPfpk} = 83.6$; Human; (Ashworth et al., 2016) $k_i^{GA3Ppfk} = 20.7$; Human; (Ashworth et al., 2016) $\beta_{PFK} = 0.75$; Human; (Ashworth et al., 2016) $V_{PFK} = 160$; Human; (Ashworth et al., 2016)

Appendix B. MATLAB Code Script

```
function dydt=Fructose_YL(t,y)
% 1. Function Inputs
% 1.1 Plasma section
B_F = y(1); % Blood Fructose
B_G = y(2); % Blood Glucose
B_L = y(3); % Blood Lactate
B_FFA = y(4); % Blood Free Fatty Acids
B_TG = y(5); % Blood Triglyceride
P_Ins = y(6); % Pancreas Insulin
P_Gcg = y(7);  % Pancreas Glucagon
% 1.2 Bloodstream Exchange section --- Hepatic blood
EX_F = y(8); % Fructose Exchange
EX_G = y(9); % Glucose Exchange
EX_L = y(10); % Lactate Exchange
EX_FFA = y(11); % Free Fatty Acids Exchange
EX_TG = y(12); % Triglyceride Exchange
EX_Ins = y(13); % Insulin Exchange
EX_Gcg = y(14);  % Glucagon Exchange
% 1.3 Hepatic section
Fru = y(15); % Hepatic fructose
F1P = y(16); % Hepatic Fructose-1-phosphate
Glu = y(17); % Hepatic Glucose
G6P = y(18); % Hepatic Glucose-6-phosphate
DHAP = y(19); % Hepatic Dihydroxyacetone phosphate
GA = y(20); % Hepatic Glyceraldehyde
GA3P = y(21); % Hepatic D-glyceraldehyde 3-phosphate
```

```
pyr = y(22); % Hepatic Pyruvate/Lactate
acoa = y(23); % Hepatic Acetyl-CoA
FA = y(24); % Hepatic Fatty acid
TG = y(25); % Hepatic Triglyceride
% 1.4 Conditional control
lipoi = y(26);
lipol = y(27);
trii = y(28);
tril = y(29);

% 2. Input of fructose and glucose in the liver
% Input of fructose (uptake rate based on portal vein concentration)
DriveFru = 4.5;
DriveGlu = 12.34;
timeref = 28800;
pow = 6;

% 3. Parameter values:
% 3.1 Bloodstream dynamic
R_BS = 0.167;
R_RL = 5.25;
R_HE = 4;
% 3.2 Transportation
% 3.2.1 Fructose
v_glut2 = 10;
k_glut2 = 76000;
v_ex2 = 30;
```

k_ex2 = 76000;

v_glut5 = 20;

k_glut5 = 6000;

v_ex5 = 60;

k_ex5 = 6000;

% 3.2.2 Glucose

v_glutG = 118;

k_glutG = 17000;

v_exG = 224;

k_exG = 17000;

% 3.2.3 Pyruvate/Lactate

v_exLac = 200;

k_exLac = 1200;

% 3.2.5 Free fatty acids

v_exFA = 1.45;

k_exFA = 200;

v_act = 0.08;

InsRef = 21.33;

k_act = 2;

% 3.2.6 Triglycerides

v_outTG = 0.3;

k_outTG = 33810;

v_exTG=0.6;

k_exTG=1000;

TTGRef=6.5;

% 3.3 Adipose & Muscle (rest of the body usage)

% 3.3.1 Glucose uptake by the rest of the body

```
k_useG = 1000;
v_useG = 5.15;
% 3.3.2 FFA uptake by the rest of the body
k_gcgFFA=1;
k_insFFA=0.6;
v_useFFA=1.4;
k_useFFA=100;
% 3.3.3 Fructose uptake
v_useF = 5.15;
k_useF = 1000;
% 3.3.3 DNL in the rest of the body
k_useDNL=4500;
v_useDNL=0.11;
% 3.3.4 TG Synthesis in the rest of the body
v_useTGS = 3;
k_useTGSg=10000;
k_useTGSffa=645;
% 3.3.5 TG consumption by the rest of the body
v_useLil=2.3;
k_useLil=2000;
% 3.4 Michaelis constant & enzymatic maximum rates (Vmax)
% Unit concentration(uM), time(s), rate (uM/s)
% Hepatic section
k_fru = 800;
v_khk = 4.5;
k_ATPkhk = 1430;
k_F1P = 230;
```

```
v_ald = 1.7;
k_DHAP = 590;
v_TPI_DHAP = 2.7;
k_GA3P_TPI= 400;
v_TPI_GA3P = 0.05;
k_GA = 18;
v_Tri = 16.7;
k_ATPMg = 770;
kiATPiTri = 380;
kiADPiTri = 1100;
k_GA3P_PK =250;
v_PK = 87;
k_ADPpk = 240;
eff = 0.8;
kiacoaPK = 30;
k_pyr = 540;
v_PDC = 15;
kiacoaPDC = 35;
v_PEPCK = 35;
k_PEPCK = 500;
k_ATPglu = 10;
k_GTPglu = 64;
% Lipogenesis
v_lipg = 4;
k_acoa = 58;
k_ATPlipg = 120;
kiFA = 300;
```

```
% Beta-oxidation
v_boxi = 3.3;
k_boxi = 5;
effac = 1;
kiacbox = 47.8;
k_ATPbox = 87;
effPPAR = 1;
kiF1P = 100;
% Triglyceride Synthesis
v_tsyn = 10;
k_GA3P_tsyn = 460;
k_FA = 645;
% Lipolysis
v_lipo = 0.085;
k_TG = 50715;
% Glucose combination (simplified from Ashworth's model)
v_GK = 132.16;
nglu = 1.4;
k_glu = 7500;
k_ATPgk = 240;
kig6pGK = 240;
nig6pGK = 4;
v_G6P = 370;
k_G6P = 2410;
hFBPPFKref = 10;
v_FBP = 68;
k_FBP = 250;
```

```
v_PFK = 160;
k_PFK = 5;
k_ATPpfk = 42.5;
kiatpPFK = 2100;
kiadpPFK = 83.6;
effpfk = 0.75;
kiga3p = 20.7;
hPEPCKref = 8.5;
hPKref = 4;
hACOAInsref = 5;
hACOAGcgref = 3;
hDNLInsref = 3;
hDNLGcgref = 7;
hboxiInsref = 2.5;
hboxiGcgref = 7;
hTGSInsref = 4;
hTGSGcgref = 4;
hLplyInsref = 4;
hplyGcgref = 5;
ATP = 2780;
ADP = 285;
GTP = 284;
% Pancreatic Hormone Release and Transport in Blood
% Insulin and Glucagon setting based on Heatherington's model
rel=5;
gr=3;
gri=2;
```

```
tauL=0.036;
tLg=1.3;
nL=2;
ML=3;
tauI=0.075;
tIg=0.9;
nI=2;
MI=4;
BloodScale=4.9999995e-4;
mins=60;
P_Ins = 266.67*P_Ins;
P_Gcg = 125*P_Gcg;
EX_Ins = 266.67*EX_Ins;
EX_Gcg = 125*EX_Gcg;
slow=15;
fast=0.07;
Lreftriw=0.3;
Ireftriw=3;
tti=1000;
ttl=10000;
tli=1000;
tll=10000;
LrefLipow=0.3;
Ireflipow=3;

% 4. Dietary Inputs
% 4.1 Dietary Input of Fructose
```

```
if t<=43200
   M_Fru = (DriveFru*((sin(2*pi*t/(timeref))).^pow));
elseif (129600>=t) && (t>=86400)
   M_Fru = (DriveFru*((sin(2*pi*t/(timeref))).^pow));
else
   M_Fru = 0;
end
% 4.2 Dietary Input of Glucose
if t<=43200
   M_Glu = (DriveGlu*((sin(2*pi*t/(timeref))).^pow));
elseif (129600>=t) && (t>=86400)
   M_Glu = (DriveGlu*((sin(2*pi*t/(timeref))).^pow));
else
   M_Glu = 0;
end

% 5. Cross-membrane transportation
% 5.1 Fructose transportation
T_GLUT2 = v_glut2*EX_F/(k_glut2+EX_F) + v_ex2*(EX_F-Fru)/(k_ex2+EX_F+Fru);
T_GLUT5 = v_glut5*EX_F/(k_glut5+EX_F) + v_ex5*(EX_F-Fru)/(k_ex5+EX_F+Fru);
% 5.2 Glucose transportation
T_GLUTG = v_glutG*EX_G/(k_glutG+EX_G) + v_exG*(EX_G-Glu) / (k_exG + EX_G
+ Glu);
% 5.3 Lactate transportation
T_Lac=v_exLac*(EX_L-pyr)/(k_exLac+EX_L+pyr);
% 5.4 Free fatty acids transportation
T_FA = v_exFA*(EX_FFA-FA) / (k_exFA + EX_FFA + FA) + v_act * EX_FFA * (1 +
EX_Ins /InsRef)/(EX_FFA+k_act);
```

```
% Triglyceride transportation

T_TG = v_exTG*(EX_TG-TG/TTGRef)/(k_exTG+TG/TTGRef+EX_TG)- (v_outTG
*TG /(k_outTG+TG));


% 6. Adipose & Muscle (rest of the body usage)

% Glucose usage

U_G=v_useG*B_G/(k_useG+B_G);

% FFA usage

U_FFA=v_useFFA*B_FFA/(B_FFA+k_useFFA)*((P_Ins+k_insFFA)/(P_Gcg+k_gcgF
FA));

% DNL

irefdenog=7;

lrefdenog=2;

U_DNL = v_useDNL*B_G/(B_G+k_useDNL) * turn ((1+P_Ins/irefdenog-P_Gcg/
lrefdenog));

% Glucose and FFA removal (Adipose & Muscle Triglyceride Synthesis)

if (P_Ins/Ireftriw-trii)>0

   dtriidt=(P_Ins/Ireftriw-trii)/tti;

else

   dtriidt=(P_Ins/Ireftriw-trii)/(slow*tti);

end

if (P_Gcg/Lreftriw-tril)>0

   dtrildt=(P_Gcg/Lreftriw-tril)/ttl;

else

   dtrildt=(P_Gcg/Lreftriw-tril)/(fast*ttl);

end

U_TGS=v_useTGS*(B_G*B_FFA)/((k_useTGSg+B_G)*(k_useTGSffa+B_FFA))*turn
(1+trii-tril);

% Triglyceride Removal (Adipose & Muscle lipolysis)
```

```
if (P_Ins/Ireflipow-lipoi)>0
   dlipoidt=(P_Ins/Ireflipow-lipoi)/tli;
else
   dlipoidt=(P_Ins/Ireflipow-lipoi)/(slow*tli);
end
if (P_Gcg/LrefLipow-lipol)>0
   dlipoldt=(P_Gcg/LrefLipow-lipol)/tll;
else
   dlipoldt=(P_Gcg/LrefLipow-lipol)/(fast*tll);
end
U_Lil = v_useLil*B_TG/(B_TG+k_useLil)*turn(1-lipoi+lipol);

% 7. Hepatic reaction rate of each enzyme
% Fructose
r_khk = v_khk*1/(k_fru/Fru+1);
r_ATPkhk = 1/(k_ATPkhk/ATP+1);
r_ald = v_ald*1/(k_F1P/F1P+1);
r_TPI_DHAP = v_TPI_DHAP*1/(k_DHAP/DHAP+1);
r_TPI_GA3P = v_TPI_GA3P*1/(k_GA3P_TPI/GA3P+1);
r_Tri = v_Tri*1/(k_GA/GA+1);
r_ATPTri = 1/(k_ATPMg/ATP+1);
r_ATPiTri = 1-eff*(1/(1+kiATPiTri/ATP));
r_ADPiTri = 1-eff*(1/(1+kiADPiTri/ADP));
r_pyr = v_PDC*1/(k_pyr/pyr+1);
r_acoaiPDC = 1-(1/(1+kiacoaPDC/acoa));
r_acoa = v_lipg*1/(k_acoa/acoa+1);
r_ATPlipg = 1/(k_ATPlipg/ATP+1);
```

```
r_FAilipg = (1-(1/(1+kiFA/FA)));

r_FA = v_tsyn*1/(k_FA/FA+1);

r_GA3Ptsyn = 1/(k_GA3P_tsyn/GA3P+1);

r_glugen = v_PEPCK*1/(k_PEPCK/pyr+1);

r_ATPglu = 1/(k_ATPglu/ATP+1);

r_GTPglu = 1/(k_GTPglu/GTP+1);

r_FAboxi = v_boxi*1/(k_boxi/FA+1);

r_aciboxi = 1-effac*(1/(1+kiacbox/acoa));

r_ATPboxi = 1/(1+k_ATPbox/ATP);

r_PPARboxi = 1-effPPAR*(1/(1+kiF1P/F1P));

r_TG = v_lipo*1/(k_TG/TG+1);

% Glucose combination

r_GK = v_GK*((Glu.^nglu)/((Glu.^nglu)+((k_glu).^nglu))) * (ATP / (ATP + k_ATPgk
))*(1-Hill(G6P,kig6pGK,nig6pGK));

r_G6Pase =v_G6P*G6P/(G6P+k_G6P);

h_FBP = (EX_Gcg+hFBPPFKref)/(EX_Ins+hFBPPFKref);

r_FBP = v_FBP*h_FBP*Hill(GA3P,k_FBP,1);

h_PFK = (EX_Ins+hFBPPFKref)/(EX_Gcg+hFBPPFKref);

r_PFK = v_PFK*h_PFK*Hill(G6P,k_PFK,1)*((ATP/(ATP+k_ATPpfk)))*(1-(ATP/
(ATP +kiatpPFK)))*(ADP/(ADP+kiadpPFK))* (1-effpfk *(GA3P/(GA3P+kiga3p)));

h_PEPCK = (EX_Gcg+hPEPCKref)/(EX_Ins+hPEPCKref);

r_PEPCK = h_PEPCK*r_glugen*r_ATPglu*r_GTPglu;

h_PK = (EX_Ins+hPKref)/(EX_Gcg+hPKref);

r_PK = v_PK*h_PK*Hill(GA3P,k_GA3P_PK,1)*(ADP/(ADP+k_ADPpk))*(1-eff*
(acoa/(acoa+kiacoaPK)));

h_PDC = 1+EX_Ins/hACOAInsref-EX_Gcg/hACOAGcgref;

r_PDC = h_PDC*r_pyr*r_acoaiPDC;

h_DNL = 1+EX_Ins/hDNLInsref-EX_Gcg/hDNLGcgref;
```

```
r_DNL = h_DNL*r_acoa*r_ATPlipg*r_FAilipg;

h_boxi =1-EX_Ins/hboxiInsref+EX_Gcg/hboxiGcgref;

r_boxi = h_boxi*r_FAboxi*r_aciboxi*r_ATPboxi*r_PPARboxi;

h_TGS = 1+EX_Ins/hTGSInsref-EX_Gcg/hTGSGcgref;

r_TGS = turn(h_TGS)*r_FA*r_GA3Ptsyn;

h_Lply = 1-EX_Ins/hLplyInsref+EX_Gcg/hplyGcgref;

r_Lply = turn(h_Lply)*r_TG;


% 8. Differential Equations:

% 8.1 Plasma section

dB_Fdt = M_Fru+(R_BS*(EX_F-B_F))/R_RL;

dB_Gdt = M_Glu+(R_BS*(EX_G-B_G))/R_RL-U_G-U_DNL-U_TGS/2;

if B_G<=4500

   B_G = 4500;

elseif B_G>=12500

   B_G = 12500;

else

   dB_Gdt = M_Glu+(R_BS*(EX_G-B_G))/R_RL-U_G-U_DNL-U_TGS/2;

end

dB_Ldt = R_BS*(EX_L-B_L)/R_RL;

dB_FFAdt = R_BS*(EX_FFA-B_FFA)/R_RL-U_FFA-U_TGS+3*U_Lil+4*U_DNL;

dB_TGdt = R_BS*(EX_TG-B_TG)/R_RL+U_TGS-U_Lil;

% Plasma hormone release

dP_Insdt = (1/(tauI*rel*mins))*(Hill(Aln(BloodScale*B_G/gri),tIg,nI)) - (R_BS*(P_Ins-
EX_Ins))/R_RL;

dP_Gcgdt = (1/(tauL*rel*mins))*(Hill(Aln(gr/(BloodScale*B_G)),tLg,nL)) -
(R_BS*(P_Gcg-EX_Gcg))/R_RL;

% 8.2 Bloodstream Exchange section --- Hepatic bloodstream
```

```
dEX_Fdt = - 1/2*(T_GLUT2+T_GLUT5)*R_HE+R_BS*(B_F-EX_F);

dEX_Gdt = - T_GLUTG*R_HE+R_BS*(B_G-EX_G);

dEX_Ldt = - T_Lac*R_HE+R_BS*(B_L-EX_L);

dEX_FFAdt = - T_FA*R_HE+R_BS*(B_FFA-EX_FFA);

dEX_TGdt = - T_TG*R_HE+R_BS*(B_TG-EX_TG);

% Hepatic hormone uptake

dEX_Insdt = -(1/(tauI*mins))*(EX_Ins/MI) +R_BS*(P_Ins-EX_Ins);

dEX_Gcgdt = -(1/(tauL*mins))*(EX_Gcg/ML) +R_BS*(P_Gcg-EX_Gcg);

% 8.3 Hepatic section

dFrudt = 1/2*T_GLUT2+1/2*T_GLUT5-r_khk*r_ATPkhk;

dF1Pdt = r_khk*r_ATPkhk-r_ald;

dGludt = T_GLUTG-r_GK+r_G6Pase ;

dG6Pdt = r_GK-r_G6Pase+r_FBP-r_PFK;

dDHAPdt = r_ald-r_TPI_DHAP+r_TPI_GA3P;

dGAdt = r_ald-r_Tri*r_ATPTri*r_ATPiTri*r_ADPiTri+r_Lply;

dGA3Pdt = r_TPI_DHAP+r_Tri*r_ATPTri*r_ATPiTri*r_ADPiTri-r_PK-r_TGS-
r_TPI_GA3P+r_PEPCK-2*r_FBP+2*r_PFK;

dpyrdt = T_Lac+r_PK-r_PDC-r_PEPCK;

dacoadt = r_PDC-8*r_DNL+8*r_boxi;

dFAdt = T_FA+r_DNL-r_boxi-r_TGS+r_Lply;

dTGdt = T_TG+1/3*r_TGS-1/3*r_Lply;

% Function Outputs

dydt =[dB_Fdt; dB_Gdt; dB_Ldt; dB_FFAdt; dB_TGdt; dP_Insdt; dP_Gcgdt;...

   dEX_Fdt; dEX_Gdt; dEX_Ldt; dEX_FFAdt; dEX_TGdt; dEX_Insdt; dEX_Gcgdt;...

   dFrudt; dF1Pdt; dGludt; dG6Pdt; dDHAPdt; dGAdt; dGA3Pdt; dpyrdt; dacoadt;
dFAdt; dTGdt;...

   dlipoidt; dlipoldt; dtriidt; dtrildt];

end
```

References

ABDELMALEK, M. F., LAZO, M., HORSKA, A., BONEKAMP, S., LIPKIN, E. W., BALASUBRAMANYAM, A., BANTLE, J. P., JOHNSON, R. J., DIEHL, A. M. & CLARK, J. M. 2012. Higher dietary fructose is associated with impaired hepatic adenosine triphosphate homeostasis in obese individuals with type 2 diabetes. *Hepatology,* 56**,** 952-960.

ABDELMALEK, M. F., SUZUKI, A., GUY, C., UNALP‐ARIDA, A., COLVIN, R., JOHNSON, R. J. & DIEHL, A. M. 2010. Increased fructose consumption is associated with fibrosis severity in patients with nonalcoholic fatty liver disease. *Hepatology,* 51**,** 1961-1971.

ABRAHA, A., HUMPHREYS, S. M., CLARK, M. L., MATTHEWS, D. R. & FRAYN, K. N. 1998. Acute effect of fructose on postprandial lipaemia in diabetic and non-diabetic subjects. *British journal of nutrition,* 80**,** 169-175.

ADEN, D. P., FOGEL, A., PLOTKIN, S., DAMJANOV, I. & KNOWLES, B. B. 1979. Controlled synthesis of HBsAg in a differentiated human liver carcinoma-derived cell line. *Nature,* 282**,** 615-616.

AINSCOW, E. K. & BRAND, M. D. 1999. Top‐down control analysis of ATP turnover, glycolysis and oxidative phosphorylation in rat hepatocytes. *European Journal of Biochemistry,* 263**,** 671-685.

AINSWORTH, S. & MACFARLANE, N. 1973. A kinetic study of rabbit muscle pyruvate kinase. *Biochemical Journal,* 131**,** 223-236.

ALBE, K. R., BUTLER, M. H. & WRIGHT, B. E. 1990. Cellular concentrations of enzymes and their substrates. *Journal of theoretical biology,* 143**,** 163-195.

ALLEN, R. J. & MUSANTE, C. J. 2017. Modeling fructose-load-induced hepatic de-novo lipogenesis by model simplification. *Gene regulation and systems biology,* 11**,** 1177625017690133.

ALLEN, R. J. & MUSANTE, C. J. 2018. A mathematical analysis of adaptations to the metabolic fate of fructose in essential fructosuria subjects. *American Journal of Physiology-Endocrinology and Metabolism,* 315**,** E394-E403.

AMIN, A. A., AGARWAL, B. & JALAN, R. 2019. Acute liver failure: updates in pathogenesis and management. *Medicine,* 47**,** 838-842.

ANISSIMOV, Y. G. & ROBERTS, M. S. 2002. A compartmental model of hepatic disposition kinetics: 1. Model development and application to linear kinetics. *Journal of pharmacokinetics and pharmacodynamics,* 29**,** 131-156.

ANSTEE, Q. M., TARGHER, G. & DAY, C. P. 2013. Progression of NAFLD to diabetes mellitus, cardiovascular disease or cirrhosis. *Nature reviews Gastroenterology & hepatology,* 10**,** 330.

ARIAS, B., FAUSTO, JAKOBY, SCHACHTER, SHAFRITZ 1994. *The Liver Biology and Pathology,* New York, Raven Press.

ASHWORTH, W. 2017. *A computational model of hepatic energy metabolism: Understanding the role of zonation in the development and treatment of non-alcoholic fatty liver disease (NAFLD).* UCL (University College London).

ASHWORTH, W. B., DAVIES, N. A. & BOGLE, I. D. L. 2016. A computational model of hepatic energy metabolism: understanding zonated damage and steatosis in NAFLD. *PLoS Comput Biol,* 12**,** e1005105.

ASIPU, A., HAYWARD, B. E., O'REILLY, J. & BONTHRON, D. T. 2003. Properties of normal and mutant recombinant human ketohexokinases and implications for the pathogenesis of essential fructosuria. *Diabetes,* 52**,** 2426-32.

BAIS, R., JAMES, H. M., ROFE, A. & CONYERS, R. 1985. The purification and properties of human liver ketohexokinase. A role for ketohexokinase and fructose-bisphosphate aldolase in the metabolic production of oxalate from xylitol. *Biochemical journal,* 230**,** 53-60.

BASARANOGLU, M., BASARANOGLU, G., SABUNCU, T. & SENTURK, H. 2013. Fructose as a key player in the development of fatty liver disease. *World J Gastroenterol,* 19**,** 1166-72.

BASCIANO, H., FEDERICO, L. & ADELI, K. 2005. Fructose, insulin resistance, and metabolic dyslipidemia. *Nutr Metab (Lond),* 2**,** 5.

BAYNES, J. W. & DOMINICZAK, M. H. 2005. Medical Biochemistry *2nd Edition,* p 555.

BEALE, E. G., HARVEY, B. J. & FOREST, C. 2007. PCK1 and PCK2 as candidate diabetes and obesity genes. *Cell biochemistry and biophysics,* 48**,** 89-95.

BENEDICT, M. & ZHANG, X. 2017. Non-alcoholic fatty liver disease: An expanded review. *World journal of hepatology,* 9**,** 715.

BERG, J., TYMOCZKO, J. & STRYER, L. 2002. Chapter 16, Glycolysis and Gluconeogenesis. Biochemistry. New York: WH Freeman.

BERNAL, W., AUZINGER, G., DHAWAN, A. & WENDON, J. 2010. Acute liver failure. *The Lancet,* 376**,** 190-201.

BERNAL, W., JALAN, R., QUAGLIA, A., SIMPSON, K., WENDON, J. & BURROUGHS, A. 2015. Acute-on-chronic liver failure. *The Lancet,* 386**,** 1576-1587.

BETTS, J. G., YOUNG, K. A., WISE, J. A., JOHNSON, E., POE, B., KRUSE, D. H., KOROL, O., JOHNSON, J. E., WOMBLE, M. & DESAIX, P. 2013. *Anatomy and Physiology*.

BIZEAU, M. E. & PAGLIASSOTTI, M. J. 2005. Hepatic adaptations to sucrose and fructose. *Metabolism,* 54**,** 1189-1201.

BRAUNERSREUTHER, V., VIVIANI, G. L., MACH, F. & MONTECUCCO, F. 2012. Role of cytokines and chemokines in non-alcoholic fatty liver disease. *World journal of gastroenterology: WJG,* 18**,** 727.

BRAY, G. A., NIELSEN, S. J. & POPKIN, B. M. 2004. Consumption of high-fructose corn syrup in beverages may play a role in the epidemic of obesity. *The American journal of clinical nutrition,* 79**,** 537-543.

BRIGGS, A. D., MYTTON, O. T., KEHLBACHER, A., TIFFIN, R., ELHUSSEIN, A., RAYNER, M., JEBB, S. A., BLAKELY, T. & SCARBOROUGH, P. 2017. Health impact assessment of the UK soft drinks industry levy: a comparative risk assessment modelling study. *The Lancet Public Health,* 2**,** e15-e22.

BRITISH LIVER TRUST 2019. The alarming impact of liver disease in the UK.

BROWN, M. S. & GOLDSTEIN, J. L. 2008. Selective versus total insulin resistance: a pathogenic paradox. *Cell metabolism,* 7**,** 95-96.

BRUNEL, D. 1999. Functionalized micelle-templated silicas (MTS) and their use as catalysts for fine chemicals. *Microporous and Mesoporous Materials,* 27**,** 329-344.

BURANT, C., TAKEDA, J., BROT-LAROCHE, E., BELL, G. & DAVIDSON, N. 1992. Fructose transporter in human spermatozoa and small intestine is GLUT5. *Journal of Biological Chemistry,* 267**,** 14523-14526.

BUZZETTI, E., PINZANI, M. & TSOCHATZIS, E. A. 2016. The multiple-hit pathogenesis of non-alcoholic fatty liver disease (NAFLD). *Metabolism,* 65**,** 1038-1048.

BYRNE, C. D. & TARGHER, G. 2015. NAFLD: a multisystem disease. *Journal of hepatology,* 62**,** S47-S64.

BYRNE, C. D. & TARGHER, G. 2020. NAFLD as a driver of chronic kidney disease. *Journal of hepatology,* 72**,** 785-801.

CHAKRABORTY, K. & RAJ, R. P. 2008. An extra-cellular alkaline metallolipase from Bacillus licheniformisMTCC 6824: purification and biochemical characterization. *Food chemistry,* 109**,** 727-736.

CHALHOUB, E., HANSON, R. W. & BELOVICH, J. M. 2007. A computer model of gluconeogenesis and lipid metabolism in the perfused liver. *American Journal of Physiology-Endocrinology And Metabolism,* 293**,** E1676-E1686.

CHENG, D., CHU, C.-H., CHEN, L., FEDER, J. N., MINTIER, G. A., WU, Y., COOK, J. W., HARPEL, M. R., LOCKE, G. A. & AN, Y. 2007. Expression, purification, and characterization of human and rat acetyl cfenzyme A carboxylase (ACC) isozymes. *Protein expression and purification,* 51**,** 11-21.

CHONG, M. F., FIELDING, B. A. & FRAYN, K. N. 2007. Mechanisms for the acute effect of fructose on postprandial lipemia. *The American journal of clinical nutrition,* 85**,** 1511-1520.

CLAYTON, R. F., RINALDI, A., KANDYBA, E. E., EDWARD, M., WILLBERG, C., KLENERMAN, P. & PATEL, A. H. 2005. Liver cell lines for the study of hepatocyte functions and immunological response. *Liver International,* 25**,** 389-402.

COHEN, J. C., HORTON, J. D. & HOBBS, H. H. 2011. Human Fatty Liver Disease: Old Questions and New Insights. *Science,* 332**,** 1519-1523.

CRAIG, R. 2014. Health survey for England. *Update*.

CRITCHLEY, L. A. & CRITCHLEY, J. A. 1999. A meta-analysis of studies using bias and precision statistics to compare cardiac output measurement techniques. *J Clin Monit Comput,* 15**,** 85-91.

DALY, M. E., VALE, C., WALKER, M., LITTLEFIELD, A., ALBERTI, K. G. & MATHERS, J. C. 1998. Acute effects on insulin sensitivity and diurnal metabolic profiles of a high-sucrose compared with a high-starch diet. *The American journal of clinical nutrition,* 67**,** 1186-1196.

DAMANIA, A., JAIN, E. & KUMAR, A. 2014. Advancements in in vitro hepatic models: application for drug screening and therapeutics. *Hepatology international,* 8**,** 23-38.

DAVY, K. P. & SEALS, D. R. 1994. Total blood volume in healthy young and older men. *J Appl Physiol (1985),* 76**,** 2059-62.

DEBOSCH, B. J., CHEN, Z., SABEN, J. L., FINCK, B. N. & MOLEY, K. H. 2014. Glucose transporter 8 (GLUT8) mediates fructose-induced de novo lipogenesis and macrosteatosis. *Journal of Biological Chemistry,* 289**,** 10989-10998.

DEKKER, M. J., SU, Q., BAKER, C., RUTLEDGE, A. C. & ADELI, K. 2010. Fructose: a highly lipogenic nutrient implicated in insulin resistance, hepatic steatosis, and the metabolic syndrome. *American Journal of Physiology-Endocrinology and Metabolism*.

DELLA CASA, L., ROSSI, E., ROMANELLI, C., GIBELLINI, L. & IANNONE, A. 2016. Effect of diets supplemented with different conjugated linoleic acid (CLA) isomers on protein expression in C57/BL6 mice. *Genes & nutrition,* 11**,** 26.

DHARMARAJAN, L., CASE, C. L., DUNTEN, P. & MUKHOPADHYAY, B. 2008. Tyr235 of human cytosolic phosphoenolpyruvate carboxykinase influences catalysis through an anion–quadrupole interaction with phosphoenolpyruvate carboxylate. *The FEBS journal,* 275**,** 5810-5819.

DIBBA, P., LI, A. A., PERUMPAIL, B. J., JOHN, N., SALLAM, S., SHAH, N. D., KWONG, W., CHOLANKERIL, G., KIM, D. & AHMED, A. 2018. Emerging therapeutic targets and experimental drugs for the treatment of NAFLD. *Diseases,* 6**,** 83.

DOMBRAUCKAS, J. D., SANTARSIERO, B. D. & MESECAR, A. D. 2005. Structural basis for tumor pyruvate kinase M2 allosteric regulation and catalysis. *Biochemistry,* 44**,** 9417-9429.

DONG, V., NANCHAL, R. & KARVELLAS, C. J. 2020. Pathophysiology of acute liver failure. *Nutrition in Clinical Practice,* 35**,** 24-29.

DOUARD, V. & FERRARIS, R. P. 2008. Regulation of the fructose transporter GLUT5 in health and disease. *American Journal of Physiology-Endocrinology and Metabolism,* 295**,** E227-E237.

DOUARD, V. & FERRARIS, R. P. 2013. The role of fructose transporters in diseases linked to excessive fructose intake. *The Journal of physiology,* 591**,** 401-414.

DOYLE, S. A. & TOLAN, D. R. 1995. Characterization of recombinant human aldolase B and purification by metal chelate chromatography. *Biochem Biophys Res Commun,* 206**,** 902-8.

DUARTE, N. C., BECKER, S. A., JAMSHIDI, N., THIELE, I., MO, M. L., VO, T. D., SRIVAS, R. & PALSSON, B. Ø. 2007. Global reconstruction of the human metabolic network based on genomic and bibliomic data. *Proceedings of the National Academy of Sciences,* 104**,** 1777-1782.

EIPEL, C., ABSHAGEN, K. & VOLLMAR, B. 2010. Regulation of hepatic blood flow: the hepatic arterial buffer response revisited. *World J Gastroenterol,* 16**,** 6046-57.

ENOMOTO, K., NISHIKAWA, Y., OMORI, Y., TOKAIRIN, T., YOSHIDA, M., OHI, N., NISHIMURA, T., YAMAMOTO, Y. & LI, Q. 2004. Cell biology and pathology of liver sinusoidal endothelial cells. *Medical Electron Microscopy,* 37**,** 208-215.

ESTES, C., ANSTEE, Q. M., ARIAS-LOSTE, M. T., BANTEL, H., BELLENTANI, S., CABALLERIA, J., COLOMBO, M., CRAXI, A., CRESPO, J. & DAY, C. P. 2018. Modeling nafld disease burden in china, france, germany, italy, japan, spain, united kingdom, and united states for the period 2016–2030. *Journal of hepatology,* 69**,** 896-904.

FAUSTO, N., CAMPBELL, J. S. & RIEHLE, K. J. 2006. Liver regeneration. *Hepatology,* 43.

FERRARIS, R. P., CHOE, J.-Y. & PATEL, C. R. 2018. Intestinal absorption of fructose. *Annual review of nutrition,* 38**,** 41-67.

FRACANZANI, A. L., VALENTI, L., BUGIANESI, E., ANDREOLETTI, M., COLLI, A., VANNI, E., BERTELLI, C., FATTA, E., BIGNAMINI, D. & MARCHESINI, G. 2008. Risk of severe liver disease in nonalcoholic fatty liver disease with normal aminotransferase levels: a role for insulin resistance and diabetes. *Hepatology,* 48**,** 792-798.

FRANDSEN, E. K. & GRUNNET, N. 1971. Kinetic properties of triokinase from rat liver. *European Journal of Biochemistry,* 23**,** 588-592.

GARFINKEL, D. 1971. Simulation of the Krebs cycle and closely related metabolism in perfused rat liver. I. Construction of a model. *Computers and Biomedical Research,* 4**,** 1-17.

GIBBONS, G. F., KHURANA, R., ODWELL, A. & SEELAENDER, M. 1994. Lipid balance in HepG2 cells: active synthesis and impaired mobilization. *Journal of lipid research,* 35**,** 1801-1808.

GILLE, C., BÖLLING, C., HOPPE, A., BULIK, S., HOFFMANN, S., HÜBNER, K., KARLSTÄDT, A., GANESHAN, R., KÖNIG, M. & ROTHER, K. 2010. HepatoNet1: a comprehensive metabolic reconstruction of the human hepatocyte for the analysis of liver physiology. *Molecular systems biology,* 6**,** 411.

GRACY, R. W. 1975. [94] Triosephosphate isomerase from human erythrocytes. *Methods in enzymology,* 41**,** 442-447.

GROISILLIER, A. & TONON, T. 2015. Determination of Fructokinase Activity from Zobellia galactanivorans.

HASHEM, K. M., HE, F. J., ALDERTON, S. A. & MACGREGOR, G. A. 2019. Cross-Sectional Survey of the Amount of Sugar and Energy in Chocolate Confectionery Sold in the UK in 1992 and 2017. *Nutrients,* 11**,** 1798.

HASHIMOTO, T., COOK, W. S., QI, C., YELDANDI, A. V., REDDY, J. K. & RAO, M. S. 2000. Defect in peroxisome proliferator-activated receptor alpha-inducible fatty acid oxidation determines the severity of hepatic steatosis in response to fasting. *J Biol Chem,* 275**,** 28918-28.

HAVEL, P. J. 2005. Dietary Fructose: Implications for Dysregulation of Energy Homeostasis and Lipid/Carbohydrate Metabolism. *Nutrition Reviews,* 63**,** 133-157.

HEALTH, U. D. O. & SERVICES, H. 2015. US Department of Agriculture. 2015–2020 dietary guidelines for Americans. Washington, DC.

HETHERINGTON, J., SUMNER, T., SEYMOUR, R., LI, L., REY, M. V., YAMAJI, S., SAFFREY, P., MARGONINSKI, O., BOGLE, I. & FINKELSTEIN, A. 2012. A composite computational model of liver glucose homeostasis. I. Building the composite model. *Journal of The Royal Society Interface,* 9**,** 689-700.

HIJMANS, B. S., GREFHORST, A., OOSTERVEER, M. H. & GROEN, A. K. 2014. Zonation of glucose and fatty acid metabolism in the liver: mechanism and metabolic consequences. *Biochimie,* 96**,** 121-9.

HOLZHUTTER, H. G., DRASDO, D., PREUSSER, T., LIPPERT, J. & HENNEY, A. M. 2012. The virtual liver: a multidisciplinary, multilevel challenge for systems biology. *Wiley Interdiscip Rev Syst Biol Med,* 4**,** 221-35.

IDEKER, T., GALITSKI, T. & HOOD, L. 2001. A new approach to decoding life: systems biology. *Annual review of genomics and human genetics,* 2**,** 343-372.

ISHIMOTO, T., LANASPA, M. A., LE, M. T., GARCIA, G. E., DIGGLE, C. P., MACLEAN, P. S., JACKMAN, M. R., ASIPU, A., RONCAL-JIMENEZ, C. A. & KOSUGI, T. 2012. Opposing effects of fructokinase C and A isoforms on fructose-induced metabolic syndrome in mice. *Proceedings of the National Academy of Sciences***,** 201119908.

JAVITT, N. B. 1990. Hep G2 cells as a resource for metabolic studies: lipoprotein, cholesterol, and bile acids. *The FASEB Journal,* 4**,** 161-168.

JENSEN, T., ABDELMALEK, M. F., SULLIVAN, S., NADEAU, K. J., GREEN, M., RONCAL, C., NAKAGAWA, T., KUWABARA, M., SATO, Y. & KANG, D.-H. 2018. Fructose and sugar: A major mediator of non-alcoholic fatty liver disease. *Journal of hepatology,* 68**,** 1063-1075.

JONES, C. 2016. The UK sugar tax–a healthy start? *British dental journal,* 221**,** 59.

JUNGERMANN, K. & KATZ, N. 1989. Functional specialization of different hepatocyte populations. *Physiological reviews,* 69**,** 708-764.

JUNGERMANN, K. & KEITZMANN, T. 1996. Zonation of parenchymal and nonparenchymal metabolism in liver. *Annual review of nutrition,* 16**,** 179-203.

KAPLAN, A. & TENG, M.-H. 1971. Interaction of beef liver lipase with mixed micelles of tripalmitin and Triton X-100. *Journal of Lipid Research,* 12**,** 324-330.

KARIM, S., ADAMS, D. H. & LALOR, P. F. 2012. Hepatic expression and cellular distribution of the glucose transporter family. *World journal of gastroenterology: WJG,* 18**,** 6771.

KATZ, N. R. 1992. Metabolic heterogeneity of hepatocytes across the liver acinus. *The Journal of nutrition,* 122**,** 843-849.

KERSTEN, S. 2014. Integrated physiology and systems biology of PPARα. *Molecular metabolism,* 3**,** 354-371.

KIM, J.-H., LEWIN, T. M. & COLEMAN, R. A. 2001. Expression and Characterization of Recombinant Rat Acyl-CoA Synthetases 1, 4, and 5 Selective Inhibition By Triacsin C And Thiazolidinediones. *Journal of Biological Chemistry,* 276**,** 24667-24673.

KISELEVSKY, Y. V., OSTROVTSOVA, S. A. & STRUMILO, S. A. 1990. Kinetic characterization of the pyruvate and oxoglutarate dehydrogenase complexes from human heart. *Acta Biochimica Polonica,* 37**,** 135-139.

KITANO, H. 2002. Computational systems biology. *Nature,* 420**,** 206-210.

KÖNIG, M., BULIK, S. & HOLZHÜTTER, H.-G. 2012. Quantifying the contribution of the liver to glucose homeostasis: a detailed kinetic model of human hepatic glucose metabolism. *PLoS Comput Biol,* 8**,** e1002577.

KOO, H.-Y., WALLIG, M. A., CHUNG, B. H., NARA, T. Y., CHO, B. S. & NAKAMURA, M. T. 2008. Dietary fructose induces a wide range of genes with distinct shift in carbohydrate and lipid metabolism in fed and fasted rat liver. *Biochimica et Biophysica Acta (BBA)-Molecular Basis of Disease,* 1782**,** 341-348.

LAUGHLIN, M. 2014. Normal roles for dietary fructose in carbohydrate metabolism. *Nutrients,* 6**,** 3117-3129.

LAVOIE, J.-M. & GAUTHIER, M.-S. 2006. Regulation of fat metabolism in the liver: link to non-alcoholic hepatic steatosis and impact of physical exercise. *Cellular and Molecular Life Sciences CMLS,* 63**,** 1393-1409.

LE, K. A., ITH, M., KREIS, R., FAEH, D., BORTOLOTTI, M., TRAN, C., BOESCH, C. & TAPPY, L. 2009. Fructose overconsumption causes dyslipidemia and ectopic lipid deposition in healthy subjects with and without a family history of type 2 diabetes. *Am J Clin Nutr,* 89**,** 1760-5.

LI, Z., SOLOSKI, M. J. & DIEHL, A. M. 2005. Dietary factors alter hepatic innate immune system in mice with nonalcoholic fatty liver disease. *Hepatology,* 42**,** 880-5.

LIAO, Y., DAVIES, N. A. & BOGLE, I. D. L. 2020. Computational Modeling of Fructose Metabolism and Development in NAFLD. *Frontiers in Bioengineering and Biotechnology,* 8.

LIBERTI, M. V. & LOCASALE, J. W. 2016. The Warburg effect: how does it benefit cancer cells? *Trends in biochemical sciences,* 41**,** 211-218.

LIEBISCH, G., FAHY, E., AOKI, J., DENNIS, E. A., DURAND, T., EJSING, C. S., FEDOROVA, M., FEUSSNER, I., GRIFFITHS, W. J. & KÖFELER, H. 2020. Update on LIPID MAPS classification, nomenclature, and shorthand notation for MS-derived lipid structures. *Journal of lipid research,* 61**,** 1539-1555.

LIM, J. S., MIETUS-SNYDER, M., VALENTE, A., SCHWARZ, J.-M. & LUSTIG, R. H. 2010. The role of fructose in the pathogenesis of NAFLD and the metabolic syndrome. *Nature reviews gastroenterology and hepatology,* 7**,** 251-264.

LOW, W. S., CORNFIELD, T., CHARLTON, C. A., TOMLINSON, J. W. & HODSON, L. 2018. Sex differences in hepatic de novo lipogenesis with acute fructose feeding. *Nutrients,* 10**,** 1263.

MA, H., SOROKIN, A., MAZEIN, A., SELKOV, A., SELKOV, E., DEMIN, O. & GORYANIN, I. 2007. The Edinburgh human metabolic network reconstruction and its functional analysis. *Molecular systems biology,* 3**,** 135.

MALAY, A. D., PROCIOUS, S. L. & TOLAN, D. R. 2002. The temperature dependence of activity and structure for the most prevalent mutant aldolase B associated with hereditary fructose intolerance. *Archives of biochemistry and biophysics,* 408**,** 295-304.

MALDONADO, E. M., FISHER, C. P., MAZZATTI, D. J., BARBER, A. L., TINDALL, M. J., PLANT, N. J., KIERZEK, A. M. & MOORE, J. B. 2018. Multi-scale, whole-system models of liver metabolic adaptation to fat and sugar in non-alcoholic fatty liver disease. *NPJ systems biology and applications,* 4**,** 1-10.

MANOLESCU, A. R., WITKOWSKA, K., KINNAIRD, A., CESSFORD, T. & CHEESEMAN, C. 2007. Facilitated hexose transporters: new perspectives on form and function. *Physiology,* 22**,** 234-240.

MARCEL, Y. L. & SUZUE, G. 1972. Kinetic studies on the specificity of long chain acyl coenzyme A synthetase from rat liver microsomes. *Journal of Biological Chemistry,* 247**,** 4433-4436.

MAYES, P. A. 1993. Intermediary metabolism of fructose. *The American Journal of Clinical Nutrition,* 58**,** 754S-765S.

MAZZA, A., FRUCI, B., GARINIS, G. A., GIULIANO, S., MALAGUARNERA, R. & BELFIORE, A. 2011. The role of metformin in the management of NAFLD. *Experimental diabetes research,* 2012.

MEIRELLES JÚNIOR, R. F., SALVALAGGIO, P., REZENDE, M. B. D., EVANGELISTA, A. S., GUARDIA, B. D., MATIELO, C. E. L., NEVES, D. B., PANDULLO, F. L., FELGA, G. E. G. & ALVES, J. A. D. S. 2015. Liver transplantation: history, outcomes and perspectives. *Einstein (Sao Paulo),* 13**,** 149-152.

MIELE, L., VALENZA, V., LA TORRE, G., MONTALTO, M., CAMMAROTA, G., RICCI, R., MASCIANA, R., FORGIONE, A., GABRIELI, M. L. & PEROTTI, G. 2009. Increased intestinal permeability and tight junction alterations in nonalcoholic fatty liver disease. *Hepatology,* 49**,** 1877-1887.

MIYAZAKI, M., DOBRZYN, A., MAN, W. C., CHU, K., SAMPATH, H., KIM, H. J. & NTAMBI, J. M. 2004. Stearoyl-CoA desaturase 1 gene expression is necessary for fructose-mediated induction of lipogenic gene expression by sterol regulatory element-binding protein-1c-dependent and -independent mechanisms. *J Biol Chem,* 279**,** 25164-71.

MOON, A. M., SINGAL, A. G. & TAPPER, E. B. 2019. Contemporary epidemiology of chronic liver disease and cirrhosis. *Clinical Gastroenterology and Hepatology*.

NAFTALIN, R. J. 2016. A computer model simulating human glucose absorption and metabolism in health and metabolic disease states. *F1000Research,* 5.

NAGAI, Y., NISHIO, Y., NAKAMURA, T., MAEGAWA, H., KIKKAWA, R. & KASHIWAGI, A. 2002. Amelioration of high fructose-induced metabolic derangements by activation of PPARα. *American Journal of Physiology-Endocrinology and Metabolism,* 282**,** E1180-E1190.

NGUYEN, T. H., WARDELL, R., CHITTURI, S., TEOH, N. & FARRELL, G. 2020. When the liver gets stiff, the tough get moving. *Journal of gastroenterology and hepatology,* 35**,** 953-959.

NOMURA, K. & YAMANOUCHI, T. 2012. The role of fructose-enriched diets in mechanisms of nonalcoholic fatty liver disease. *The Journal of nutritional biochemistry,* 23**,** 203-208.

O'GRADY, J., SCHALM, S. & WILLIAMS, R. 1993. Acute liver failure: redefining the syndromes. *The Lancet,* 342**,** 273-275.

O'LEARY, J. G., LEPE, R. & DAVIS, G. L. 2008. Indications for liver transplantation. *Gastroenterology,* 134**,** 1764-1776.

OHASHI, K., MUNETSUNA, E., YAMADA, H., ANDO, Y., YAMAZAKI, M., TAROMARU, N., NAGURA, A., ISHIKAWA, H., SUZUKI, K. & TERADAIRA, R. 2015. High fructose consumption induces DNA methylation at PPARα and CPT1A promoter regions in the rat liver. *Biochemical and biophysical research communications,* 468**,** 185-189.

OHNO, H., YASUHIRO NAITO, HIROMU NAKAJIMA, AND MASARU TOMITA. 2008. Construction of a biological tissue model based on a single-cell model: a computer simulation of metabolic heterogeneity in the liver lobule. *Artificial life,* 14**,** 3-28.

OUYANG, X., CIRILLO, P., SAUTIN, Y., MCCALL, S., BRUCHETTE, J. L., DIEHL, A. M., JOHNSON, R. J. & ABDELMALEK, M. F. 2008. Fructose consumption

as a risk factor for non-alcoholic fatty liver disease. *Journal of hepatology,* 48**,** 993-999.

PATEL, C., SUGIMOTO, K., DOUARD, V., SHAH, A., INUI, H., YAMANOUCHI, T. & FERRARIS, R. P. 2015. Effect of dietary fructose on portal and systemic serum fructose levels in rats and in KHK−/− and GLUT5−/− mice. *American Journal of Physiology-Gastrointestinal and Liver Physiology,* 309**,** G779-G790.

PERUMPAIL, B. J., KHAN, M. A., YOO, E. R., CHOLANKERIL, G., KIM, D. & AHMED, A. 2017. Clinical epidemiology and disease burden of nonalcoholic fatty liver disease. *World journal of gastroenterology,* 23**,** 8263.

PETÄJÄ, E. M. & YKI-JÄRVINEN, H. 2016. Definitions of normal liver fat and the association of insulin sensitivity with acquired and genetic NAFLD—a systematic review. *International journal of molecular sciences,* 17**,** 633.

PETTA, S., VALENTI, L., BUGIANESI, E., TARGHER, G., BELLENTANI, S., BONINO, F., FERRANNINI, E., LOGUERCIO, C., LONARDO, A. & MARRA, F. 2016. A "systems medicine" approach to the study of non-alcoholic fatty liver disease. *Digestive and Liver Disease,* 48**,** 333-342.

PHILLIPS, M. I. & DAVIES, D. R. 1985. The mechanism of guanosine triphosphate depletion in the liver after a fructose load. The role of fructokinase. *Biochemical Journal,* 228**,** 667-671.

PIAZZOLLA, V. A. & MANGIA, A. 2020. Noninvasive Diagnosis of NAFLD and NASH. *Cells,* 9**,** 1005.

PRATT, D. S. & KAPLAN, M. M. 2000. Evaluation of abnormal liver-enzyme results in asymptomatic patients. *New England Journal of Medicine,* 342**,** 1266-1271.

PUBLIC HEALTH ENGLAND AND THE FOOD STANDARDS AGENCY 2019. National Diet and Nutrition Survey

Rolling programme Years 9 to 11 (2016/2017 to 2018/2019).

RANI, H., SHEU, T. W., CHANG, T. & LIANG, P. 2006. Numerical investigation of non-Newtonian microcirculatory blood flow in hepatic lobule. *Journal of biomechanics,* 39**,** 551-563.

REAVEN, G. M., HOLLENBECK, C., JENG, C.-Y., WU, M. S. & CHEN, Y.-D. I. 1988. Measurement of plasma glucose, free fatty acid, lactate, and insulin for 24 h in patients with NIDDM. *Diabetes,* 37**,** 1020-1024.

RODRIGUES, J. R., COUTO, A., CABEZAS, A., PINTO, R. M., RIBEIRO, J. M., CANALES, J., COSTAS, M. J. & CAMESELLE, J. C. 2014. Bifunctional Homodimeric Triokinase/FMN Cyclase CONTRIBUTION OF PROTEIN DOMAINS TO THE ACTIVITIES OF THE HUMAN ENZYME AND MOLECULAR DYNAMICS SIMULATION OF DOMAIN MOVEMENTS. *Journal of Biological Chemistry,* 289**,** 10620-10636.

ROGLANS, N., SANGUINO, E., PERIS, C., ALEGRET, M., VÁZQUEZ, M., ADZET, T., DÍAZ, C., HERNÁNDEZ, G., LAGUNA, J. C. & SÁNCHEZ, R. M. 2002. Atorvastatin treatment induced peroxisome proliferator-activated receptor α expression and decreased plasma nonesterified fatty acids and liver triglyceride in fructose-fed rats. *Journal of Pharmacology and Experimental Therapeutics,* 302**,** 232-239.

ROGLANS, N., VILA, L., FARRÉ, M., ALEGRET, M., SÁNCHEZ, R. M., VÁZQUEZ‐CARRERA, M. & LAGUNA, J. C. 2007. Impairment of hepatic

Stat‐3 activation and reduction of PPARα activity in fructose‐fed rats. *Hepatology,* 45**,** 778-788.

RONCAL-JIMENEZ, C. A., LANASPA, M. A., RIVARD, C. J., NAKAGAWA, T., SANCHEZ-LOZADA, L. G., JALAL, D., ANDRES-HERNANDO, A., TANABE, K., MADERO, M. & LI, N. 2011. Sucrose induces fatty liver and pancreatic inflammation in male breeder rats independent of excess energy intake. *Metabolism,* 60**,** 1259-1270.

RUTLEDGE, A. C. & ADELI, K. 2007. Fructose and the Metabolic Syndrome: Pathophysiology and Molecular Mechanisms. *Nutrition Reviews,* 65**,** 13-23.

RYOO, J. H., SUH, Y. J., SHIN, H. C., CHO, Y. K., CHOI, J. M. & PARK, S. K. 2014. Clinical association between non‐alcoholic fatty liver disease and the development of hypertension. *Journal of gastroenterology and hepatology,* 29**,** 1926-1931.

SANCHEZ-LOZADA, L. G., MU, W., RONCAL, C., SAUTIN, Y. Y., ABDELMALEK, M., REUNGJUI, S., LE, M., NAKAGAWA, T., LAN, H. Y., YU, X. & JOHNSON, R. J. 2010. Comparison of free fructose and glucose to sucrose in the ability to cause fatty liver. *Eur J Nutr,* 49**,** 1-9.

SANTOLERI, D. & TITCHENELL, P. M. 2019. Resolving the paradox of hepatic insulin resistance. *Cellular and molecular gastroenterology and hepatology,* 7**,** 447-456.

SCHMILOVITZ-WEISS, H., HOCHHAUSER, E., COHEN, M., CHEPURKO, Y., YITZHAKI, S., GROSSMAN, E., LEIBOWITZ, A., ACKERMAN, Z. & BEN-ARI, Z. 2013. Rosiglitazone and bezafibrate modulate gene expression in a rat model of non-alcoholic fatty liver disease-A historical prospective. *Lipids in health and disease,* 12**,** 41.

SCHULTZ, A., BARBOSA-DA-SILVA, S., AGUILA, M. B. & MANDARIM-DE-LACERDA, C. A. 2015. Differences and similarities in hepatic lipogenesis, gluconeogenesis and oxidative imbalance in mice fed diets rich in fructose or sucrose. *Food & function,* 6**,** 1684-1691.

SEFRIED, S., HÄRING, H.-U., WEIGERT, C. & ECKSTEIN, S. S. 2018. Suitability of hepatocyte cell lines HepG2, AML12 and THLE-2 for investigation of insulin signalling and hepatokine gene expression. *Royal Society Open Biology,* 8**,** 180147.

SELLMANN, C., PRIEBS, J., LANDMANN, M., DEGEN, C., ENGSTLER, A. J., JIN, C. J., GÄRTTNER, S., SPRUSS, A., HUBER, O. & BERGHEIM, I. 2015. Diets rich in fructose, fat or fructose and fat alter intestinal barrier function and lead to the development of nonalcoholic fatty liver disease over time. *The Journal of nutritional biochemistry,* 26**,** 1183-1192.

SENGUPTA, A., GROVER, M., CHAKRABORTY, A. & SAXENA, S. 2015. HEPNet: A Knowledge Base Model of Human Energy Pool Network for Predicting the Energy Availability Status of an Individual. *PLoS One,* 10**,** e0127918.

SHAFIEE-MORREL, F., GRUSAK, M., GUSTAFSON, S., LILA, M. & NICULESCU, M. 2012. Lower concentrations of blueberry polyphenolic-rich extract differentially alter HepG2 cell proliferation and expression of genes related to cell-cycle, oxidation and epigenetic machinery. *Journal of Nutritional Disorders & Therapy,* 3**,** 120.

SHIMIZU, S., UGI, S., MAEGAWA, H., EGAWA, K., NISHIO, Y., YOSHIZAKI, T., SHI, K., NAGAI, Y., MORINO, K., NEMOTO, K., NAKAMURA, T., BRYER-ASH, M. & KASHIWAGI, A. 2003. Protein-tyrosine phosphatase 1B as new activator for hepatic lipogenesis via sterol regulatory element-binding protein-1 gene expression. *J Biol Chem,* 278**,** 43095-101.

SIBULESKY, L. 2013. Normal liver anatomy. *Clinical Liver Disease,* 2.

SILLERO, M., SILLERO, A. & SOLS, A. 1969. Enzymes involved in fructose metabolism in liver and the glyceraldehyde metabolic crossroads. *European Journal of Biochemistry,* 10**,** 345-350.

SILLIMAN, K. & COULSTON, A. 1991. Sugars in the diet. *Sugars and sweeteners.***,** 17-35.

SMITH, P. E., KROHN, R. I., HERMANSON, G. T., MALLIA, A. K., GARTNER, F. H., PROVENZANO, M., FUJIMOTO, E. K., GOEKE, N. M., OLSON, B. J. & KLENK, D. 1985. Measurement of protein using bicinchoninic acid. *Analytical biochemistry,* 150**,** 76-85.

SNYDER, R. & LEE, E. W. 1975. [91] Triosephosphate isomerase from human and horse liver. *Methods in enzymology,* 41**,** 430-434.

SOFTIC, S., COHEN, D. E. & KAHN, C. R. 2016. Role of dietary fructose and hepatic de novo lipogenesis in fatty liver disease. *Digestive diseases and sciences,* 61**,** 1282-1293.

SONG, M., SCHUSCHKE, D. A., ZHOU, Z., CHEN, T., SHI, X., ZHANG, J., ZHANG, X., PIERCE, W. M., JR., JOHNSON, W. T., VOS, M. B. & MCCLAIN, C. J. 2013. Modest fructose beverage intake causes liver injury and fat accumulation in marginal copper deficient rats. *Obesity (Silver Spring),* 21**,** 1669-75.

STAELS, B., RUBENSTRUNK, A., NOEL, B., RIGOU, G., DELATAILLE, P., MILLATT, L. J., BARON, M., LUCAS, A., TAILLEUX, A., HUM, D. W., RATZIU, V., CARIOU, B. & HANF, R. 2013. Hepatoprotective effects of the dual peroxisome proliferator-activated receptor alpha/delta agonist, GFT505, in rodent models of nonalcoholic fatty liver disease/nonalcoholic steatohepatitis. *Hepatology,* 58**,** 1941-52.

STANHOPE, K. L., GRIFFEN, S. C., BAIR, B. R., SWARBRICK, M. M., KEIM, N. L. & HAVEL, P. J. 2008. Twenty-four-hour endocrine and metabolic profiles following consumption of high-fructose corn syrup-, sucrose-, fructose-, and glucose-sweetened beverages with meals. *The American journal of clinical nutrition,* 87**,** 1194-1203.

STANHOPE, K. L., SCHWARZ, J. M., KEIM, N. L., GRIFFEN, S. C., BREMER, A. A., GRAHAM, J. L., HATCHER, B., COX, C. L., DYACHENKO, A. & ZHANG, W. 2009. Consuming fructose-sweetened, not glucose-sweetened, beverages increases visceral adiposity and lipids and decreases insulin sensitivity in overweight/obese humans. *The Journal of clinical investigation,* 119**,** 1322-1334.

STARZL, T. E., IWATSUKI, S., VAN THIEL, D. H., CARLTON GARTNER, J., ZITELLI, B. J., JEFFREY MALATACK, J., SCHADE, R. R., SHAW JR, B. W., HAKALA, T. R. & THOMAS ROSENTHAL, J. 1982. Evolution of liver transplantation. *Hepatology,* 2**,** 614S-636S.

STINNETT, L., LEWIN, T. M. & COLEMAN, R. A. 2007. Mutagenesis of rat acyl-CoA synthetase 4 indicates amino acids that contribute to fatty acid binding. *Biochimica et Biophysica Acta (BBA)-Molecular and Cell Biology of Lipids,* 1771**,** 119-125.

STOKKELAND, K., LAGEBORN, C. T., EKBOM, A., HÖIJER, J., BOTTAI, M., STÅL, P. & SÖDERBERG‐LÖFDAL, K. 2018. Statins and angiotensin‐converting enzyme inhibitors are associated with reduced mortality and morbidity in chronic liver disease. *Basic & clinical pharmacology & toxicology,* 122**,** 104-110.

SUMNER, T., HETHERINGTON, J., SEYMOUR, R. M., LI, L., VARELA REY, M., YAMAJI, S., SAFFREY, P., MARGONINSKI, O., BOGLE, I. D., FINKELSTEIN, A. & WARNER, A. 2012. A composite computational model of liver glucose homeostasis. II. Exploring system behaviour. *J R Soc Interface,* 9**,** 701-6.

SUN, S. Z. & EMPIE, M. W. 2012. Fructose metabolism in humans–what isotopic tracer studies tell us. *Nutrition & metabolism,* 9**,** 1.

TAGHIBIGLOU, C., RASHID-KOLVEAR, F., VAN IDERSTINE, S. C., LE-TIEN, H., FANTUS, I. G., LEWIS, G. F. & ADELI, K. 2002. Hepatic very low density lipoprotein-ApoB overproduction is associated with attenuated hepatic insulin signaling and overexpression of protein-tyrosine phosphatase 1B in a fructose-fed hamster model of insulin resistance. *J Biol Chem,* 277**,** 793-803.

TAILLEUX, A., WOUTERS, K. & STAELS, B. 2012. Roles of PPARs in NAFLD: potential therapeutic targets. *Biochim Biophys Acta,* 1821**,** 809-18.

TAPPY, L. & LÊ, K.-A. 2010. Metabolic effects of fructose and the worldwide increase in obesity. *Physiological reviews,* 90**,** 23-46.

TAYLOR, R., MAGNUSSON, I., ROTHMAN, D. L., CLINE, G. W., CAUMO, A., COBELLI, C. & SHULMAN, G. I. 1996. Direct assessment of liver glycogen storage by 13C nuclear magnetic resonance spectroscopy and regulation of glucose homeostasis after a mixed meal in normal subjects. *The Journal of clinical investigation,* 97**,** 126-132.

THORENS, B. 1992. Molecular and Cellular Physiology of GLUT-2, a High-K~ m Facilitated Diffusion Glucose Transporter. *International review of cytology***,** 209-209.

TSOCHATZIS, E. A., BOSCH, J. & BURROUGHS, A. K. 2014. Liver cirrhosis. *The Lancet,* 383**,** 1749-1761.

VAN HORN, C. G., CAVIGLIA, J. M., LI, L. O., WANG, S., GRANGER, D. A. & COLEMAN, R. A. 2005. Characterization of recombinant long-chain rat acyl-CoA synthetase isoforms 3 and 6: identification of a novel variant of isoform 6. *Biochemistry,* 44**,** 1635-1642.

VANCURA, A. & HALDAR, D. 1994. Purification and characterization of glycerophosphate acyltransferase from rat liver mitochondria. *Journal of Biological Chemistry,* 269**,** 27209-27215.

VENTURA, E. E., DAVIS, J. N. & GORAN, M. I. 2011. Sugar content of popular sweetened beverages based on objective laboratory analysis: focus on fructose content. *Obesity,* 19**,** 868-874.

VOS, J. J., WIETASCH, J. G., ABSALOM, A. R., HENDRIKS, H. G. & SCHEEREN, T. W. 2014. Green light for liver function monitoring using indocyanine green? An overview of current clinical applications. *Anaesthesia,* 69**,** 1364-1376.

VOS, M. B. & LAVINE, J. E. 2013. Dietary fructose in nonalcoholic fatty liver disease. *Hepatology,* 57**,** 2525-2531.

WANG, S., PESSAH, M., INFANTE, J., CATALA, D., SALVAT, C. & INFANTE, R. 1988. Lipid and lipoprotein metabolism in Hep G2 cells. *Biochimica et Biophysica Acta (BBA)-Lipids and Lipid Metabolism,* 961**,** 351-363.

WEBER, G., LEA, M. A. & STAMM, N. B. 1967. Inhibition of pyruvate kinase and glucokinase by acetyl CoA and inhibition of glucokinase by phosphoenolpyruvate. *Life Sciences,* 6**,** 2441-2452.

WILKENING, S., STAHL, F. & BADER, A. 2003. Comparison of primary human hepatocytes and hepatoma cell line Hepg2 with regard to their biotransformation properties. *Drug Metabolism and Disposition,* 31**,** 1035-1042.

WILLIAMS, R., ALEXANDER, G., ARMSTRONG, I., BAKER, A., BHALA, N., CAMPS-WALSH, G., CRAMP, M. E., DE LUSIGNAN, S., DAY, N. & DHAWAN, A. 2018. Disease burden and costs from excess alcohol consumption, obesity, and viral hepatitis: fourth report of the Lancet Standing Commission on Liver Disease in the UK. *The Lancet,* 391**,** 1097-1107.

WILLIAMS, R., ASPINALL, R., BELLIS, M., CAMPS-WALSH, G., CRAMP, M., DHAWAN, A., FERGUSON, J., FORTON, D., FOSTER, G. & GILMORE, I. 2014. Addressing liver disease in the UK: a blueprint for attaining excellence in health care and reducing premature mortality from lifestyle issues of excess consumption of alcohol, obesity, and viral hepatitis. *The Lancet,* 384**,** 1953-1997.

WRIGHT, E. M., SALA-RABANAL, M., LOO, D. D. F. & HIRAYAMA, B. A. 2012. Chapter 58 - Sugar Absorption. *In:* JOHNSON, L. R., GHISHAN, F. K., KAUNITZ, J. D., MERCHANT, J. L., SAID, H. M. & WOOD, J. D. (eds.) *Physiology of the Gastrointestinal Tract (Fifth Edition).* Boston: Academic Press.

YE, Q., ZOU, B., YEO, Y. H., LI, J., HUANG, D. Q., WU, Y., YANG, H., LIU, C., KAM, L. Y. & TAN, X. X. E. 2020. Global prevalence, incidence, and outcomes of non-obese or lean non-alcoholic fatty liver disease: a systematic review and meta-analysis. *The Lancet Gastroenterology & Hepatology,* 5**,** 739-752.

YOUNOSSI, Z. M., KOENIG, A. B., ABDELATIF, D., FAZEL, Y., HENRY, L. & WYMER, M. 2016. Global epidemiology of nonalcoholic fatty liver disease—meta‐analytic assessment of prevalence, incidence, and outcomes. *Hepatology,* 64**,** 73-84.

YOUNOSSI, Z. M., LOOMBA, R., RINELLA, M. E., BUGIANESI, E., MARCHESINI, G., NEUSCHWANDER‐TETRI, B. A., SERFATY, L., NEGRO, F., CALDWELL, S. H. & RATZIU, V. 2018. Current and future therapeutic regimens for nonalcoholic fatty liver disease and nonalcoholic steatohepatitis. *Hepatology,* 68**,** 361-371.

YOUNOSSI, Z. M., RINELLA, M. E., SANYAL, A., HARRISON, S. A., BRUNT, E., GOODMAN, Z., COHEN, D. E. & LOOMBA, R. 2020. From NAFLD to MAFLD: implications of a premature change in terminology. *Hepatology*.

YUAN, P., DEWAN, R., ZAUN, M., THOMPSON, R. & GRACY, R. 1979. Isolation and characterization of triosephosphate isomerase isozymes from human placenta. *Archives of biochemistry and biophysics,* 198**,** 42-52.

ZELBER–SAGI, S., KESSLER, A., BRAZOWSKY, E., WEBB, M., LURIE, Y., SANTO, M., LESHNO, M., BLENDIS, L., HALPERN, Z. & OREN, R. 2006. A double-blind randomized placebo-controlled trial of orlistat for the treatment of nonalcoholic fatty liver disease. *Clinical Gastroenterology and Hepatology,* 4**,** 639-644.

ZHAO, F.-Q. & KEATING, A. F. 2007. Functional properties and genomics of glucose transporters. *Current genomics,* 8**,** 113-128.

ZIERZ, S. & ENGEL, A. G. 1987. Different sites of inhibition of carnitine palmitoyltransferase by malonyl-CoA, and by acetyl-CoA and CoA, in human skeletal muscle. *Biochemical Journal,* 245**,** 205-209.